



THE HONG KONG
POLYTECHNIC UNIVERSITY

香港理工大學

Pao Yue-kong Library

包玉剛圖書館

Copyright Undertaking

This thesis is protected by copyright, with all rights reserved.

By reading and using the thesis, the reader understands and agrees to the following terms:

1. The reader will abide by the rules and legal ordinances governing copyright regarding the use of the thesis.
2. The reader will use the thesis for the purpose of research or private study only and not for distribution or further reproduction or any other purpose.
3. The reader agrees to indemnify and hold the University harmless from and against any loss, damage, cost, liability or expenses arising from copyright infringement or unauthorized usage.

IMPORTANT

If you have reasons to believe that any materials in this thesis are deemed not suitable to be distributed in this form, or a copyright owner having difficulty with the material being included in our database, please contact lbsys@polyu.edu.hk providing details. The Library will look into your claim and consider taking remedial action upon receipt of the written requests.

**OPTIMAL PLANNING OF POWER SYSTEMS WITH
RENEWABLE ENERGY INTEGRATION**

XU XU

PhD

The Hong Kong Polytechnic University

2019

The Hong Kong Polytechnic University

Department of Electrical Engineering

**Optimal Planning of Power Systems with
Renewable Energy Integration**

Xu XU

A thesis submitted in partial fulfillment of the requirements for the
degree of Doctor of Philosophy

May 2019

Certificate of Originality

I hereby declare that this thesis is my own work and that, to the best of my knowledge and belief, it reproduces no material previously published or written, nor material that has been accepted for the award of any other degree or diploma, except where due acknowledgement has been made in the text.

_____ (Signed)

_____ Xu XU (Name of student)

To my parents,

Xiqiang Xu and Aihong Han

Abstract

In the last decade, the growth of renewable energy capacity has been increased rapidly in power systems. Large-scale renewable energy integration of the power systems may bring many economic interests and environmental benefits. However, due to the stochastic characteristics of renewable generation output, widespread installation of renewable generators will pose some great challenges to the normal power system operation. For example, power flow patterns of transmission lines will significantly change and become inevitably fluctuating due to high renewable penetration. This may result in some potential negative effects, including but are not limited to line congestion, increased active power loss and large voltage deviation. To deal with these issues, the traditional power system expansion can be taken into consideration, such as power system line expansion and reconstruction, new electrical plants installation and existing facilities upgrade. However, these system expansion options are usually investment-intensive and time-consuming and may cause environmental problems. In this regard, this thesis focuses on dealing with negative concerns caused by renewable energy integration via optimal advanced flexible AC transmission systems (FACTS) devices planning in transmission networks, and enhancing renewable energy hosting capacity via optimal advanced electrical devices in distribution networks, respectively.

The thesis firstly focuses on planning in transmission networks, which is to cope with the negative effects introduced by high wind power penetration. To tackle the negative impacts caused by wind energy integration, a stochastic optimal TCSC location-allocation model is proposed. This planning model is formulated as a two-stage optimization program, where the planning decisions including sites and sizes for TCSC devices installation are determined in the first stage and the second stage is to

minimize the expected operation cost of transmission systems under various wind-load uncertainty scenarios. The proposed planning model is firstly formulated as a mixed integer nonlinear programming (MINLP), and then both the linearization technique as well as the approximation approach are used to transform this MINLP to a mixed integer linear programming (MILP), which can be directly solved by commercial solvers such as CPLEX and GUROBI. The TCSC planning model considers uncertainties of wind energy output and load demand, which are represented by wind-load scenarios. These scenarios are originally generated by using classical copula theory and then reduced by a well-established backward-reduction algorithm. Finally, a modified IEEE 57-bus transmission system is utilized to verify the effectiveness of the proposed planning model.

The thesis secondly focuses on planning in distribution networks, which is to improve the ability of distribution networks to accommodate more photovoltaic (PV) generations. To improve PV hosting capacity, a two-stage optimal var compensator (SVC) planning model is proposed. In detail, the first stage is to determine the PV hosing capacity of the given sites and SVC location-allocation decisions and the second stage is to minimize the operation cost of SVC devices in all considered uncertainty scenarios. Besides, the concept of PV accommodation capability (PVAC) is proposed to describe the amount of PV generation that can be reliably accommodated at a certain node of a distribution network within a certain time period. To enhance the daily PVAC, this thesis proposes two-stage MILP based voltage regulator (VR) placement model, where the hourly PVAC and VR allocation decisions are determined in the first stage and a stochastic programming based feasibility checking model is developed to ensure the network constraints security in the second stage. These two planning problems are both intractable due to numerous operation

scenarios involved as well as the time-coupling constraints. In this regard, to reduce the computational complexity, a Benders decomposition algorithm based solution method is developed to solve the proposed two-stage stochastic problems. IEEE distribution systems are utilized to verify the effectiveness of the proposed planning model and solution method.

List of Publications Arisen from the Thesis

Journal Papers

- 1 **Xu Xu**, Jiayong Li, Zhao Xu, Jian Zhao and Chunsing Lai, "Enhancing photovoltaic hosting capacity—A stochastic approach to optimal planning of static var compensator devices in distribution networks," *Applied Energy*, vol. 238, pp. 952-962, 2019. Published.
- 2 **Xu Xu**, Jian Zhao, Zhao Xu, Songjian Chai, Jiayong Li, Yi Yu, "Stochastic optimal TCSC placement in power system considering high wind power penetration," *IET Generation, Transmission & Distribution*, vol. 12, no. 12, pp. 3052-3060, 2018. Published.
- 3 **Xu Xu**, Jiayong Li, Youwei Jia, Zhao Xu, "Two-stage stochastic optimal voltage regulator placement in distribution grid considering photovoltaic accommodation capability improvement", *Energy*, 2019, Under Review.

Conference Papers

- 1 **Xu Xu**, Zhao Xu, Jiayong Li, Jian Zhao, Xue Lyu, "Optimal Placement of Voltage Regulators for Photovoltaic Hosting Capacity Maximization," in *2018 IEEE Innovative Smart Grid Technologies-Asia (ISGT Asia)*, 2018, pp. 1278-1282: IEEE. **(The solo best student paper award)**
- 2 **Xu Xu**, Zhao Xu, Xue Lyu, Jiayong Li, Jian Zhao, "Optimal SVC Placement for Maximizing PV Hosting Capacity in Distribution Network", in *10th Symposium on Control of Power and Energy Systems*, 2018, vol. 51, no. 28, pp. 356-361.
- 3 **Xu Xu**, Zhao Xu, Loong Chan, Jian Zhao, Songjian Chai, Yi Yu, Jiayong Li, Xue Lyu, "Probabilistic TCSC Placement Considering Wind Power Penetration Based on Line Flow Equations", in *2017 International Conference on Electrical Engineering*.

Acknowledgements

This work is accomplished at the Department of Electrical Engineering, The Hong Kong Polytechnic University (HKPU) during my PhD candidature period from 2016 to 2019.

I am very grateful to all the people who helped and supported me during my Ph.D. study in The Hong Kong Polytechnic University. First and foremost, I would like to express my deepest appreciation to my chief supervisor, Prof. Zhao Xu, for his continuous guidance, encouragement, support and patience throughout my entire PhD study. He is always very kind and patient in offering insightful suggestions to improve my research works. I will remember his kindness and patience during my lifetime.

I would also like to express special thanks to my parents and my relatives for their unconditional love, support and encouragement. Special thanks should go to dear fiancée, Qingzhi Cai, who has always been there for me. My thanks also go to my research colleagues who make progress together with me, inspire each other and become better than ever before during my precious lifetime in Hong Kong. Especially, I would thank the seniors, Dr. Jian Zhao, Dr. Jiayong Li, Dr. Youwei Jia and Dr. Songjia Chai, for their help and suggestions on my research.

Table of Contents

Abstract	i
List of Publications Arisen from the Thesis.....	iv
Acknowledgements	v
Table of Contents	vi
List of Figures	ix
List of Tables.....	xiii
List of Abbreviations.....	xiv
Chapter 1 Introduction.....	1
1.1 Background.....	1
1.2 Purpose of the Thesis.....	5
1.3 Primary Contributions.....	7
1.4 Thesis Layout.....	9
Chapter 2 Stochastic Thyristor Controlled Series Capacitor Devices Planning with High Wind Energy Penetration	12
2.1 Introduction.....	12
2.2 Uncertainties Consideration in Transmission Networks.....	18
2.2.1 Uncertainties Modeling.....	18
2.2.2 Scenarios Generation and Reduction.....	18
2.3 Mathematical Formulation of the Stochastic TCSC Planning Model	20
2.3.1 Line Flow based Model	20
2.3.2 TCSC Installed LFB Model.....	22
2.3.3 Linearization of LFB-TCSC Model.....	24
2.3.4 Stochastic TCSC Planning Model	26
2.4 Numerical Results.....	28

2.4.1	The Approximation Approach Verification.....	31
2.4.2	TCSC Devices Location-allocation Results	33
2.4.3	Comparisons on Total cost.....	33
2.4.4	Comparison of Power Loss.....	34
2.4.5	Comparison of Transmission Line Capacity Margin.....	35
2.4.6	Sensitivity Analysis on Wind Power Penetration	37
2.5	Summary.....	39
Chapter 3 Improving Photovoltaic Hosting Capacity via Optimal Location-		
allocation of Static Var Compensators		
3.1	Introduction.....	40
3.2	Formulation of SVC Planning Problem.....	45
3.2.1	Two-stage Stochastic Framework.....	45
3.2.2	Distribution Network Model.....	47
3.2.3	PV Hosting Capacity Improvement.....	48
3.2.4	Mathematical Formulation of the SVC Planning Problem.....	48
3.3	Solution Methodology	52
3.3.1	Subproblem and Master problem.....	52
3.3.2	Benders Decomposition Algorithm Procedure	54
3.4	Numerical Results.....	55
3.4.1	IEEE 37-node Distribution Network	55
3.4.2	IEEE 123-node Distribution Network	70
3.5	Summary.....	72
Chapter 4 Optimal Voltage Regulators Placement Considering Photovoltaic		
Accommodation Capability Enhancement.....		
4.1	Introduction.....	74

4.2	Problem Formulation	78
4.2.1	Mathematical Formulation based on Deterministic Mixed Integer Nonlinear Programming.....	79
4.2.2	Linearization Techniques for DMINLP Model.....	82
4.2.3	Stochastic Programming based Feasibility Checking Model	83
4.2.4	Final Formulation of Stochastic VR Placement Model	87
4.3	Decomposition Algorithm for Solving SMILP	88
4.3.1	Subprograms Formulation	88
4.3.2	Master Program Formulation.....	90
4.3.3	Solution Algorithm Process	91
4.4	Numerical Results.....	91
4.4.1	Performance of Computational Efficiency	93
4.4.2	Performance of Optimal VR Placement	94
4.4.3	Comparison with Deterministic Model	97
4.4.4	Tradeoff Curve between Daily PVAC and VR Planning Cost.....	99
4.4.5	Impact of VR Installation Number on PVAC Enhancement	100
4.5	Summary.....	100
Chapter 5	Conclusions and Future Works	103
5.1	Conclusions.....	103
5.2	Future Works.....	105
References	108

List of Figures

Fig. 1-1 Renewable generation capacity by energy source in 2018 [4]	2
Fig. 1-2 Renewable capacity growth form 2014-2018 [4].....	2
Fig. 1-3 Renewable generation capacity at the regional level in 2018[4].....	3
Fig. 2-1 Simple diagram of a TCSC device	23
Fig. 2-2 Simplified model of the transmission line with a TCSC device installed	23
Fig. 2-3 Modified IEEE 57-bus test system	30
Fig. 2-4 Representative wind-load scenarios with their probabilities.....	30
Fig. 2-5 Maximum mismatches of residue value E1	32
Fig. 2-6 Maximum mismatches of residue value E2	32
Fig. 2-7 Maximum mismatches of residue value E3	32
Fig. 2-8 Comparison of total power loss given the expected wind-load scenario	34
Fig. 2-9 Maximum apparent power of all transmission lines given the expected load-wind output	35
Fig. 2-10 Maximum apparent power of all transmission lines given the critical scenario of load-wind output.....	35
Fig. 2-11 Comparison of transmission line security in five representative scenarios under the deterministic model.....	36
Fig. 2-12 Comparison of transmission line security in five representative scenarios under the stochastic model.....	36
Fig. 2-13 Impact of wind power penetration level on maximum apparent power flow	38
Fig. 2-14 Impact of wind power penetration level on transmission line capacity margin	38

Fig. 3-1 Diagram of the two-stage stochastic framework	46
Fig. 3-2 The radial distribution network	47
Fig. 3-3 IEEE 37-node test system.....	56
Fig. 3-4 PV output factor for daily PV generations	56
Fig. 3-5 Load factor for daily load consumptions.....	57
Fig. 3-6 Performance of convergence	58
Fig. 3-7 PV hosting capacity with and without SVC installation	61
Fig. 3-8 Comparison on daily voltage profiles	61
Fig. 3-9 Daily voltage profiles of node 30 in scenario 7 with and without SVC installation.....	62
Fig. 3-10 Daily voltage deviations of node 30 in scenario 7 with and without SVC installation.....	63
Fig. 3-11 Daily voltage profiles on node 4 in scenario 26 with and without SVC installation.....	63
Fig. 3-12 Daily voltage deviations on node 4 in scenario 26 with and without SVC installation.....	64
Fig. 3-13 Daily voltage profiles on node 15 in scenario 54 with and without SVC installation.....	64
Fig. 3-14 Daily voltage deviations on node 15 in scenario 54 with and without SVC installation.....	65
Fig. 3-15 Daily voltage profiles on node 23 in scenario 81 with and without SVC installation.....	65
Fig. 3-16 Daily voltage deviations on node 23 in scenario 81 with and without SVC installation.....	66
Fig. 3-17 Daily voltage profiles obtained from the deterministic scheme under the	

critical scenario	67
Fig. 3-18 Daily voltage profiles obtained from the stochastic scheme under the critical scenario	67
Fig. 3-19 Tradeoff curve between PV hosting capacity and SVC planning cost.....	68
Fig. 3-20 Impact of SVC installation capacity on PV hosting capacity (with same installation number)	69
Fig. 3-21 Impact of SVC installation number on PV hosting capacity (with same installation capacity: 0.05p.u.)	70
Fig. 3-22 The modified IEEE 123-node test system	71
Fig. 3-23 Daily voltage profiles of the modified 123-node distribution system under the critical scenario	72
Fig. 4-1 One distribution branch diagram with a voltage regulator.....	82
Fig. 4-2 Decision-making process of the proposed VR placement problem	84
Fig. 4-3 Two-stage stochastic framework of the proposed voltage regulator placement problem	85
Fig. 4-4 IEEE 33-node test distribution system	91
Fig. 4-5 Load factor.....	92
Fig. 4-6 Solar energy output factor	92
Fig. 4-7 Evolution of Benders decomposition algorithm.....	93
Fig. 4-8 Comparison on daily PVAC	95
Fig. 4-9 Comparison on voltage magnitude.....	95
Fig. 4-10 Comparison of maximum apparent power in scenario 17.....	96
Fig. 4-11 Comparison of maximum apparent power in scenario 55	96
Fig. 4-12 Voltage profile of the deterministic model under the critical scenario.....	98
Fig. 4-13 Voltage profile of the stochastic model under the critical scenario	98

Fig. 4-14 Optimal tradeoff curve between the daily PVAC and VR planning cost ...99

Fig. 4-15 Impact of VR installation number on PVAC 100

List of Tables

Table 2-1 TCSC devices planning results of the stochastic model and deterministic model.....	33
Table 2-2 Total costs of investment and power loss using the stochastic model and deterministic model.....	34
Table 3-1 Comparison of the computation time under two methods.....	58
Table 3-2 PV hosting capacity of candidate locations in the 37-node test system.....	58
Table 3-3 SVC planning decisions in the 37-node test system.....	58
Table 3-4 Comparison on different candidate nodes for PV energy connection (The underlined numbers indicate the different candidate nodes with Case A).....	59
Table 3-5 PV hosting capacity value of candidate locations in the 123-node system.....	71
Table 3-6 SVC planning decisions in the 123-node system.....	71
Table 4-1 Comparison of computation time by two methods.....	93
Table 4-2 The result of the daily PVAC in the 33-node test system.....	94
Table 4-3 The result of VR placement in the 33-node test system.....	94

List of Abbreviations

ADN	Active distribution network
CB	Capacity bank
CPUC	California Public Utilities Commission
DNO	Distribution network operator
EPRI	Electric Power Research Institute
ESS	Energy storage system
FACTS	Flexible AC transmission systems
GA	Genetic algorithm
KD	Kantorovich Distance
LFB	Line flow based
LV	Low voltage
MILP	Mixed integer linear programming
MINLP	Mixed integer nonlinear programming
OPF	Optimal power flow
OTLC	On load tap changer
PSO	Particle swarm optimization
PV	Photovoltaic
PVAC	Photovoltaic accommodation capability
RHC	Renewable hosting capacity
RO	Robust optimization
SVC	Static var compensator
TCSC	Thyristor-controlled series capacitor
VR	Voltage regulator

Chapter 1 Introduction

1.1 Background

In recent years, the installation of renewable generators has been increased rapidly in power systems worldwide due to increased environmental awareness and fast development of advanced renewable generation technologies, e.g. distributed photovoltaic (PV) generators and wind turbines [1-3]. According to a recent report [4], the global capacity of renewable generation has reached 2351 GW by the end of 2018, and it is estimated to rise by about 4000 GW in the next decade. The increase rate of renewable power capacity in 2018 was the same as in 2017, 7.9% (171 GW). PV energy capacity increased mostly, which was 24% (94 GW), followed by wind power capacity with an increase of 10% (49 GW), as shown in Fig. 1-1 and Fig. 1-2. Besides, Fig. 1-3 shows the detailed information of renewable generation capacity at the regional level. By the end of 2018, 61% of new renewable generation capacity was installed in Asia, resulting in 1024 GW (44%) of renewable energy capacity. Europe and North America expanded 24 GW (4.6%) and 19 GW (5.4%) of renewable resources, respectively. Renewable energy capacity growth in Africa was the same as in 2017, with an increase of 3.6 GW (+8.4%). In addition, thanks to the decreasing investment cost of renewable generators and hortative government policies introduced by many countries, distributed renewable generators become popular among end-use customers [5-7]. For example, due to favorable policies made by the California Public Utilities Commission (CPUC), more than 230,000 houses in California have installed rooftop PV panels since 2014 [8]. Besides, other countries like Australia, Canada,

Germany and Denmark have also carried out attractive subsidy schemes to encourage the customers to install distributed renewable generators [9].

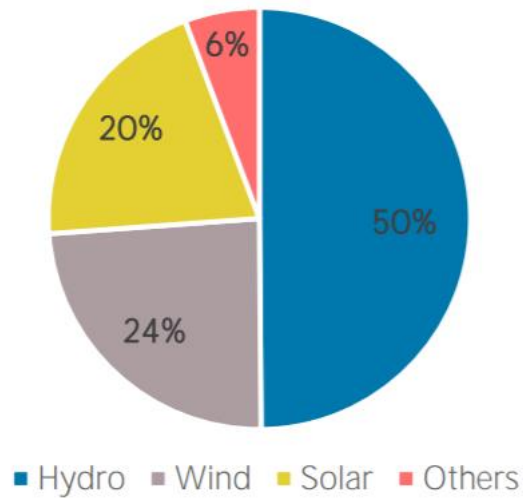


Fig. 1-1 Renewable generation capacity by energy source in 2018 [4]

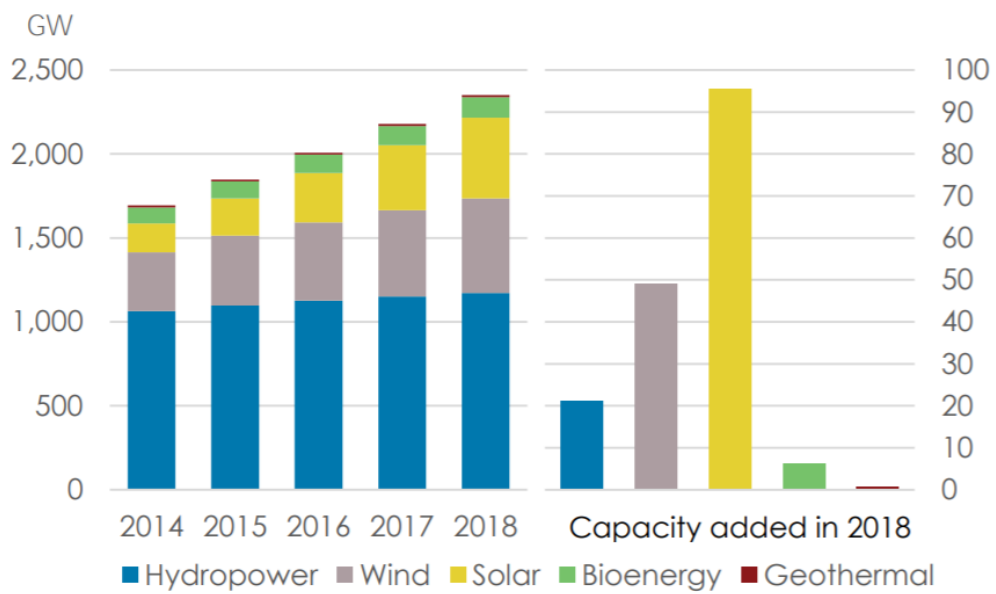


Fig. 1-2 Renewable capacity growth form 2014-2018 [4]

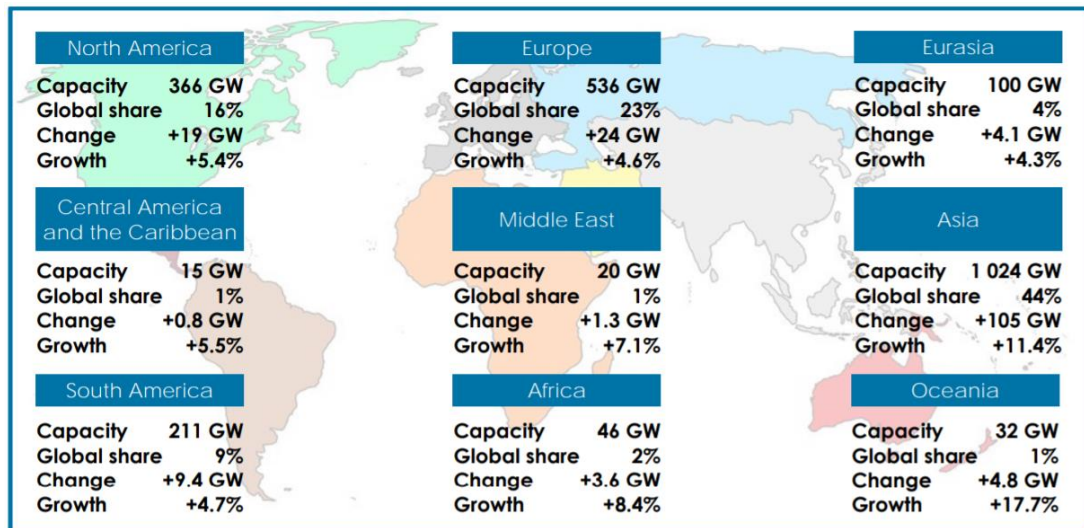


Fig. 1-3 Renewable generation capacity at the regional level in 2018[4]

With the widespread installation of renewable generators, many economic and environmental benefits can be obtained [10-13]. Firstly, renewable energy can not only reduce greenhouse gas emission but also reduce air pollution. This is because renewable energy can relieve energy dependence on fossil fuels, leading to a positive effect on the natural environment. Secondly, compared with traditional generation expansion, the installation of renewable generators has the advantages of lower operation cost and shorter construction time. Thirdly, renewable energy systems have the potentials to provide ancillary services to the power systems, such as voltage regulation and contingency reserves, thus supporting the reliability and resilience of power systems. However, with the rapid growth of renewable energy integration, the stochastic renewable energy output presents significant uncertainties to the power systems, including but are not limited to line congestion, increased active power loss and large voltage deviation [14-16].

In order to handle the negative effects caused by renewable energy integration in the transmission networks, installing flexible AC transmission

systems (FACTS) devices in the transmission systems is an effective option. The FACTS comprises a group of power electronic devices which is able to control one or more parameters of the power systems [17]. Many potential benefits can be obtained from FACTS controllers, such as the power quality improvement, power transfer capability enhancement, power flow control, transient and dynamic stability improvement, damping of power system oscillations, better voltage regulation, flexible operation and control of the system, secure loading of the transmission lines close to their thermal limits, prevention of cascading outages, etc. [18-20]. Due to the rapid development of power electronics technology, optimal FACTS devices installation becomes a promising way to enhance the operational capacity of the existing power system. Besides, FACTS devices placement has two main advantages, including installation flexibility and economic efficiency [21]. Therefore, compared with transmission system expansion, investing FACTS devices is economically preferable by transmission network planners. Thyristor controlled series capacitor (TCSC) [22] is one of the most useful FACTS devices since it can be inserted into the transmission lines to improve the system loadability, increase the power transmission capacity, improve the transient stability, reduce transmission loss and suppress the network low frequency oscillation by adjusting the transmission line impedances [23, 24]. In order to acquire these benefits, the optimal locations and sizes of TCSC devices should be optimally determined [25, 26].

High renewable energy integration in the distribution networks will pose significant challenges to the power system operation, e.g. overvoltage and overload of certain distribution lines [27-29]. In this regard, it is important to

continuously evaluate and improve the renewable hosting capacity (RHC) of the distribution networks before PV generators deployment or during actual operation. RHC is defined by Electric Power Research Institute (EPRI) as “the amount of renewable generation that can be accommodated without adversely impacting quality or reliability under existing control configurations and without requiring infrastructure upgrades” [30]. RHC can be affected by two main factors [31-33]. The first one is related to the configuration of distribution networks, including voltage control approach, system topology, load consumption, thermal limits and weather conditions. The second one is about the characteristics of renewable generators, such as renewable generator type, control functions, manufacture technology, installation locations and generation efficiency.

1.2 Purpose of the Thesis

This thesis intends to hedge against the negative impacts introduced by high renewable energy integration in transmission networks by optimally planning FACTS devices, and evaluate and enhance RHC to safeguard distribution system operation by developing efficient approaches. Therefore, the purpose of the thesis can be summarized to two aspects: the first one is to address negative issues caused by large-scale renewable energy integration in transmission networks and the second one is to enable the distribution networks to securely improve its capability of accommodating more renewable generations.

Firstly, this thesis proposes a novel FACTS device planning framework considering uncertainties of wind energy output and load demand in

transmission networks. Flexible FACTS device investment in transmission networks can be another alternative to address the aforementioned negative impacts and enhance the operational capacity of the existing transmission network. Among the most useful FACTS devices, TCSC is selected to be optimally deployed to increase the loadability of the existing transmission network. To handle the issues caused by wind power penetration in the transmission network, a two-stage stochastic planning model is proposed. With optimal planning of TCSC devices, several goals can be achieved, which includes maximizing the use of existing transmission facilities, reducing the active power loss cost and improving the loadability of transmission networks.

Secondly, this thesis proposes a novel stochastic programming based static var compensator (SVC) location-allocation framework in the distribution networks. It aims at enhancing PV hosting capacity to safeguard distribution network operation. PV hosting capacity plays an important role in identifying the capability of accommodating PV generations without operational constraints violations. Uncertainties including PV energy output and load consumption should be considered since these uncertainties may affect the optimal solutions. After solving this SVC planning model, a tradeoff relationship between PV hosting capacity and SVC planning cost can be obtained. After optimal SVC installation, significant PV hosting capacity enhancement can be achieved. This means that the distribution network can accommodate more PV power generators, which can bring economic and environmental benefits such as reduction of greenhouse gas emission and energy cost.

Thirdly, this thesis improves the daily PV accommodation capability (PVAC) of distribution networks via optimal voltage regulator (VR) allocation. The concept of PV accommodation capability is proposed to describe the amount of PV generation that can be reliably accommodated at a certain node of a distribution network within a certain time period. The PVAC dynamically varies according to operation conditions, such as time-varying demand and PV generation. Optimal VR placement is another alternative to tackle the aforementioned negative influences though providing continuous voltage regulation. Two criteria are introduced to maintain the safety and reliability of the distribution network operation, i.e., voltage variation and distribution line capacity. A stochastic feasibility check model is proposed to guarantee the security of distribution networks for any considered operation scenarios.

1.3 Primary Contributions

To achieve the objectives of the research, the main contributions achieved in this thesis are summarized as follows,

- 1) In this thesis, the classical copula theory is used to sample uncertainties of wind generation and load demand in transmission networks, where the temporal interdependence between wind energy output and load is taken into account. Especially, the inverse transform method is used to model these two uncertainties. Previous works usually use Monte Carlo simulation method to generate scenarios. In comparison, this method has been widely applied to the generation of forecasted operational scenarios for renewable production, which can better resemble reality.

- 2) The stochastic programming based framework is proposed for TCSC planning model considering uncertainties in the transmission networks. This planning model is formulated to a two-stage model where the first stage determines the TCSC location-allocation decisions and the second stage is to minimize the expected system operation cost under different wind-load scenarios. The proposed TCSC planning model is originally formulated a mixed integer nonlinear programming (MINLP), then a linearization technique and an approximation method are utilized to transform this MINLP into a mixed integer linear programming (MILP). Numerical results demonstrate that the performance of the proposed stochastic scheme is better than that of the traditional deterministic scheme.
- 3) The PV hosting capacity is innovatively modeled as a decision variable in the optimization text. Empirically, PV hosting capacity is difficult to be evaluated and it is generally assessed by using simulation-based approaches. In this thesis, the PV hosting capacity is incorporated into the objective function of optimal SVC planning problem by using sum weighted method. Therefore, the tradeoff between the PV hosting capacity and the SVC planning cost can be obtained, which is enforceable for practical application.
- 4) VR has the potential to improve the hourly PVAC of distribution networks since it can handle the overvoltage issue caused by PV energy integration through its continuous voltage regulation, which is not well studied in the existing works. To fill this research gap, a novel two-stage framework is proposed to investigate the extent of the potential benefits from optimal VR placement as an option to improve the PVAC. The hourly PVAC is

modeled as a continuous variable which is formulated in the objective function. Two criteria are introduced to maintain the safety and reliability of the distribution network operation, i.e., voltage variation and distribution line capacity. Moreover, a stochastic programming based feasibility checking model is established to ensure that the distribution network always remains secure operation under different uncertainty scenarios. Considering the widespread application of VR in power systems, this thesis has practical significance.

- 5) Time-coupling constraints across the time periods and numerous uncertainty scenarios result in an intractable two-stage stochastic planning problem. To reduce the computation burden, an efficient solution approach based on Benders decomposition is developed to solve this two-stage problem. Specifically, the two-stage problem can be decomposed into a master problem and multiple subproblems corresponding to all time periods in all scenarios. Furthermore, stochastic Benders cuts are built to link the master problem with the subproblems. To the best knowledge, this is the first study to employ the Benders decomposition algorithm to solve the two-stage planning problem for PV hosting capacity improvement by far.

1.4 Thesis Layout

The remainder of the thesis is organized as follows,

Chapter 2 proposes a two-stage stochastic programming based optimal TCSC location-allocation model. This planning model is formulated as a two-stage problem in which the planning variables of sites and sizes for TCSC

investment are optimized in the first stage and the power flow is optimized under representative wind-load scenarios in the second stage. The objective is to minimize the total costs of power system operation and TCSC investment, subject to linear power flow equations. This planning model is a MINLP, and then a general linear relaxation technique is employed to formulate this nonlinear model to a MILP. Wind-load scenarios are adopted to represent uncertainties, which are derived by using the classical copula theory where the temporal interdependence between wind power and load is considered. Finally, the modified IEEE 57-bus power system is used to verify the effectiveness of the proposed planning model.

Chapter 3 propose a two-stage stochastic optimal SVC location-allocation model. The primary goal of this planning model is to maximize the PV hosting capacity of the distribution networks by finding the optimal sites and sizes of SVC devices. In this two-stage problem, the PV hosting capacity and the corresponding SVC location-allocation decisions are determined in the first-stage before the uncertainty realization, while the SVC operation decisions are optimized under representative PV-load scenarios in the second stage. The numerous coupled constraints result in an intractable problem, so a solution approach is developed where the Benders decomposition algorithm is used to decompose the original problem into master problem and subproblems. Thus, commercial solvers can be used to directly solve this two-stage problem. The modified IEEE 37-node and 123-node distribution networks are employed to demonstrate the effectiveness of the proposed model and the solution method.

Chapter 4 proposes an optimal VR placement model for maximizing daily PVAC in distribution systems while maintaining the safety and reliability of

the distribution network operation. This allocation model is firstly formulated as a deterministic MINLP problem, subject to piecewise linearized DistFlow equations. The General linearization techniques are employed to transform the original nonlinear program into a MILP. The stochastic operation scenarios of PV outputs and load demand are considered, which creates a two-stage stochastic MILP problem. The first stage determines the hourly PVAC values and the corresponding VR allocation decisions while the second stage is related to the proposed stochastic feasibility checking model which is imposed to ensure that the distribution network operation always remains secure under different uncertainty scenarios. The decomposition-based method is adopted to reduce the computation complexity caused by a mass of time-coupled constraints. The modified 33-node distribution system is utilized to verify the effectiveness of the proposed model and solution method.

Eventually, Chapter 5 concludes this thesis and provides perspectives for future work.

Chapter 2 Stochastic Thyristor Controlled Series Capacitor Devices Planning with High Wind Energy Penetration

2.1 Introduction

In the last decade, wind energy capacity investments have been increased rapidly. Large-scale wind power integration of the power system brings about many economic interests and environmental benefits. However, due to the stochastic characteristic of wind power output, widespread wind farms installation poses some great challenges to the normal power system operation. Due to high wind power penetration, power flows on the transmission lines will be significantly changed and become inevitably fluctuating [14, 15]. This may result in some potential negative effects, including transmission line congestion, increased active power loss and large voltage deviation. In order to deal with these issues caused by uncertainties and risks associated with high wind power penetration, the traditional transmission system expansion can be taken into consideration [34]. However, the transmission system expansion, such as transmission line expansion and reconstruction, novel electrical plants installation and existing facilities upgrade, is usually investment-intensive and time-consuming and may cause environmental problems.

In this regard, flexible AC transmission systems (FACTS) devices investment in the transmission networks can be regarded as an attractive alternative to improve the operational capacity of the power system. FACTS devices are able to be inserted into the transmission lines or installed on the transmission buses to control the phase angle, consume or generate reactive

power, improve voltage files and adjust transmission line impedances [35]. Hence, many advantages can be obtained by planning FACTS devices, such as maximizing of the use of existing electrical facilities, deferring the transmission systems upgrade and improving the transmission loadability [36]. Besides, FACTS devices placement has two main characters, installation flexibility and economic efficiency, due to their short installation period and less capital cost. Therefore, compared with transmission system expansion options, investing FACTS devices is economically preferable for transmission network planners. Thyristor controlled series capacitor (TCSC) [22] is one of the most useful FACTS devices since it can be inserted into the transmission lines to improve the system loadability, increase the power transmission capacity, improve the transient stability, reduce transmission loss and suppress the network low frequency oscillation by adjusting the transmission line impedances [23, 24]. In order to acquire these benefits, the optimal locations and sizes of TCSC devices should be optimally determined [25, 26].

In the past, sensitivity analysis-based approaches are widely investigated for solving optimal TCSC allocation problems. The main idea of these kinds of approaches is to calculate sensitivity indexes for optimal TCSC locations. Ref. [37] proposes a method to obtain the sensitivity index by calculating indicators to find the most critical transmission lines for installing TCSC devices. Ref. [38] presents a TCSC placement model where the sensitivity index is introduced for seeking the optimal locations for TCSC devices allocation. However, the sensitivity analysis-based approaches have their own disadvantages on low computation efficiency since the computation runs repeatedly given different inputs [15]. In addition, these methods cannot

optimize the sitting and sizing of TCSC devices simultaneously [39]. Therefore, in order to handle the issues described above, heuristic algorithms are extensively developed for obtaining the optimal TCSC planning decisions. In Ref. [40], the genetic algorithm (GA) is employed to acquire the suitable sitting and sizing of TCSC devices in the transmission networks. Ref. [41] uses the particle swarm optimization (PSO) algorithm to optimize the position and parameter of TCSC devices considering the capital cost minimization and network loadability enhancement. Nevertheless, these heuristic algorithms have two main disadvantages, one is that the global optimality of the solutions cannot be guaranteed and the other one is that the huge computation burden may occur in the large-scale test systems. Another popular method is to formulate the TCSC planning problem as a mixed-integer linear programming (MILP), which can be directly solved by some commercial solvers. As the TCSC devices are inserted into the transmission lines, the line parameters are transformed to the decision variables, resulting in the mixed integer nonlinear programming (MINLP). Due to the great computation complex in solving MINLP, reach efforts are paid to transform the MINLP the MILP via relaxation or approximation of the nonlinear terms. In Ref. [42], the MILP is formulated for TCSC location-allocation problems where the approximation method is adopted. In Ref. [42], the DC load flow model is utilized for neglecting the nonlinear power flow appearing in the TCSC planning problem. Ref. [43] uses a decomposition method to decompose the complicated MINLP based TCSC planning problem into some MILPs. Refs [44, 45] give more examples about MILP based approach for TCSC installation problems. Although these methods exhibit high computation efficiency in solving complex TCSC

investment problems, most researchers consider simply or even overlook the uncertainties of wind energy out and load consumption. Note that these uncertainties have a direct effect on TCSC planning results. With the increasing wind power integration, the existing TCSC location-allocation methodology may be not suitable.

In this chapter, a stochastic programming based TCSC location-allocation model considering the uncertainties in the transmission networks is proposed. This planning model is formulated to a two-stage model in which the first stage determines the TCSC location-allocation decisions and the second stage is to minimize the expected system operation cost under different wind-load scenarios given the first-stage results. To present the uncertainties of wind energy output and load demand, the scenario approach is adopted to describe these uncertainties with the form of several daily wind-load scenarios. Subject to line flow-based equations, optimal locations and sizes of TCSC devices can be obtained by minimizing the sum of power loss cost and TCSC planning cost. The classical copula theory is used to develop these scenarios where the temporal interdependence between wind energy output and load demand is considered. The proposed TCSC planning model is originally formulated a MINLP, then a linearization technique and an approximation method are utilized to transform this MINLP into a MILP. Finally, the modified IEEE 57-bus transmission system is employed to verify the effectiveness of the proposed model.

The nomenclature of symbols used in this chapter is given as follows,

Sets and Indices

j/J	Index/set of transmission buses.
i/I	Index/set of child transmission buses.

n/N	Index/set of transmission lines.
$\delta(j)$	Set of child nodes of the bus j .
$\varphi(j)$	Set of transmission lines all connected to the bus j .
t/T	Index/set of time slots.
w/W	Index/set of net load scenarios.
k/K	Index/set of generation units.
Variables	
$P_{n,t,w}/Q_{n,t,w}$	Active/Reactive power flow through transmission line n at t, w .
$P_{k,t,w}^g/Q_{k,t,w}^g$	Active/Reactive power generation at k, t, w .
$L_{n,t,w}^P/L_{n,t,w}^Q$	Active/Reactive power loss of transmission line n at t, w .
$L_{n,t,w}^K$	Derived variable of transmission line n at t, w , as defined in (4c).
x_n^{TCSC}	Compensation rate of TCSC of transmission line n .
u_n	Binary decision variable flagging TCSC placement of line n .
$V_{j,t,w}$	Bus voltage at j, t, w .
Parameters	
c^P	Objective function coefficient associated with the electricity price (\$/kWh).
c^{TCSC}	Objective function coefficient associated with the amortized cost price of installed TCSC (\$/day).
F, F^{LOSS}, F^{INV}	Total cost, power loss cost, and investment cost.
N_b, N_l	The total number of busbars, lines.
p^w	Probability of scenario w .
B_n^i	The element of bus-line incidence matrix, 1 when bus i is the sending bus of line n , -1 when bus j is the receiving bus of line n , 0 otherwise.
B_n^m	The element of modified bus-line incidence matrix.
B_j^q	The element of the diagonal matrix associated with reactive power compensation devices of bus j .

B_k^g	The element of the coefficient matrix of $P_{k,t,w}^g$ and $Q_{k,t,w}^g$.
R_n/X_n	Resistance/Reactance of transmission line n .
$P_{j,t,w}^d/Q_{j,t,w}^d$	Active/Reactive net load at j, t, w .
P_n^{min}/P_n^{max}	Lower/Upper bound of active power flow through transmission line n .
Q_n^{min}/Q_n^{max}	Lower/Upper bound of reactive power flow through transmission line n .
$P_k^{g,min}/P_k^{g,max}$	Lower/Upper bound of active power generation of generator unit k .
$Q_k^{g,min}/Q_k^{g,max}$	Lower/Upper bound of reactive power generation of generator unit k .
$R_k^{P,min}/R_k^{P,max}$	Active power generator ramp down/up limitation of generator unit k .
$R_k^{Q,min}/R_k^{Q,max}$	Reactive power generator ramp down/up limitation of generator unit k .
$L_n^{P,min}/L_n^{P,max}$	Lower/Upper bound of active power loss of transmission line n .
$L_n^{Q,min}/L_n^{Q,max}$	Lower/Upper bound of reactive power loss of transmission line n .
$L_n^{K,min}/L_n^{K,max}$	Lower/Upper bound of the derived variable of transmission line n .
V_j^{min}/V_j^{max}	Lower/Upper bound of bus voltage of bus j .
$V_j^{d,min}/V_j^{d,max}$	Lower/Upper bound of bus voltage deviation of bus j .
$x_n^{TCSC,min}/x_n^{TCSC,max}$	Lower/Upper bound of TCSC compensation rate, 20% to 80% of line n (p.u.).
TL_n	Thermal limits of the transmission line n .
N_{TCSC}^{max}	Maximum allowed TCSC installation number.

2.2 Uncertainties Consideration in Transmission Networks

2.2.1 Uncertainties Modeling

In this TCSC planning model, time-varying wind energy output and uncertain load demand are taken into consideration. The wind power generation is highly related to the wind speed which can be modeled by Weibull distribution [46] and load demand can be considered as the normal distribution in the long-term run [47]. On the bus j within time period t , the Weibull distribution of active wind energy generation is $Y_{j,t}^p \sim W(\lambda_{j,t}, k_{j,t})$, where $\lambda_{j,t}$ and $k_{j,t}$ are scale and shape parameters, respectively, and the normal distribution of active load demand is $X_{j,t}^p \sim N(\mu_{j,t}, \sigma_{j,t}^2)$, where $\mu_{j,t}$ and $\sigma_{j,t}$ are the mean value and variance, respectively. Besides, the active net load on the bus with both load demand and wind energy integration can be expressed as $P_{j,t}^d = X_{j,t}^p - Y_{j,t}^p$. Therefore, the active net load is generally regarded as a negative load demand because the active wind power output can reduce the overall active load on the same bus. The additive results of these two independent variables can be derived by a well-studied approach based on Gram-Charlier Series expressions and cumulants [23]. In the same way, the reactive net load $Q_{j,t}^d$ can be obtained.

2.2.2 Scenarios Generation and Reduction

As described in the previous subsection, the marginal distribution of the net load within each time period can be acquired. Then the Gaussian copula theory [48] is adopted to generate numerous scenarios with consideration of temporal dependence. Specifically, in the first step, a multivariate Gaussian random number generator is used to address uncertainty realizations W set

$\{\chi_{j,t_1}^w, \chi_{j,t_2}^w, \dots, \chi_{j,t_{24}}^w\}$, $w = 1, \dots, W$ with a chosen covariance structure. In some realistic cases [48], the covariance structure is issued by an exponential covariance function considering the empirical correlations, given as follows,

$$\text{cov}(X_{j,t_1}, X_{j,t_2}) = \exp\left(-\frac{|t_1 - t_2|}{\gamma}\right), \forall j \in J, 0 \leq t_1, t_2 \leq T \quad (2.1)$$

where $X_{j,t}$ represents the Gaussian random variable on the bus j within time period t , and γ denotes the range parameter which controls the strength of the random variable correlation among the set of lead time periods. In this thesis, an empirical value $\gamma = 10$ is utilized [48].

In the second step, inverse probit function Φ and the marginal distribution $F_{j,t}$ are used to transform these multivariate Gaussian realizations $\chi_{j,t}^w$ into trajectories $y_{j,t}$ of net load at j, t .

$$y_{j,t} = F_{j,t}^{-1}(\Phi(\chi_{j,t}^w)), \forall j \in J, \forall t \in T, \forall w \in W \quad (2.2)$$

To reduce the computational complexity of the proposed TCSC planning problem, as the inputs of the second stage of the TCSC planning model, the representative scenarios should be distinguished from the obtained numerous ones. With this consideration, a scenario selection approach based on backward-reduction algorithm [49] is adopted since this approach can select scenarios with corresponding probabilities which can show the importance of the associated scenarios. After scenario reduction, the remains of probabilistic scenarios are fed into the stochastic TCSC planning model.

2.3 Mathematical Formulation of the Stochastic TCSC

Planning Model

2.3.1 Line Flow based Model

Generally, the AC model [50] and the DC model [51] can be used to model complex power flow in power systems. The AC model has advantages in describing the electrical networks precisely. However, most operation or planning optimization problems based on AC model are formulated as nonlinear and nonconvex problems, which are difficult to be solved due to heavy computational burden and only local optimal solutions can be found. Hence, the AC model is not applicable in large-scale systems with consideration of uncertainties. As for the DC model, it is widely used for power system planning and operation problems, which can be efficiently solved by some commercial solvers. It should be noted that the DC model ignores the reactive power balance, tap dependence and power loss, so this model is not suitable for the proposed optimal TCSC planning model. By contrast, line flow based (LFB) model [52] is based on voltage magnitudes and line power flow, which directly relate to TCSC device variables. Besides, the LFB model has a good performance on computation efficiency [53]. In this regard, the advantageous LFB model is adopted to model the power flow in the proposed TCSC planning model, given as follows,

$$\sum_{n \in \varphi(j)} B_n^i P_n = \sum_{k \in \delta(j)} B_k^g P_k^g - P_j^d - \sum_{n \in \varphi(j)} B_n^m \frac{(P_n^2 + Q_n^2)}{V_j^2} R_n, \forall j \in J \quad (2.3)$$

$$\sum_{n \in \varphi(j)} B_n^i Q_n = \sum_{k \in \delta(j)} B_k^g Q_k^g - Q_j^d + B_j^q U_j - \sum_{n \in \varphi(j)} B_n^m \frac{(P_n^2 + Q_n^2)}{V_j^2} X_n, \forall j \in J \quad (2.4)$$

$$U_j = U_i + 2 \sum_{n \in \varphi(j)} (R_n P_n + X_n Q_n) + \sum_{n \in \varphi(j)} \frac{(P_n^2 + Q_n^2)}{V_j^2} (R_n^2 + X_n^2), \forall j \in J, \forall i \in \delta(j) \quad (2.5)$$

$$U_j = V_j^2, U_i = V_i^2 \quad (2.6)$$

where (2.3) defines the active power injection P_n which is summarized by the active generation output, active load demand and the total active power loss of transmission lines connected to this bus; (2.4) defines the reactive power injection Q_n which is summarized by the reactive generation output, reactive load demand, reactive power compensation (related with voltage) and the total reactive power loss of transmission lines connected to this bus; and (2.5) describes the voltage transmit along the transmission line, the voltage drop is determined by the quadratic active/reactive power, quadratic voltage (2.6) and line conductance. B_n^i , B_k^g , B_j^q , B_n^m are bus incidence matrixes for P_n , P_k^g and Q_k^g , V_j^2 , active and reactive power loss, respectively. Detailed expressions of these incidence matrixes can be found in [54].

As shown in (2.3)-(2.6), the LFB model is nonlinear so it is difficult to be solved. In order to linear the LFB model, two continuous variables L_n^P and L_n^Q are introduced to denote the active power loss term and the reactive power loss term appearing in (2.3) and (2.4), respectively. Besides, the variable L_n^K is introduced to describe the nonlinear term in (2.5). The expressions of these three auxiliaries are as follows,

$$L_n^P = \frac{(P_n^2 + Q_n^2)}{U_j} R_n, \forall j \in J, \forall n \in \varphi(j) \quad (2.7)$$

$$L_n^Q = \frac{(P_n^2 + Q_n^2)}{U_j} X_n, \forall j \in J, \forall n \in \varphi(j) \quad (2.8)$$

$$L_n^K = \frac{(P_n^2 + Q_n^2)}{U_j} (R_n^2 + X_n^2), \forall j \in J, \forall n \in \varphi(j) \quad (2.9)$$

After substituting $L_{n,t,w}^P$, $L_{n,t,w}^Q$ and $L_{n,t,w}^K$ for active power loss, reactive power loss and nonlinear term in (2.5), respectively, the linear LFB model in the time period t of the scenario w is written as follows,

$$\sum_{n \in \varphi(j)} B_n^i P_{n,t,w} = \sum_{k \in \delta(j)} B_k^g P_{k,t,w}^g - P_{j,t,w}^d - \sum_{n \in \varphi(j)} B_n^m L_n^P, \quad (2.10)$$

$$\forall n \in N, \forall t \in T, \forall w \in W$$

$$\sum_{n \in \varphi(j)} B_n^i Q_{n,t,w} = \sum_{k \in \delta(j)} B_k^g Q_{k,t,w}^g - Q_{j,t,w}^d + B_j^q U_{j,t,w} - \sum_{n \in \varphi(j)} B_n^m L_n^Q, \quad (2.11)$$

$$\forall n \in N, \forall t \in T, \forall w \in W$$

$$U_{j,t,w} = U_{i,t,w} + 2 \sum_{n \in \varphi(j)} (R_n P_{n,t,w} + X_n Q_{n,t,w}) + \sum_{n \in \varphi(j)} L_{n,t,w}^K, \quad (2.12)$$

$$\forall n \in N, \forall t \in T, \forall w \in W$$

The following two equations (2.13) and (2.14) define the relationships among $L_{n,t,w}^P$, $L_{n,t,w}^Q$ and $L_{n,t,w}^K$.

$$X_n L_{n,t,w}^P - R_n L_{n,t,w}^Q = 0, \forall n \in N, \forall t \in T, \forall w \in W \quad (2.13)$$

$$R_n L_{n,t,w}^P + X_n L_{n,t,w}^Q - L_{n,t,w}^K = 0, \forall n \in N, \forall t \in T, \forall w \in W \quad (2.14)$$

2.3.2 TCSC Installed LFB Model

From the perspective of the long term, the TCSC device can be ideally regarded as a variant capacitive reactance compensator consisting of a series capacitor and a shunt thyristor-controlled reactor [23], as shown in Fig. 2-1. For the steady-state power flow study, after a TCSC device installation on a transmission line, the reactive $-jx_n^{TCSC}$ is offered by the TCSC, as shown in Fig. 2-2.

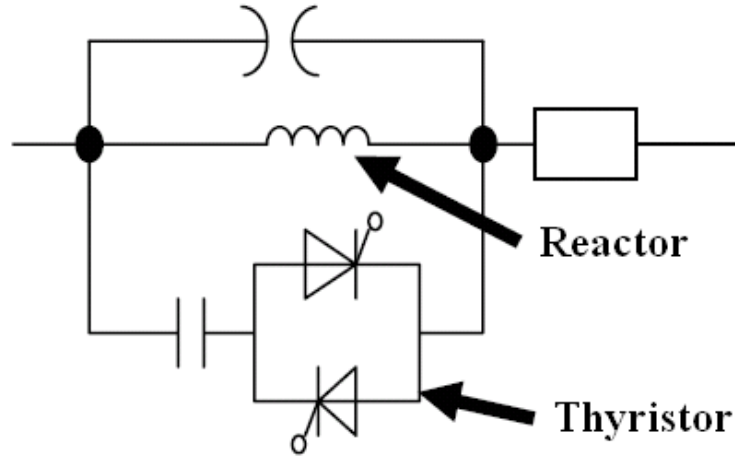


Fig. 2-1 Simple diagram of a TCSC device

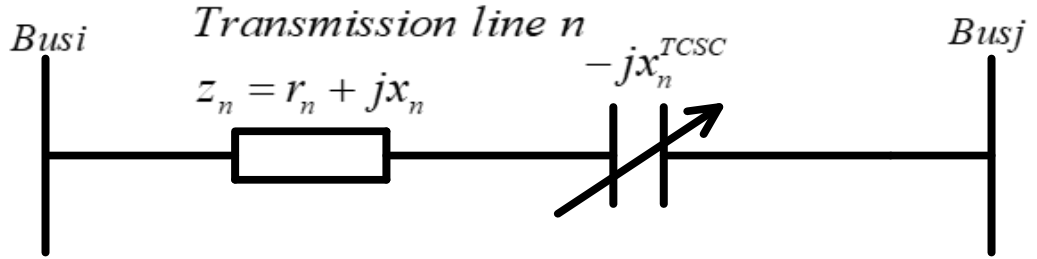


Fig. 2-2 Simplified model of the transmission line with a TCSC device installed

Therefore, the original transmission line reactance X_n is changed to the new reactance X'_n , described as follows,

$$X'_n = X_n + x_n^{TCSC} u_n, \forall n \in N \quad (2.15)$$

where the binary variable u_n denotes the TCSC device placement status on the transmission line n , $u_n = 1$ denoting the TCSC device installation, otherwise, $u_n = 0$.

Then X_n should be replaced by X'_n in the LFB model so that the LFB-TCSC model is derived from (2.10)-(2.14), given as follows,

$$\sum_{n \in \varphi(j)} B_n^i P_{n,t,w} = \sum_{k \in \delta(j)} B_k^g P_{k,t,w}^g - P_{j,t,w}^d - \sum_{n \in \varphi(j)} B_n^m L_n^P, \quad (2.16)$$

$$\forall n \in N, \forall t \in T, \forall w \in W$$

$$\sum_{n \in \varphi(j)} B_n^i Q_{n,t,w} = \sum_{k \in \delta(j)} B_k^g Q_{k,t,w}^g - Q_{j,t,w}^d + B_j^q U_{j,t,w} - \sum_{n \in \varphi(j)} B_n^m L_n^Q, \quad (2.17)$$

$$\forall n \in N, \forall t \in T, \forall w \in W$$

$$U_{j,t,w} = U_{i,t,w} + 2 \sum_{n \in \varphi(j)} (R_n P_{n,t,w} + X_n Q_{n,t,w} + x_{n,t,w}^{TCSC} u_n Q_{n,t,w}) + \sum_{n \in \varphi(j)} L_{n,t,w}^K, \quad (2.18)$$

$$\forall n \in N, \forall t \in T, \forall w \in W$$

$$X_n L_{n,t,w}^P + x_{n,t,w}^{TCSC} u_n L_{n,t,w}^P - R_n L_{n,t,w}^Q = 0, \quad (2.19)$$

$$\forall n \in N, \forall t \in T, \forall w \in W$$

$$R_n L_{n,t,w}^P + X_n L_{n,t,w}^Q + x_{n,t,w}^{TCSC} u_n L_{n,t,w}^Q - L_{n,t,w}^K = 0, \quad (2.20)$$

$$\forall n \in N, \forall t \in T, \forall w \in W$$

2.3.3 Linearization of LFB-TCSC Model

Note that the LFB-TCSC model (2.16)-(2.20) is formulated as a MINLP including cubic terms $x_n^{TCSC} u_n Q_{n,t,w}$, $x_n^{TCSC} u_n L_{n,t,w}^P$, and $x_n^{TCSC} u_n L_{n,t,w}^Q$. This MINLP problem cannot be directly solved by commercial solvers since it is nonconvex. To linear these three cubic terms, a two-step transformation is developed. In the first step, an auxiliary continuous variable z_n^{TCSC} is introduced for representing $z_n^{TCSC} = x_n^{TCSC} u_n$. Then the LFB-TCSC model is reformulated as follows,

$$\sum_{n \in \varphi(j)} B_n^i P_{n,t,w} = \sum_{k \in \delta(j)} B_k^g P_{k,t,w}^g - P_{j,t,w}^d - \sum_{n \in \varphi(j)} B_n^m L_n^P, \quad (2.21)$$

$$\forall n \in N, \forall t \in T, \forall w \in W$$

$$\sum_{n \in \varphi(j)} B_n^i Q_{n,t,w} = \sum_{k \in \delta(j)} B_k^g Q_{k,t,w}^g - Q_{j,t,w}^d + B_j^q U_{j,t,w} - \sum_{n \in \varphi(j)} B_n^m L_n^Q, \quad (2.22)$$

$$\forall n \in N, \forall t \in T, \forall w \in W$$

$$U_j = U_i + 2 \sum_{n \in \phi(j)} (R_n P_{n,t,w} + X_n Q_{n,t,w} + z_n^{TCSC} Q_{n,t,w}) + \sum_{n \in \phi(j)} L_{n,t,w}^K, \quad (2.23)$$

$$\forall n \in N, \forall t \in T, \forall w \in W$$

$$X_n L_{n,t,w}^P + z_n^{TCSC} L_{n,t,w}^P - R_n L_{n,t,w}^Q = 0, \forall n \in N, \forall t \in T, \forall w \in W \quad (2.24)$$

$$R_n L_{n,t,w}^P + X_n L_{n,t,w}^Q + z_n^{TCSC} L_{n,t,w}^Q - L_{n,t,w}^K = 0, \forall n \in N, \forall t \in T, \forall w \in W \quad (2.25)$$

Meanwhile, the following auxiliary constraints should be considered in the LFB-TCSC formulation to make the equation $z_n^{TCSC} = x_n^{TCSC} u_n$ workable,

$$-x_n^{TCSC, \max} u_n + z_n^{TCSC} \leq 0, \forall n \in N \quad (2.26)$$

$$x_n^{TCSC, \min} u_n - z_n^{TCSC} \leq 0, \forall n \in N \quad (2.27)$$

$$-x_n^{TCSC, \min} u_n + z_n^{TCSC} \leq x_n^{TCSC} - x_n^{TCSC, \min}, \forall n \in N \quad (2.28)$$

$$-x_n^{TCSC, \max} u_n + z_n^{TCSC} \leq -x_n^{TCSC} + x_n^{TCSC, \max}, \forall n \in N \quad (2.29)$$

In the second step, the bilinear terms $z_n^{TCSC} Q_{n,t,w}$, $z_n^{TCSC} L_{n,t,w}^P$ and $z_n^{TCSC} L_{n,t,w}^Q$ in (2.23)-(2.25) should be linearized. Here, an approximation method is utilized to transform three equality constraints (2.23)-(2.25) to six inequality constraints (2.30)-(2.35) where the reactive power flow $Q_{n,t,w}$, active power loss $L_{n,t,w}^P$ and reactive power loss $L_{n,t,w}^Q$ are replaced by their upper and lower bounds.

$$-U_j + U_i + 2 \sum_{n \in \phi(j)} (R_n P_{n,t,w} + X_n Q_{n,t,w} + z_n^{TCSC} Q_{n,t,w}^{\max}) + \sum_{n \in \phi(j)} L_{n,t,w}^K \leq 0, \quad (2.30)$$

$$\forall j \in J, \forall i \in \delta(j), \forall t \in T, \forall w \in W$$

$$U_j - U_i - 2 \sum_{n \in \phi(j)} (R_n P_{n,t,w} + X_n Q_{n,t,w} + z_n^{TCSC} Q_{n,t,w}^{\min}) - \sum_{n \in \phi(j)} L_{n,t,w}^K \leq 0, \quad (2.31)$$

$$\forall j \in J, \forall i \in \delta(j), \forall t \in T, \forall w \in W$$

$$X_n L_{n,t,w}^P + z_n^{TCSC} L_{n,t,w}^{P, \max} - R_n L_{n,t,w}^Q \leq 0, \forall n \in N, \forall t \in T, \forall w \in W \quad (2.32)$$

$$-X_n L_{n,t,w}^P - z_n^{TCSC} L_{n,t,w}^{P,\min} + R_n L_{n,t,w}^Q \leq 0, \forall n \in N, \forall t \in T, \forall w \in W \quad (2.33)$$

$$R_n L_{n,t,w}^P + X_n L_{n,t,w}^Q + z_n^{TCSC} L_{n,t,w}^{Q,\max} - L_{n,t,w} \leq 0, \forall n \in N, \forall t \in T, \forall w \in W \quad (2.34)$$

$$-R_n L_{n,t,w}^P - X_n L_{n,t,w}^Q - z_n^{TCSC} L_{n,t,w}^{Q,\min} + L_{n,t,w} \leq 0, \forall n \in N, \forall t \in T, \forall w \in W \quad (2.35)$$

2.3.4 Stochastic TCSC Planning Model

The primary goal of the stochastic programming based TCSC devices planning model is to obtain the optimal sitting and sizing of TCSC devices by minimizing the sum of TCSC investment cost and expected power loss cost under considered uncertainty scenarios. This planning model is formulated to a two-stage model in which the first stage determines the TCSC location-allocation decisions and the second stage is to minimize the expected system operation cost under different wind-load scenarios given the first-stage results.

The objective of this planning problem is given as follows,

$$\text{Minimize } F_{\theta} \quad (2.36)$$

$$F = F^{LOSS} + F^{INV} \quad (2.37)$$

$$F^{LOSS} = \sum_{w \in W} p^w \sum_{t \in T} \sum_{n \in N} c^p L_{n,t,w}^P \quad (2.38)$$

$$F^{INV} = \sum_{n \in N} c^{TCSC} z_n^{TCSC} \quad (2.39)$$

where the variable set $\theta = \{P_{n,t,w}, Q_{n,t,w}, U_{j,t,w}, P_{k,t,w}^g, Q_{k,t,w}^g, P_{n,t,w}^l, Q_{n,t,w}^l, L_{n,t,w}, x_n^{TCSC}, u_n, z_n^{TCSC}\}$. The objective (2.36) comprises two terms, the first one F^{LOSS} (2.38) is to minimize the expected power loss cost overall operation scenarios and the second one F^{INV} (2.39) is to minimize the TCSC investment cost. It should be noted that c^{TCSC} representing the daily TCSC capital cost is presented in an amortized way [43] so as to match the daily power loss cost F^{LOSS} .

The constraints of this planning problem are given as follows,

(1) Power flow balance constraints: (2.21)-(2.35).

(2) Power flow limits

$$P_n^{\min} \leq P_{n,t,w} \leq P_n^{\max}, \forall n \in N, \forall t \in T, \forall w \in W \quad (2.40)$$

$$Q_n^{\min} \leq Q_{n,t,w} \leq Q_n^{\max}, \forall n \in N, \forall t \in T, \forall w \in W \quad (2.41)$$

$$P_n^{\max 2} + Q_n^{\max 2} \leq TL_n, \forall n \in N \quad (2.42)$$

where the active and reactive power flow limits are defined in (2.40) and (2.41), respectively. (2.42) considers the transmission line capacity limit to ensure no thermal limit violations.

(3) Bus voltage limits

$$U_j^{\min} \leq U_{j,t,w} \leq U_j^{\max}, \forall j \in J, \forall t \in T, \forall w \in W \quad (2.43)$$

$$U_j^{\min} = V_j^{\min 2}, U_j^{\max} = V_j^{\max 2} \quad (2.44)$$

(4) Conventional generator limits

$$P_k^{g,\min} \leq P_{k,t,w}^g \leq P_k^{g,\max}, \forall k \in K, \forall t \in T, \forall w \in W \quad (2.45)$$

$$Q_k^{g,\min} \leq Q_{k,t,w}^g \leq Q_k^{g,\max}, \forall k \in K, \forall t \in T, \forall w \in W \quad (2.46)$$

$$R_k^{P,\text{down}} \leq P_{k,t,w}^g - P_{k,t-1,w}^g \leq R_k^{P,\text{up}}, \forall k \in K, \forall t \in T, \forall w \in W \quad (2.47)$$

$$R_k^{Q,\text{down}} \leq Q_{k,t,w}^g - Q_{k,t-1,w}^g \leq R_k^{Q,\text{up}}, \forall k \in K, \forall t \in T, \forall w \in W \quad (2.48)$$

where active and reactive generation limits are described in (2.45) and (2.46), respectively. Active and reactive generation ramp limits are given in (2.47) and (2.48), respectively.

(5) Power loss limits

$$L_n^{P,\min} \leq L_{n,t,w}^P \leq L_n^{P,\max}, \forall n \in N, \forall t \in T, \forall w \in W \quad (2.49)$$

$$L_n^{Q,\min} \leq L_{n,t,w}^Q \leq L_n^{Q,\max}, \forall n \in N, \forall t \in T, \forall w \in W \quad (2.50)$$

$$L_n^{K,\min} \leq L_{n,T,W}^K \leq L_n^{K,\max}, \forall n \in N, \forall t \in T, \forall w \in W \quad (2.51)$$

where the constraints (2.49)-(2.51) give the bounds of active power loss $L_{n,t,w}^P$, reactive power loss $L_{n,t,w}^Q$ and derived variable $L_{n,t,w}^K$. It should be noted that the upper and lower bounds of active and reactive power loss are quite important to the linearization of this planning model. Consider that one objective of the proposed TCSC planning model is to reduce power loss cost, in this regard, upper bounds of active and reactive power loss are assumed to be equal to the maximum active and reactive power loss obtained from the optimal power flow (OPF) before TCSC installation. Therefore, the power loss after TCSC placement is ensured to be less than that without TCSC installation. Besides, the lower bounds of active and reactive power loss are both zero.

(6) TCSC device installation number limit

$$\sum_{n \in N} u_n \leq N_{TCSC}^{\max}, N_{TCSC}^{\max} = \{0, 1, 2, \dots, N_b\}, u_n \in \{0, 1\}, \forall n \in N \quad (2.52)$$

From the practical view, (2.52) is included to limit the maximum investment number of TCSC devices in transmission networks, where N_{TCSC}^{\max} is the maximum TCSC installation number which can be given by transmission network planners with practical considerations.

2.4 Numerical Results

In this section, a modified IEEE 57-bus transmission system is used to verify the effectiveness of the proposed TCSC planning model. The total active and reactive loads of this system are set as 1250.8 MW and 336.4 MVar

respectively. The test system comprises seven conventional generators, 42 load buses and 80 transmission lines. Other detailed parameters of this 57-bus test system can be referred to the MATPOWER [55]. Two wind farms are assumed to be connected to bus 8 and bus 36 of the test system, with each capacity at 200MVA, as depicted in Fig. 2-3. Besides, in this section, it is assumed that the operation and maintenance cost of these two wind farms are zero. Ten thousand wind-load scenarios are generated and ten representative ones are selected. As the inputs of the proposed stochastic programming-based planning model, these ten wind-load scenarios can reduce the computational complexity with acceptable optimal solutions. Fig. 2-4 shows the representative active wind-load (net load) scenarios with their probabilities. The widely-used commercial solver YALMIP [56] based on the platform CPLEX [57] is adopted to directly solve the two-stage stochastic TCSC device planning problem. Besides, in this section, the deterministic TCSC placement model is regarded as the benchmark. The deterministic model only considers one wind-load scenario where the wind energy output and load demand are set as their mean values, which is quite different from the proposed stochastic model.

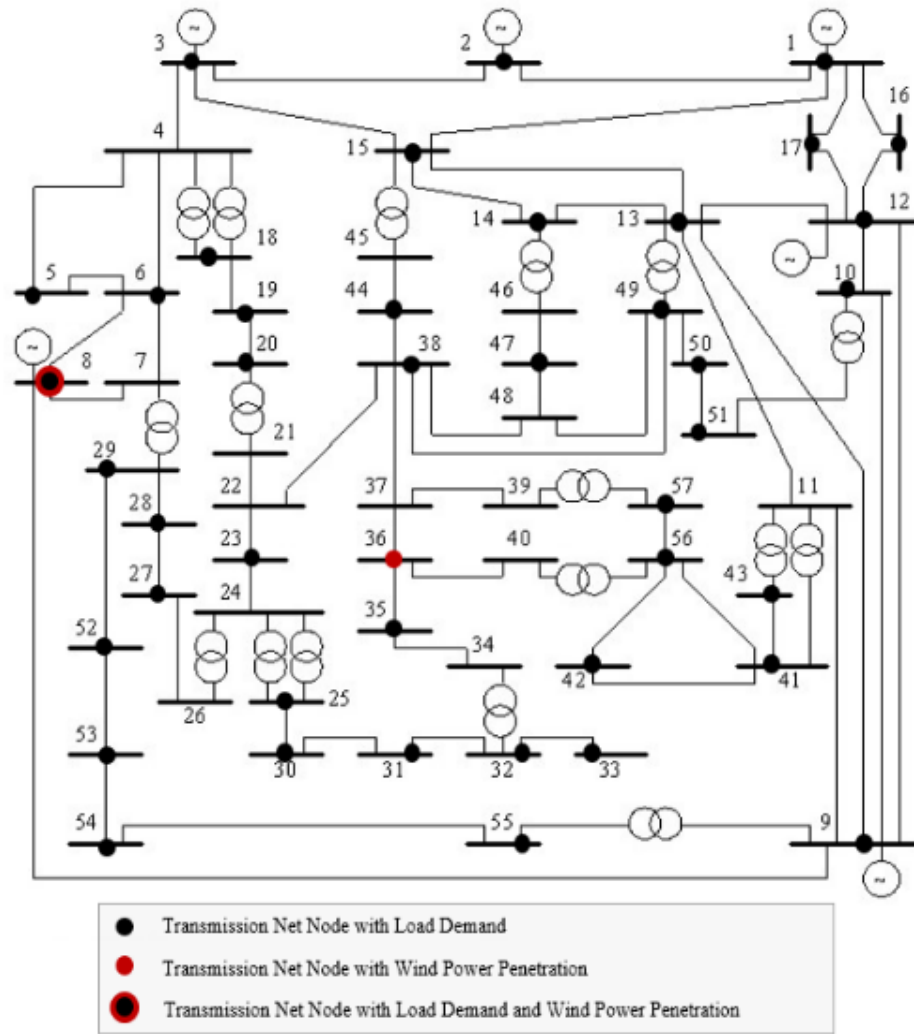


Fig. 2-3 Modified IEEE 57-bus test system

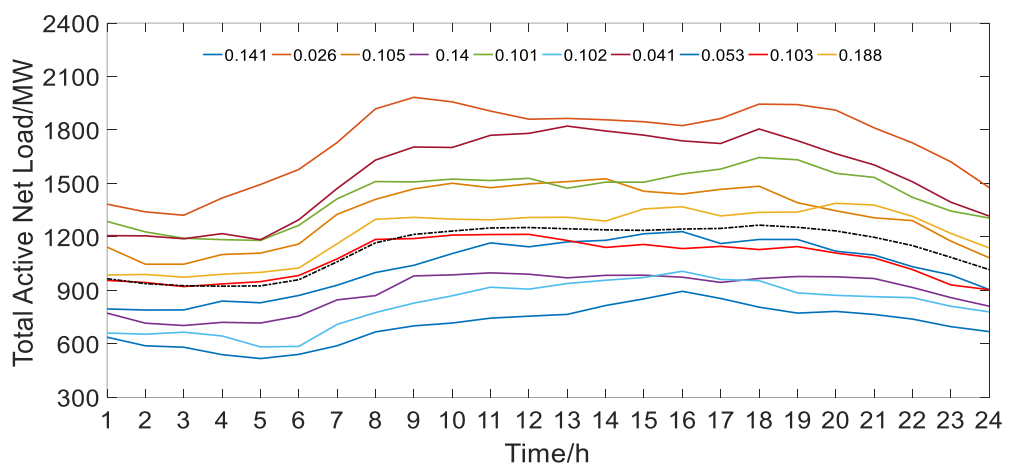


Fig. 2-4 Representative wind-load scenarios with their probabilities

2.4.1 The Approximation Approach Verification

In this chapter, six linear inequality constraints (2.30)-(2.35) are introduced to substitute for three original nonlinear equality constraints (2.23)-(2.25). However, the accuracy of this approximation approach needs to be concerned. To denote the mismatch values of equations (2.23)-(2.25), E_1 , E_2 and E_3 are defined as follows,

$$E_1 = V_j^2 - V_i^2 - 2 \sum_{n \in \phi(j)} (R_n P_{n,t,w} + X_n Q_{n,t,w} + z_n^{TCSC} Q_{n,t,w}) - \sum_{n \in \phi(j)} L_{n,t,w}^K, \quad (2.53)$$

$$\forall j \in J, \forall i \in \delta(j), \forall t \in T, \forall w \in W$$

$$E_2 = X_n L_{n,t,w}^P + z_n^{TCSC} L_{n,t,w}^P - R_n L_{n,t,w}^Q, \quad (2.54)$$

$$\forall j \in J, \forall i \in \delta(j), \forall t \in T, \forall w \in W$$

$$E_3 = R_n L_{n,t,w}^P + X_n L_{n,t,w}^Q + z_n^{TCSC} L_{n,t,w}^Q - L_{n,t,w}^K, \quad (2.55)$$

$$\forall j \in J, \forall i \in \delta(j), \forall t \in T, \forall w \in W$$

To verify the accuracy of this approximation approach, a wind-load scenario with the maximum probability is utilized to calculate the values of E_1 , E_2 and E_3 . The maximum mismatch values of E_1 , E_2 and E_3 in all time periods are illustrated in Fig. 2-5, Fig. 2-6 and Fig. 2-7, respectively. As shown in these three figures, the maximum errors caused by approximation are quite small. Moreover, for the transmission line without TCSC devices placement, the approximation approach is not applied so the errors are zero. Hence, it can be concluded that this reasonable approximation approach has a minor effect on the optimal solutions. Considering that this approximation approach is able to linearize the nonlinear constraints containing quadratic terms so as to make the original problem become convex, these small errors are acceptable for a planning solution.

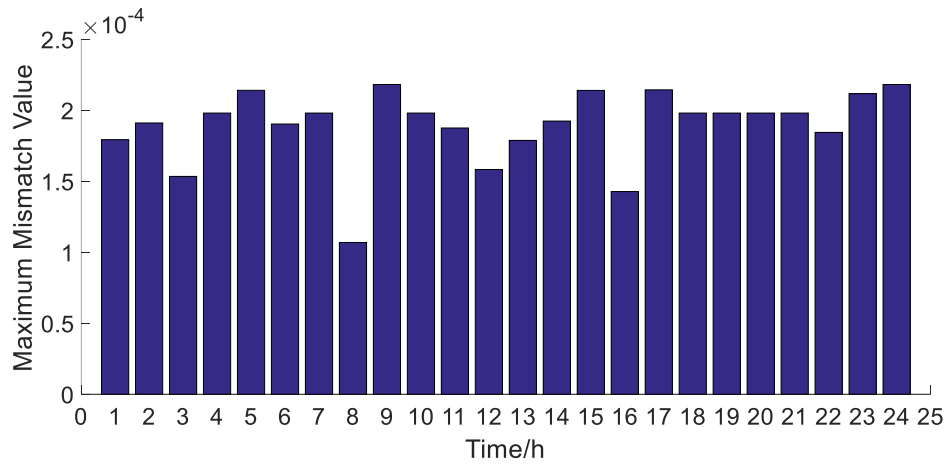


Fig. 2-5 Maximum mismatches of residue value E_1

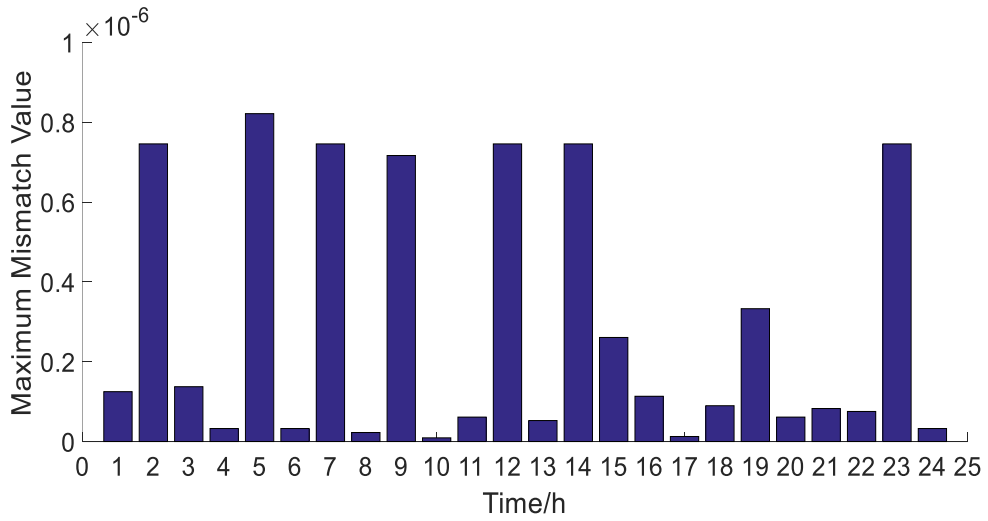


Fig. 2-6 Maximum mismatches of residue value E_2

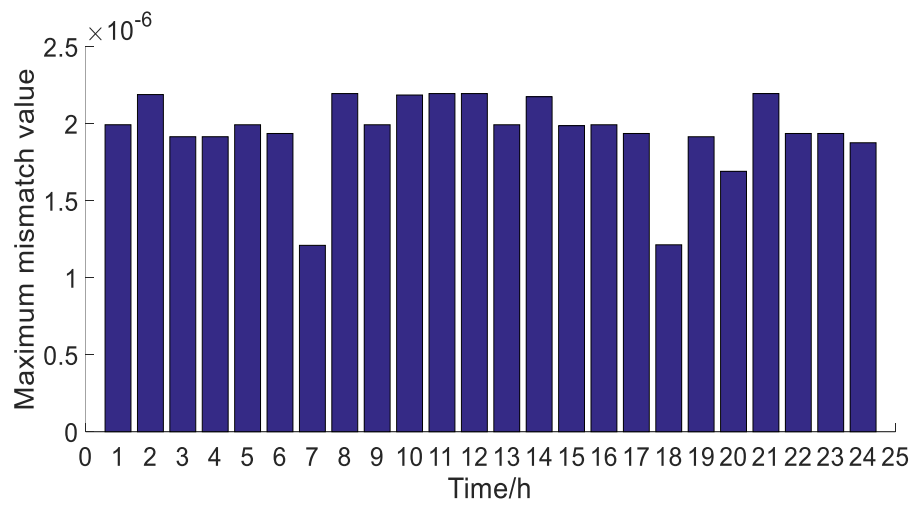


Fig. 2-7 Maximum mismatches of residue value E_3

2.4.2 TCSC Devices Location-allocation Results

The optimal location and allocation results of TCSC devices obtained by the deterministic model and the stochastic model are shown in Table 2-1. It can be observed from this table that the TCSC devices installation number and capacity of the stochastic model are both larger than those of the deterministic model. This is because uncertainties of wind energy output and load demand are taken into account in the stochastic model so more TCSC devices with larger capacity are installed in the transmission lines to achieve a good performance on all considered operational scenarios.

Table 2-1 TCSC devices planning results of the stochastic model and deterministic model

	Line from-to	Compensation value, p.u.	Original reactance, p.u.	Reactance after TCSC installation, p.u.	Installation Number
stochastic model	3-4	-0.0112	0.0366	0.0254	9
	4-6	-0.1184	0.148	0.0296	
	9-13	-0.1264	0.158	0.0316	
	13-15	-0.0277	0.0869	0.0592	
	1-17	-0.0864	0.108	0.0216	
	4-18	-0.2622	0.43	0.1678	
	24-26	-0.0292	0.0473	0.0181	
	56-42	-0.2832	0.354	0.0708	
	39-57	-0.853	1.355	0.502	
	deterministic model	4-6	-0.1184	0.148	
1-16		-0.0412	0.206	0.1648	
1-17		-0.0864	0.108	0.0216	
4-18		-0.2638	0.43	0.1662	
24-26		-0.0292	0.0473	0.0181	
15-45		-0.0412	0.1042	0.063	

2.4.3 Comparisons on Total cost

This subsection gives a comparison of total cost consisting of TCSC devices investment cost and system power loss cost. The corresponding costs of the stochastic model and the deterministic model under the expected wind-load scenario are listed in Table 2-2. It can be observed from this table that the total cost obtained by the stochastic model is lower than that of the deterministic model. In detail, the planning decisions of the stochastic model result in higher TCSC devices investment cost but lower power loss cost.

Table 2-2 Total costs of investment and power loss using the stochastic model and deterministic model

	Stochastic model	Deterministic approach
F^{LOSS} , \$/day	6.332×10^3	6.751×10^3
F^{INV} , \$/day	1.345×10^3	3.274×10^2
F , \$/day	7.677×10^3	7.078×10^3

2.4.4 Comparison of Power Loss

This subsection compares the performance of the stochastic model and the deterministic model on decreasing transmission system power loss. Under the expected wind-load scenario, the comparison of total power loss is shown in Fig. 2-8. It can be seen from this figure that the stochastic model is able to produce less power loss. Since the wind power output and load demand are both uncertain and time-varying, the proposed stochastic TCSC planning model is more suitable and realistic than the traditional deterministic model.

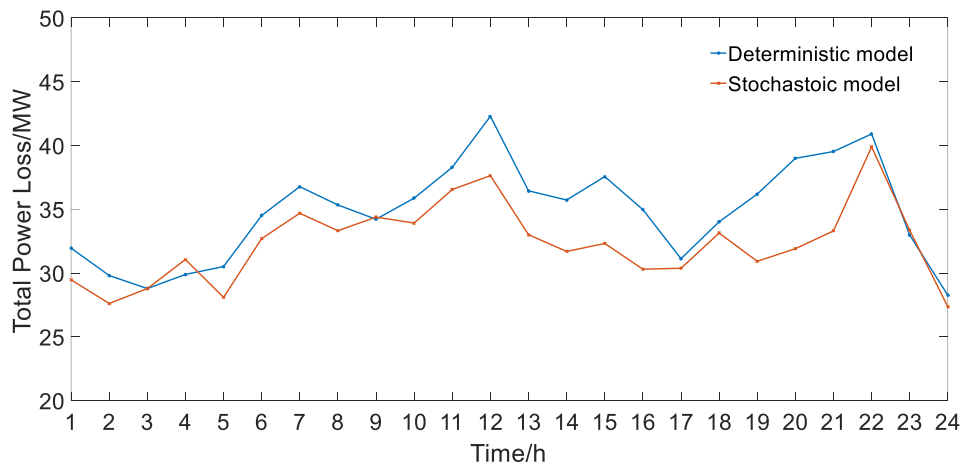


Fig. 2-8 Comparison of total power loss given the expected wind-load scenario

2.4.5 Comparison of Transmission Line Capacity Margin

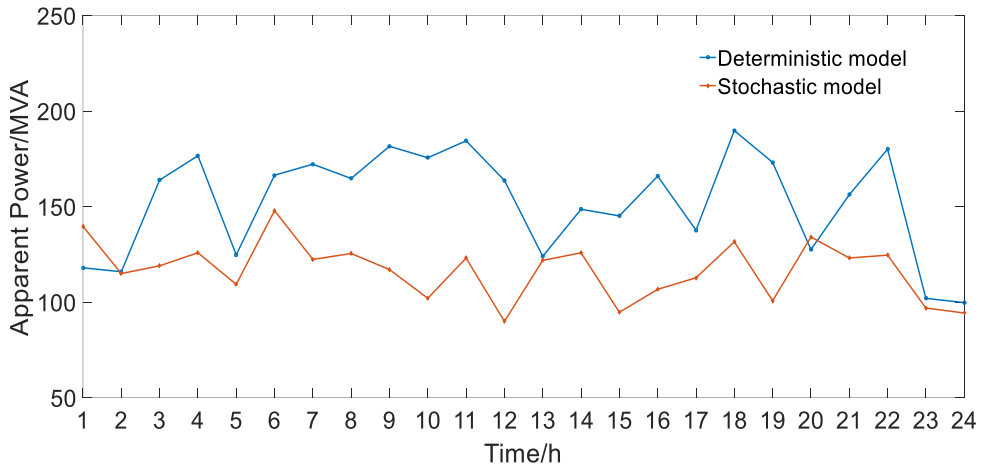


Fig. 2-9 Maximum apparent power of all transmission lines given the expected load-wind output

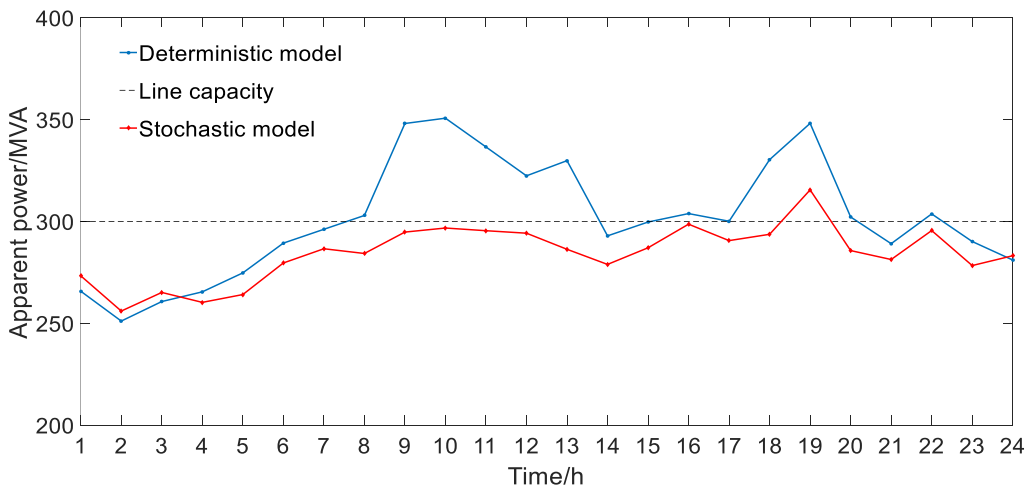


Fig. 2-10 Maximum apparent power of all transmission lines given the critical scenario of load-wind output

In this subsection, the performance of the stochastic model and the deterministic model on transmission line capacity margin improvement is compared. The transmission line capacity margin is defined as the difference value between the transmission line capacity and apparent power flow along this line. The transmission line capacity of this modified 57-bus test system is

assumed to be 300 MVA [55]. Fig. 2-9 depicts the apparent power of these two models under the expected wind-load scenario. As seen in this figure, the apparent power flow on the transmission lines with stochastic TCSC planning is smaller and less fluctuant than that of deterministic TCSC planning.

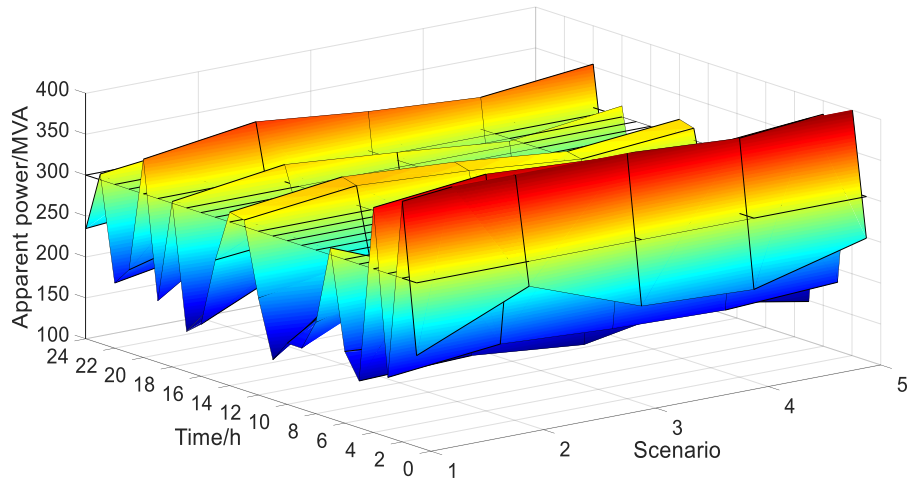


Fig. 2-11 Comparison of transmission line security in five representative scenarios under the deterministic model

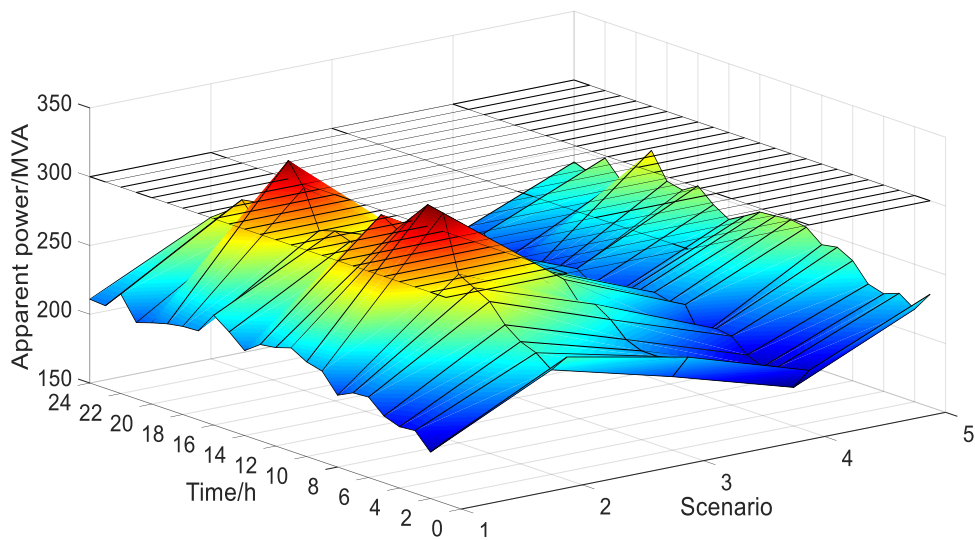


Fig. 2-12 Comparison of transmission line security in five representative scenarios under the stochastic model

To further demonstrate the effectiveness of the stochastic model, the critical wind-load scenario (high wind energy output and low load consumption) is employed. Fig. 2-10 shows the apparent power of these two models under the critical wind-load scenario. It can be seen from this figure that the apparent power of the stochastic model is quite smaller than that of the deterministic model. Besides, the apparent power of the deterministic model exceeds the transmission line capacity within some time periods, which may cause line congestion. Moreover, Fig. 2-11 and Fig. 2-12 illustrate the maximum apparent power of the deterministic model and stochastic model given all ten representative scenarios as shown in Fig. 2-4, respectively. The overload can be seen in the deterministic model while it is alleviated by the stochastic model. The reason is that the stochastic model considers uncertain wind power output and load consumption, so the transmission line congestion can be relieved since more TCSC devices with large capacity are installed. Hence, after stochastic TCSC placement, the marginal security of transmission line is higher.

2.4.6 Sensitivity Analysis on Wind Power Penetration

In this subsection, sensitivity analysis is conducted to investigate the impact of increased wind power penetration level on marginal security of transmission line capacity with stochastic and deterministic TCSC placement. Fig. 2-13 shows the maximum apparent power flow along all transmission lines with stochastic and deterministic TCSC placement under different wind energy integration levels. Then the corresponding marginal security of the transmission line capacity is shown in Fig. 2-14. As depicted in these two

figures, the apparent power flow rises with increasing wind energy integration level and the marginal security of transmission lines is accordingly decreases. However, the stochastic model shows better performance on maintaining the marginal security of the transmission lines. After stochastic TCSC planning, the transmission network is more robust so as to be capable of dealing with uncertainties of wind power output and load consumption.

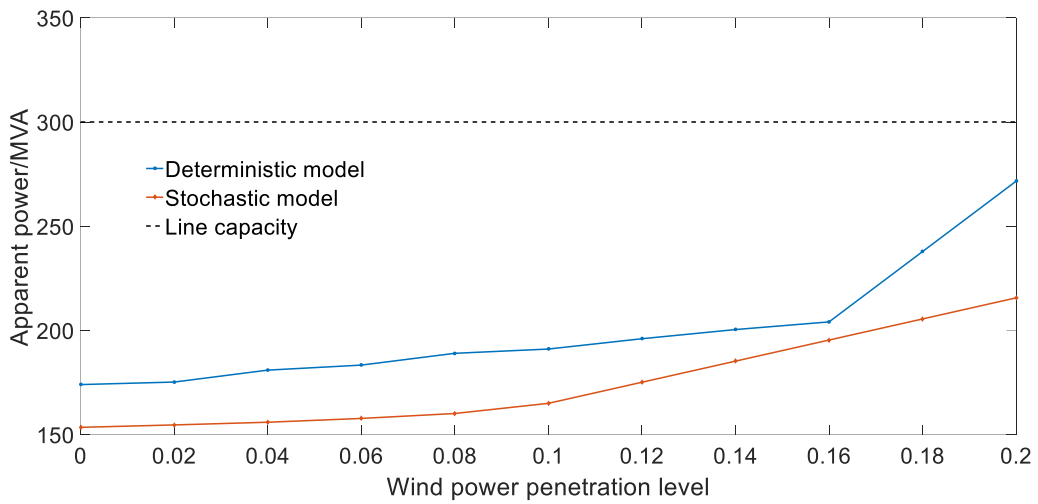


Fig. 2-13 Impact of wind power penetration level on maximum apparent power flow

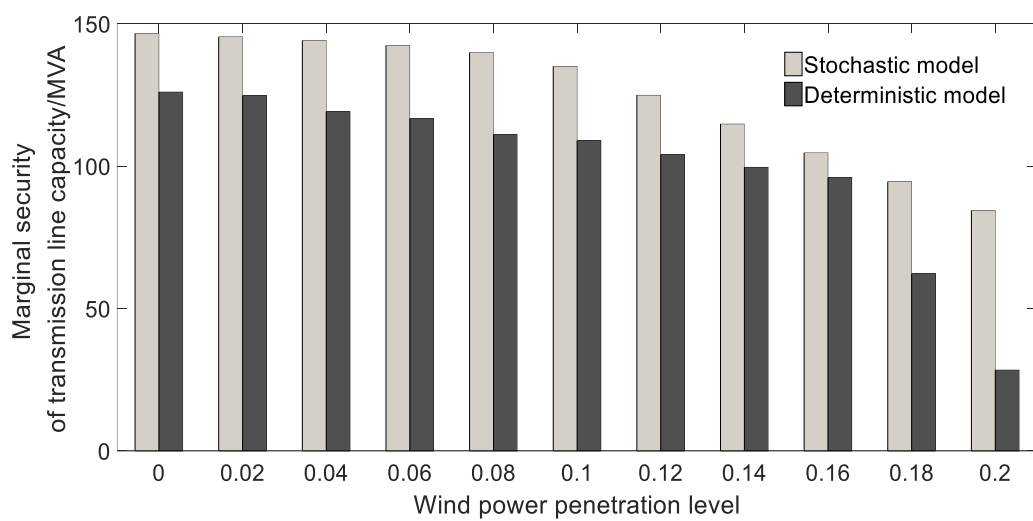


Fig. 2-14 Impact of wind power penetration level on transmission line capacity margin

2.5 Summary

In this chapter, a stochastic programming based TCSC location-allocation model considering the uncertainties of the transmission networks is proposed. This planning model is formulated to a two-stage model in which the first stage determines the TCSC location-allocation decisions and the second stage is to minimize the expected system operation cost under different wind-load scenarios given the first-stage results. To present the uncertainties of wind energy output and load demand, the scenario approach is adopted to describe these uncertainties with the form of daily wind-load scenarios. Subject to line flow-based equations, optimal locations and sizes of TCSC devices can be obtained by minimizing the sum of power loss cost and TCSC planning cost. The classical copula theory is used to develop these scenarios where the temporal interdependence between wind energy output and load demand is considered. The proposed TCSC planning model is originally formulated a MINLP, then a linearization technique and an approximation method are utilized to transform this MINLP into a MILP. Finally, the modified IEEE 57-bus transmission system is utilized to verify the effectiveness of the proposed model. The numerical results indicate that the proposed stochastic model outperforms the traditional deterministic model in reducing active power loss cost and enhancing the marginal security of transmission lines.

Chapter 3 Improving Photovoltaic Hosting Capacity via Optimal Location-allocation of Static Var Compensators

3.1 Introduction

Chapter 2 intends to hedge against the negative impacts introduced by wind energy integration in transmission networks by optimally planning thyristors controlled series capacitors (TCSCs). However, this chapter tries to eliminate the negative effects caused by photovoltaic (PV) energy penetration in distribution networks by enhancing the PV hosting capacity via efficient planning approaches. Distributed PV generation technology is becoming a promising solution to the global energy crisis and environmental pollution problem [58, 59]. However, with the rapid growth of PV power systems in the distribution networks, the stochastic PV energy output presents significant uncertainties to the distribution networks. Besides, the over-proliferation of PV generators brings various negative effects to normal operating conditions of distribution networks [27-29]. These negative impacts limit the ability of the distribution networks to accommodate more PV generation. Thus, PV curtailment frequently happens [60], resulting in PV energy waste. In this regard, the distribution network planners need a reasonable and effective method to improve PV hosting capacity in distribution networks meanwhile ensure no violations of normal distribution system operation constraints, especially voltage magnitude violations and distribution line capacity violations.

PV hosting capacity is defined as the amount of PV production that can be accommodated by the distribution network without endangering the reliability

and security of the network operation [31-33]. Several methods have been proposed to improve PV energy penetration of distribution networks. Monte Carlo simulation-based analysis is used to assess the ability to hold PV generations in Ref. [61] and then an active distribution network (ADN) management approach is presented to increase PV hosting capacity by optimally deploying control devices and smart inverters. Ref. [62] formulates a multi-objective optimization model to enhance the ability to hold wind energy in distribution networks and minimize costs of the purchased energy from the upstream network, which is an effective tool for distribution network operators (DNOs) to consider both technical and economic aspects of wind energy hosting capacity. In Ref. [63], to increase the PV hosting capacity of the low-voltage (LV) grid, a voltage droop control is presented to efficiently control the active medium-voltage to low-voltage transformers in the condition of high PV energy integration. Ref. [64] provides an approach in which a multi-objective and multi-period nonlinear programming optimization model is formulated where the demand response is used as to enhance the ability to hold PV generations and decrease the active power losses simultaneously. Ref. [65] presents a control approach based on the voltage sensitivity analysis to prevent overvoltage occurrence and increase the PV hosting capacity of LV grids by determining dynamic set points for distributed electrical energy storage systems (ESS) management. In Ref. [66], distributed generation hosting capacity is improved by modifying the operating parameters of existing components, including on load tap changer (OLTC) and static var compensators (SVCs). However, most of these existing works only focus on increasing PV energy penetration by using short-term operation strategies but

overlook the long-term effects arising from the planning perspective. This may limit renewable energy hosting capacity improvement. Since the PV power integration increases continuously, the distribution network planners need a considerate way to improve the ability of the grid to absorb PV generation. In this regard, this chapter maximizes the PV hosting capacity of distribution networks from the perspective of long-term planning.

Optimal SVC devices planning provides an outlook of enhancing the PV hosting capacity in distribution networks since SVC has the ability to regulate voltage magnitude and adjust power flow by consuming or generating reactive power. Capacity banks (CBs) are widely used in the distribution network since it has advantages on the low cost of installation and maintenance. Nevertheless, CB can only provide reactive power by the discontinuous adjustment which results in a low lifetime of CB components. By contrast, SVC can not only release reactive power but also absorb reactive power by continuous adjustment. Besides, SVC is capable of reacting sensitively in response to the nodal voltage variations. Therefore, SVC can be used to relieve the overvoltage issues caused by the high level of PV power integration, so optimal SVC devices planning results in a positive effect on PV hosting capacity enhancement. Classical studies related to SVC location-allocation problems regard the considerable potential of SVC planning on improving PV hosting capacity. Ref. [67] aims to improve the voltage profiles via optimal sitting and sizing of SVC and Ref. [68] focuses on improving the system load margin by finding SVC installation locations. Instead of improving the performance of voltage regulation and system loadability, the primary goal of this planning

model is to enhance the PV hosting capacity by optimally determining the SVC devices planning decisions.

When dealing with uncertainties, two typical approaches including stochastic programming [69] and robust optimization (RO) [70] are generally used for power system planning problems. In many cases, compared with the stochastic programming solutions, the solutions obtained by RO are usually over-conservative. This is because the worst-case scenarios are excessively considered in RO models but the occurrence probabilities of these scenarios are practically low. In General, stochastic programming is used to model operation or planning problems in electrical networks considering representative uncertainties scenarios, aiming at minimizing expected operation or planning cost in all considered scenarios subject to network constraints. Therefore, the stochastic programming solutions are less conservative than the RO solutions but more robust than the traditional deterministic optimization solutions. In this regard, stochastic programming is employed to model this planning problem.

In this chapter, a two-stage stochastic optimal SVC location-allocation model is proposed. The primary goal of this planning model is to maximize the PV hosting capacity of the distribution networks by finding the optimal sites and sizes of SVC devices. In this two-stage problem, the PV hosting capacity and the corresponding SVC location-allocation decisions are determined in the first-stage which is before the uncertainty realization, while the operational constraints are evaluated with given first-stage results under representative PV-load scenarios in the second stage. The numerous coupled constraints result in an intractable problem, so a solution approach is developed where the Benders

decomposition algorithm is used to decompose the original problem into master problem and subproblems. Thus, commercial solvers can be used to directly solve this two-stage problem. The modified IEEE 37-node and 123-node distribution networks are employed to demonstrate the effectiveness of the proposed model and the solution method. The major contributions are summarized in threefold as below,

1) The main contribution of this work is that it investigates the extent of the potential benefits from optimal SVC planning as an option to improve the PV hosting capacity of distribution networks. Considering the widespread application of SVC in power systems, this work has practical significance.

2) Simulation-based methods are widely adopted to assess PV hosting capacity but they are inapplicable in studying its improvement. Conversely, in this thesis, the PV hosting capacity is originally modeled as the decision variable and incorporate it into the objective function. Hence, a tradeoff between PV hosting capacity and SVC planning cost can be achieved.

3) The proposed two-stage stochastic optimal SVC location-allocation problem is practically intractable because coupled objective and constraints across the time periods and numerous uncertainty scenarios. In this regard, based on Benders decomposition, an efficient solution approach is developed to solve this two-stage problem so as to reduce computational complexity.

The nomenclature of symbols used in this chapter is given as follows,

Sets and Indices

i / N	Index/set of distribution node.
$m / N^{PV}(i)$	Index/set of candidate distribution node for PV generation installation.
t / T	Index/set of the time period.

s / S	Index/set of PV-load scenario.
Variables	
a_i^{SVC}	Binary decision variable flagging SVC installation status at the node i .
Q_i^{SVC}	SVC installation capacity at the node i .
q_{its}^{SVC}	Reactive power support of SVC at the node i in t, s .
P_{its} / Q_{its}	Active/Reactive power flow through the distribution line between node $i-1$ and node i in t, s .
V_{its}	Voltage magnitude at the node i in t, s .
E_m^{PV}	PV hosting capacity allocated to the node m .
Parameters	
C_F^{SVC}	The Objective coefficient associated with the fixed capital cost of SVC (\$).
C_V^{SVC}	The objective coefficient associated with the varying operation cost of SVC (\$/h).
w^{PV}	Weight factor of the PV hosting capacity.
w^{SVC}	Weight factor of the SVC planning cost (SVC investment cost and SVC operation cost).
p_s	The occurrence probability of the scenario s .
N_{inv}^{SVC}	Maximum SVC installation number.
ξ_{ts}^{PV}	PV output factor (ratio of PV hosting capacity) in the period t, s , $\xi_{ts}^{PV} \in [0,1]$

3.2 Formulation of SVC Planning Problem

3.2.1 Two-stage Stochastic Framework

Fig. 3-1 demonstrates the basic two-stage stochastic framework planning model. The first-stage variables comprise sitting and sizing of SVC devices and the PV hosting capacity values of candidate locations. These first-stage results are obtained before the uncertainty realizations, so they are named as

here-and-now decisions. The second-stage variables comprise the distribution network operation decisions within all time periods in all uncertainty scenarios with the given first-stage variables. These second-stage variables are optimized after the uncertainty realizations, named as *wait-and-see* decisions.

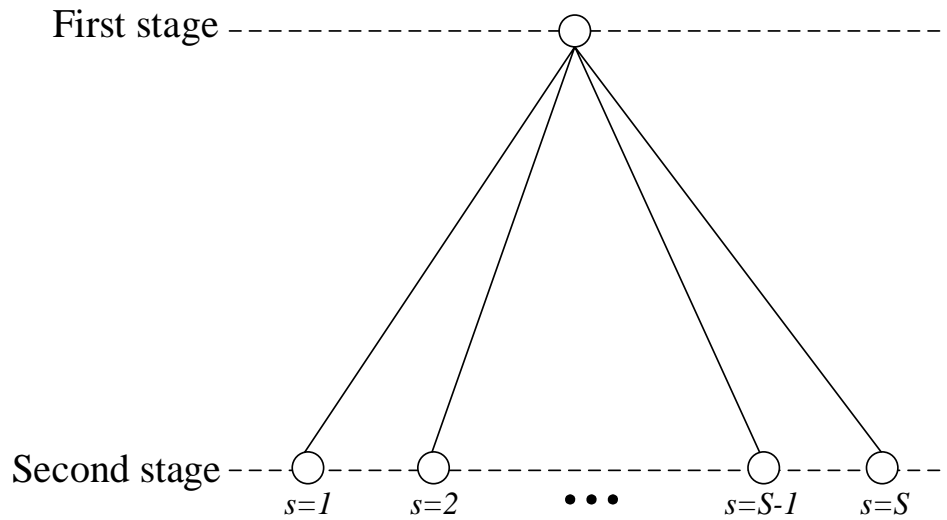


Fig. 3-1 Diagram of the two-stage stochastic framework

Uncertainties of PV energy output and load consumption of the distribution network are taken into account in the second stage of the proposed stochastic SVC planning model. Based on historical data collected from [71], daily uncertainty scenarios are used to represent uncertainties. In detail, ten thousand daily scenarios including five thousand PV energy output scenarios and five thousand load demand scenarios are gathered. To improve the computation efficiency, representative scenarios need to be selected from collected numerous scenarios. In this chapter, a scenario reduction approach based on Kantorovich Distance (KD) is utilized since this approach is able to select most potential scenarios associated with their probabilities which can have a direct effect on the optimal solutions. The detailed procedure of this scenario reduction method can be referred to [49].

3.2.2 Distribution Network Model

In this chapter, the widely-used DistFlow model [72, 73] is adopted to describe the power flow equations of a radial distribution network, as depicted in Fig. 3-2,

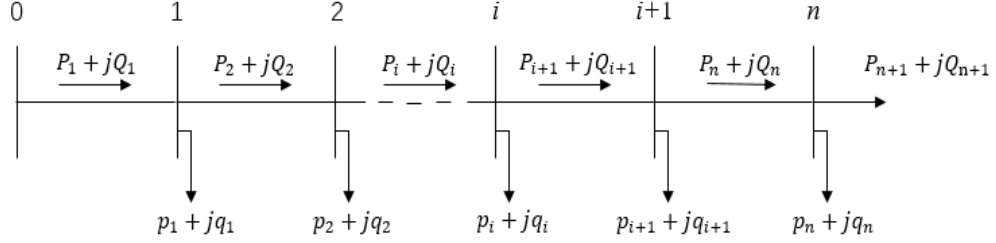


Fig. 3-2 The radial distribution network

The DistFlow equations are given as follows,

$$P_{i+1} = P_i - r_i \frac{P_i^2 + Q_i^2}{V_i^2} + p_i^g - p_i^d, \forall i \in N \quad (3.1)$$

$$Q_{i+1} = Q_i - x_i \frac{P_i^2 + Q_i^2}{V_i^2} + q_i^g - q_i^d, \forall i \in N \quad (3.2)$$

$$V_{i+1}^2 = V_i^2 - 2(r_{i+1}P_{i+1} + x_{i+1}Q_{i+1}) + (r_{i+1}^2 + x_{i+1}^2) \frac{P_{i+1}^2 + Q_{i+1}^2}{V_i^2}, \forall i \in N \quad (3.3)$$

where active and reactive power flow balance at each node of the distribution network are denoted in (3.1) and (3.2), respectively. (3.3) represents the voltage transmit along each distribution line connected to two adjacent nodes. To reduce the computation complexity, the original DistFlow model can be transformed into a linear one by ignoring the second-order terms P_i^2 , Q_i^2 and V_i^2 [74]. Refs. [72, 73] verifies the effectiveness of this linearized DistFlow model, which is given as follows,

$$P_{i+1} = P_i + p_i^g - p_i^d, \forall i \in N \quad (3.4)$$

$$Q_{i+1} = Q_i + q_i^g - q_i^d, \forall i \in N \quad (3.5)$$

$$V_{i+1} = V_i - \frac{r_{i+1}P_{i+1} + x_{i+1}Q_{i+1}}{V_0}, \forall i \in N \quad (3.6)$$

3.2.3 PV Hosting Capacity Improvement

As shown in the voltage transmit equation (3.6), the voltage increasement ΔV can be expressed as follows,

$$\Delta V = V_i - V_{i+1} = \frac{r_{i+1}P_{i+1} + x_{i+1}Q_{i+1}}{V_0} \quad (3.7)$$

According to (3.7), when the PV generation increases at the node i , the inverse active power flow P_{i+1} increases, resulting in voltage increasement ΔV increase. Therefore, the overvoltage problem may be caused. However, SVC is able to relieve the voltage rise by absorbing reactive power. Specifically, SVC is able to absorb reactive power so as to decrease reactive power flow Q_{i+1} , leading to the decrease of voltage increasement ΔV . In this regard, optimal SVC planning poses a positive effect on PV hosting capacity improvement.

3.2.4 Mathematical Formulation of the SVC Planning Problem

This subsection describes the mathematical formulation of the stochastic SVC location-allocation problem. In this formulation, two objectives are considered, including the maximization of PV hosting capacity (3.8) and minimization of SVC planning cost (installation cost and operation cost) (3.9).

$$\text{Max} \sum_m E_m^{PV} \quad (3.8)$$

$$\text{Min} \sum_i \eta C_F^{SVC} a_i^{SVC} + \sum_s p_s \sum_t \sum_i C_V^{SVC} a_i^{SVC} |q_{its}^{SVC}| \quad (3.9)$$

where $\eta = \frac{r(1+r)^y}{365[(1+r)^y - 1]}$ is introduced to denote the daily recovery factor of SVC devices, r denotes the interest rate and y represents the planning horizon of this problem.

Then the multi-objective function is constructed by using the weighted sum approach [75] to address objectives (3.8) and (3.9) simultaneously, given as follows,

$$\begin{aligned} \text{Min}_{\psi_1, \psi_2} \quad & -w^{PV} \sum_m E_m^{PV} \\ & +w^{SVC} \left(\sum_i \eta C_F^{SVC} a_i^{SVC} + \sum_s P_s \sum_t \sum_i C_V^{SVC} a_i^{SVC} \tilde{q}_{its}^{SVC} \right) \end{aligned} \quad (3.10)$$

$$\text{where } \tilde{q}_{its}^{SVC} := |q_{its}^{SVC}|$$

where $\psi_1 = \{a_i^{SVC}, Q_i^{SVC}, E_m^{PV}\}$ and $\psi_2 = \{P_{its}, Q_{its}, V_{its}, q_{its}^{SVC}\}$ denote the first-stage variables set and the second-stage variables set, respectively. Here, the unit of the first term related to PV hosting capacity (kV) is different from that of the rest two terms (\$). Therefore, to sum these three terms in the single-dimensional case (\$), weight factors w^{PV} and w^{SVC} are employed to represent weight factors of PV hosting capacity and SVC planning cost, respectively, subject to $w^{PV} + w^{SVC} = 1$. Note that different combinations of weight factors will result in different tradeoff relationships between PV hosting capacity and SVC planning cost. From the perspective of practical implementation, these two weight factors can be adjusted according to the preference of distribution network planners. For example, if the distribution network planners want the system to have a relative high PV hosting capacity, w^{PV} should be large and the corresponding w^{SVC} should be small.

The constraints are classified into first-stage constraints and second-stage constraints, where the first-stage constraints are given as,

a) PV hosting capacity limit

$$E_m^{PV} \geq 0, \forall m \in N^{PV}(i) \quad (3.11)$$

where (3.11) ensures that the PV hosting capacity is non-negative.

b) SVC devices investment limit

$$0 \leq Q_i^{SVC} \leq \bar{Q}_i^{SVC}, \forall i \in N \quad (3.12)$$

$$\sum_i a_i^{SVC} \leq N_{inv}^{SVC}, \forall i \in N \quad (3.13)$$

where (3.12) limits the SVC investment capacity. (3.13) describes that the total SVC installation number cannot exceed a predefined number considering the limit of the total capital cost in practical application.

The second-stage constraints are given as,

a) Power flow limits

$$P_{i+1ts} = P_{its} + p_{mts}^{PV} - p_{its}^d, \forall i \in N, \forall m \in N^{PV}(i), \forall t \in T, \forall s \in S \quad (3.14)$$

$$Q_{i+1ts} = Q_{its} + q_{its}^{SVC} - q_{its}^d, \forall i \in N, \forall t \in T, \forall s \in S \quad (3.15)$$

$$V_{i+1ts} = V_{its} - \frac{r_{i+1} P_{i+1ts} + x_{i+1} Q_{i+1ts}}{V_0}, \forall i \in N, \forall t \in T, \forall s \in S \quad (3.16)$$

$$p_{mts}^{PV} = \xi_{ts}^{PV} E_m^{PV} \quad (3.17)$$

$$P_{i+1ts} \leq \bar{P}_i, \forall i \in N, \forall t \in T, \forall s \in S \quad (3.18)$$

$$Q_{i+1ts} \leq \bar{Q}_i, \forall i \in N, \forall t \in T, \forall s \in S \quad (3.19)$$

where (3.14)-(3.16) are derived from the linearized from the DistFlow equations (3.4)-(3.6). In (3.17), PV energy output factor $\xi_{ts}^{PV} \in [0,1]$ is

introduced to capture uncertain PV energy output which is $\xi_{ts}^{PV} E_m^{PV}$. (3.18)

and (3.19) demonstrate the active and reactive power flow limits, respectively.

b) Voltage magnitude limits

$$V_{its} \geq \underline{V}_i, \forall i \in N, \forall t \in T, \forall s \in S \quad (3.20)$$

$$V_{its} \leq \bar{V}_i, \forall i \in N, \forall t \in T, \forall s \in S \quad (3.21)$$

where (3.20) and (3.21) give the lower and upper bounds of voltage magnitude, respectively.

c) SVC operation limits

$$-a_i^{SVC} Q_i^{SVC} \leq q_{its}^{SVC} \leq a_i^{SVC} Q_i^{SVC}, \forall i \in N, \forall t \in T, \forall s \in S \quad (3.22)$$

$$\tilde{q}_{its}^{SVC} \geq q_{its}^{SVC}, \forall i \in N, \forall t \in T, \forall s \in S \quad (3.23)$$

$$\tilde{q}_{its}^{SVC} \geq -q_{its}^{SVC}, \forall i \in N, \forall t \in T, \forall s \in S \quad (3.24)$$

where (3.22) is considered to limit reactive compensation provided by SVC devices. (3.23) and (3.24) are imposed to convert $|q_{its}^{SVC}|$ to \tilde{q}_{its}^{SVC} .

Note that the bilinear $a_i^{SVC} Q_i^{SVC}$ in (3.22) renders the proposed planning problem nonconvex, resulting in low computational efficiency. To linear this nonlinear term, a continuous variable z_i^{SVC} is introduced to substitute for $a_i^{SVC} Q_i^{SVC}$ with the following linear inequality constraints,

$$-a_i^{SVC} \bar{Q}_i^{SVC} + z_i^{SVC} \leq 0, \forall i \in N \quad (3.25)$$

$$a_i^{SVC} \underline{Q}_i^{SVC} - z_i^{SVC} \leq 0, \forall i \in N \quad (3.26)$$

$$-a_i^{SVC} \underline{Q}_i^{SVC} + z_i^{SVC} \leq \underline{Q}_i^{SVC} - \bar{Q}_i^{SVC}, \forall i \in N \quad (3.27)$$

$$a_i^{SVC} \bar{Q}_i^{SVC} - z_i^{SVC} \leq -\underline{Q}_i^{SVC} + \bar{Q}_i^{SVC}, \forall i \in N \quad (3.28)$$

Therefore, (3.22) can be rewritten as (3.29), given as follows,

$$-z_i^{SVC} \leq q_{its}^{SVC} \leq z_i^{SVC}, \forall i \in N, \forall t \in T, \forall s \in S \quad (3.29)$$

3.3 Solution Methodology

This section proposes a solution approach in which the Benders decomposition algorithm [76] is employed to decompose the proposed two-stage stochastic SVC location-allocation problem. The original problem is a mixed integer nonlinear program (MINLP) and it is intractable because of the time-coupling constraints as well as numerous scenarios. Therefore, commercial solvers, like CPLEX [77] and GUROBI [78], cannot be directly used to solve this complicated problem. However, Benders decomposition algorithm is properly applied to solve this two-stage problem. Specifically, the original two-stage problem is decomposed into a master problem corresponding to the first-stage problem and many subproblems corresponding to all second-stage problems. Note that each subproblem is associated with one time period in one scenario. During the Benders decomposition procedure, Benders cuts are built to link the master problem with subproblems.

3.3.1 Subproblem and Master problem

The subproblem is to minimize the penalty cost for voltage magnitude violation and the expected SVC cost over all time periods in all scenarios. The subproblem for the time period t of scenario s in Benders iterative v is formulated as follows,

$$Z_{ts}^{sub(v)} := \underset{w^{sp}}{\text{Min}} w^{SVC} \sum_i C_V^{SVC} a_i^{SVC(v)} \tilde{q}_{its}^{SVC(v)} \quad (3.30)$$

$$\text{s.t. (3.14)-(3.21), (3.23) and (3.24), (3.29)} \quad (3.31)$$

$$E_m^{PV(v)} = E_m^{PV,fix} : \varphi_{mts}^{PV(v)}, \forall m \in N^{PV} (i) \quad (3.32)$$

$$z_i^{SVC(v)} = z_i^{SVC,fix} : \varphi_{its}^{SVC(v)}, \forall i \in N \quad (3.33)$$

The decision variables set of the subproblem is given by follows,

$$\psi^{sp} = \{Z_{ts}^{sub(v)}, E_m^{PV(v)}, z_i^{SVC(v)}, P_{its}^{(v)}, Q_{its}^{(v)}, Q_i^{SVC(v)}, a_i^{SVC(v)}, q_{its}^{SVC(v)}, \tilde{q}_{its}^{SVC(v)}, V_{its}^{(v)}, \varphi_{mts}^{PV(v)}, \varphi_{its}^{SVC(v)}\}$$

(3.31) summarizes all second-stage constraints. In (3.32) and (3.33), PV hosting capacity $E_m^{PV(v)}$ and SVC planning decision $z_i^{SVC(v)}$ are fixed to the given value obtained by solving the master problem. After solving all subproblems which correspond to all time periods of all scenarios, the upper bound of $Z_{upper}^{(v)}$ for the optimal value of original problem (3.10)-(3.29) can be acquired by the following equation,

$$Z_{upper}^{(v)} = \sum_s p_s \sum_t Z_{ts}^{sub(v)} - w^{PV} \sum_m E_m^{PV,fix} + w^{SVC} \sum_i \eta C_F^{SVC} a_i^{SVC,fix} \quad (3.34)$$

The master problem is to determine the PV hosting capacity and SVC planning decisions before the uncertainty realizations. The master problem for the time period t of scenario s in Benders iterative v is formulated as follows,

$$Z_{lower}^{(v)} := \underset{\psi^{mp}}{\text{Min}} \lambda^{(v)} - w^{PV} \sum_m E_m^{PV(v)} + w^{SVC} \sum_i \eta C_F^{SVC} a_i^{SVC(v)} \quad (3.35)$$

$$\text{s.t. (3.11)-(3.13), (3.25)-(3.28)} \quad (3.36)$$

$$\begin{aligned} \lambda^{(v)} \geq & \sum_s p_s \sum_t Z_{ts}^{Sub(k)} + \sum_m \sum_s p_s \sum_t \varphi_{mts}^{PV(k)} (E_m^{PV(v)} - E_m^{PV(k)}) \\ & + \sum_i \sum_s p_s \sum_t \varphi_{its}^{SVC(k)} (z_i^{SVC(v)} - z_i^{SVC(k)}), k = 1, 2, \dots, v-1 \end{aligned} \quad (3.37)$$

$$\lambda^{(v)} \geq \lambda^{down} \quad (3.38)$$

$$\lambda^{(v)} - w^{PV} \sum_m E_m^{PV(v)} + w^{SVC} \sum_i \eta C_F^{SVC} a_i^{SVC(v)} \leq Z^{opt} \quad (3.39)$$

The decision variables set of the master problem is given by follows,

$$\psi^{mp} = \{Z_{lower}^{(v)}, E_m^{PV(v)}, z_i^{SVC(v)}, Q_i^{SVC(v)}, a_i^{SVC(v)}, \lambda^{(v)}\}$$

The master problem (3.35)-(3.39) is a MILP problem which can be directly by most commercial solvers. (3.36) summarizes the first-stage constraints. (3.37) describes the Benders cut, which is utilized to build a link between the master problem and subproblems. Note that Dual variables $\varphi_{mts}^{PV(v)}$ and $\varphi_{its}^{SVC(v)}$ of first-stage variables $E_m^{PV(v)}$ and $z_i^{SVC(v)}$ are used to calculate the sensitivities $\sum_s p_s \sum_t \varphi_{mts}^{PV(k)}$ and $\sum_s p_s \sum_t \varphi_{its}^{SVC(k)}$ for generating Benders cuts. (3.38) is added to accelerate the iteration convergence, where a lower bound λ^{down} is introduced. (3.39) is imposed to ensure that the lower bound $Z_{lower}^{(v)}$ of the original problem is lower or equal to the minimum upper bound Z^{opt} obtained from the subproblems.

3.3.2 Benders Decomposition Algorithm Procedure

The convergence is guaranteed until the upper bound meets the lower bound. Detailed proof process of Benders decomposition convergence condition can be referred to [79]. The proposed Benders decomposition algorithm procedure for solving the proposed two-stage planning model is given as follows,

Step 1. Initialization:

Set the iteration index $v = 1$. Set the initial upper bound $Z_{upper}^{(v)} = \infty$ and lower bound $Z_{lower}^{(v)} = -\infty$. Set the convergence tolerance ε . Initialize the first-stage variables, $E_m^{PV(0)}$ and $z_i^{SVC(0)}$. Set $E_m^{PV,fix} = E_m^{PV(0)}$ and $z_i^{SVC,fix} = z_i^{SVC(0)}$.

Step 2. Iteration

Solve the subproblem (3.30)-(3.33) for each time period and each uncertainty scenario. Obtain the upper bound $Z_{upper}^{(v)}$ of the original problem according to (3.34).

Step 3. Minimum upper bound update

If $Z_{upper}^{(v)} \leq Z^{opt}$, update the global solution $Z^{opt} = Z_{upper}^{(v)}$.

Step 4. Convergence check

If $|Z_{upper}^{(v)} - Z_{lower}^{(v)}| \leq \varepsilon$, then stop the procedure. Otherwise, set $v \leftarrow v + 1$.

Step 5. Solve master problem

Solve the master problem (3.35)-(3.39), calculate $Z_{lower}^{(v)}$ and update the values of $E_m^{PV,fix}$ and $z_i^{SVC,fix}$. Go back to **Step 2** and continue.

3.4 Numerical Results

3.4.1 IEEE 37-node Distribution Network

In this subsection, the IEEE 37-node distributing network is utilized to verify the proposed planning model and solution method, as depicted in Fig. 3-3. The base power value is 1 MVA and the voltage value is 12.66 kV. The 37-node test system is modified by randomly selecting six potential locations for PV generators installation, such as nodes 3, 8, 11, 23, 29 and 33. Practically, these sites are considered based on many factors, such as irradiation and regulations, more information can be referred to [80]. One hundred representative scenarios (10*10) of PV generation and load consumption are taken into account. Fig. 3-4 and Fig.3-5 show these daily uncertainty scenarios

with their probabilities. As an example, the combination of weight factors, $w^{PV} = 0.5$ and $w^{SVC} = 0.5$, is employed to demonstrate the performance of the proposed planning model and solution approach.

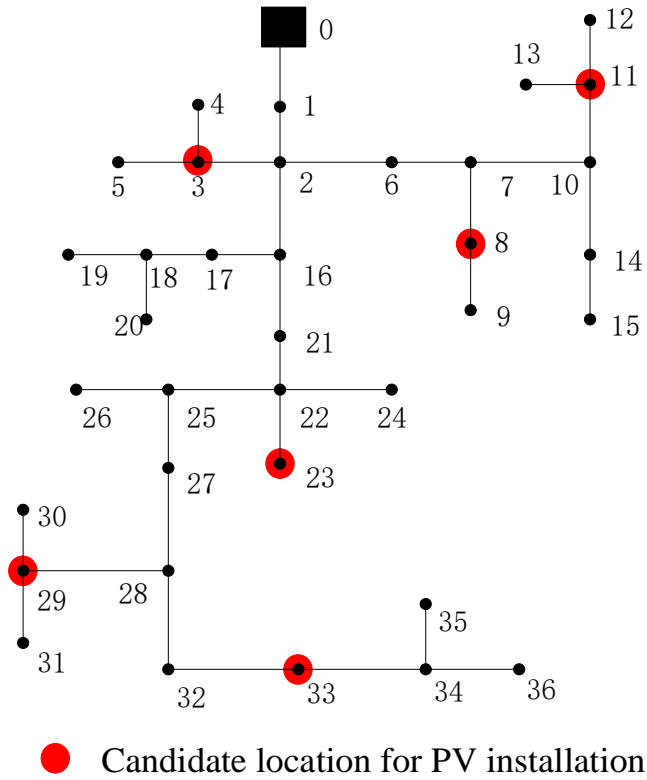


Fig. 3-3 IEEE 37-node test system

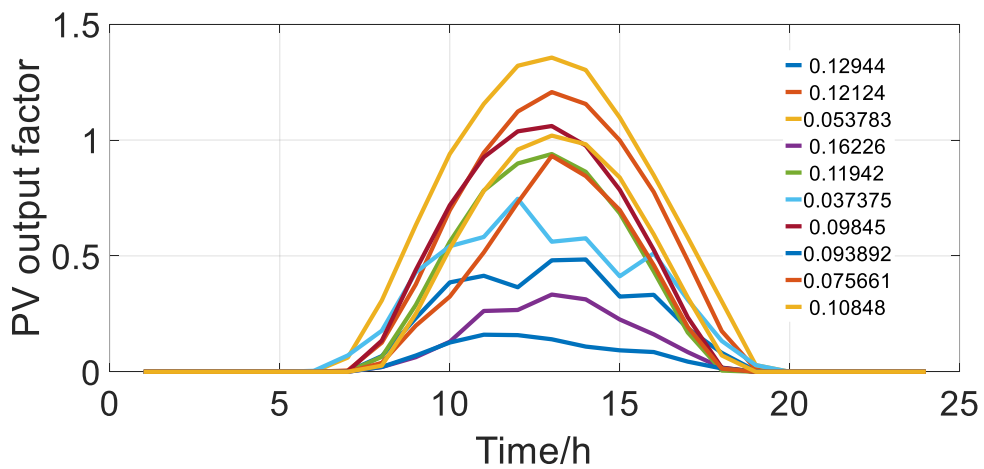


Fig. 3-4 PV output factor for daily PV generations

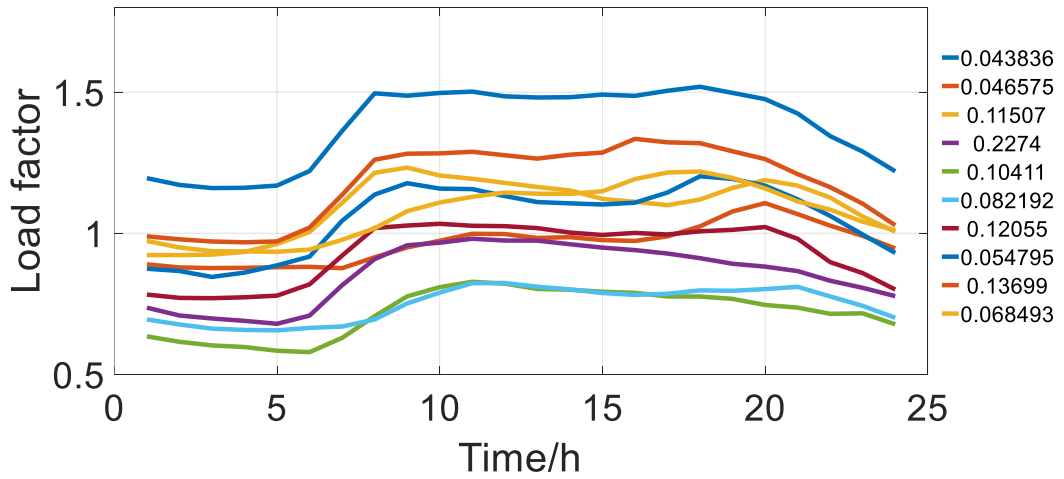


Fig. 3-5 Load factor for daily load consumptions

The convergence performance of the developed Benders decomposition algorithm based solution approach is shown in Fig. 3-6. The optimal solutions including SVC planning decisions and PV hosting capacity decision can be obtained after the sixteen iterations in which the upper bound meets the lower bound. To illustrate the efficiency of the developed solution method, as the benchmark, a widely-used commercial solver GUROBI [78] on the platform of CVX [81] is used to directly solve the original problem (3.10)-(3.29), denoted as CVX-GUROBI. Table 3-1 lists the comparison between CVX-GUROBI and CVX_BD-GUROBI which is the proposed solution method via the same solver and platform. As shown in this table, CVX-GUROBI cannot directly solve the original problem since it contains a mass of variables and coupled constraints. By contrast, CVX_BD-GUROBI is able to solve the same problem with acceptable computation time. This is because the proposed solution method decomposes the complicated original problems into a master

problem and subproblems, which can significantly reduce the computation complexity.

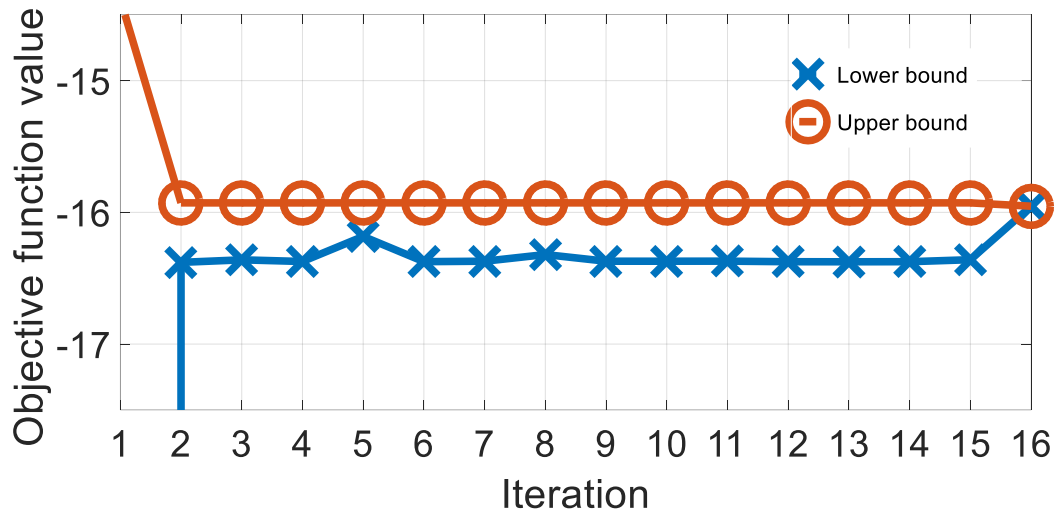


Fig. 3-6 Performance of convergence

Table 3-1 Comparison of the computation time under two methods

CVX-GUROBI	CVX_BD-GUROBI	
Non convergence	[sec.] 8211	[iterations] 16

Table 3-2 PV hosting capacity of candidate locations in the 37-node test system

Candidate location (Node)	PV size (p.u.)	Candidate location (Node)	PV size (p.u.)
3	0.121	23	0.109
8	0.082	29	0.036
11	0.062	33	0.081

Table 3-3 SVC planning decisions in the 37-node test system

Location (Node)	SVC size (p.u.)	Location (Node)	SVC size (p.u.)
3	0.050	23	0.050
4	0.032	24	0.050
7	0.042	26	0.041
8	0.050	29	0.050
9	0.027	33	0.050
10	0.022	34	0.031
11	0.050	–	–

Table 3-2 and Table 3-3 list the PV hosting capacity on candidate each location and the corresponding optimal results of SVC planning, respectively. To investigate the effects of candidate locations for PV generations connection on PV hosting capacity, several cases are designed with different candidate sites of PV energy integration. Case A is regarded as the benchmark which is the original assumption and the following cases are given as follows,

1) Case B: according to Case A, move PV generation installation from nodes 29, 33 to nodes 25, 35, respectively.

2) Case C: according to Case A, move PV generation installation from nodes 23, 29, 33 to nodes 17, 21, 32, respectively.

3) Case D: according to Case A, move PV generation installation from nodes 11, 23, 29, 33 to nodes 10, 16, 26, 34, respectively.

4) Case E: according to Case A, move PV generation installation from nodes 8, 11, 23, 29, 33 to nodes 5, 12, 19, 24, 31, respectively.

5) Case F: according to Case A, move PV generation installation from nodes 3, 8, 11, 23, 29, 33 to nodes 4, 7, 13, 18, 22, 30, respectively.

Table 3-4 Comparison on different candidate nodes for PV energy connection (The underlined numbers indicate the different candidate nodes with Case A)

	Candidate nodes	PV size (p.u.)	PV hosting capacity (p.u.)	SVC planning cost (\$ 10 ⁶)
Case A	(3, 8, 11, 23, 29, 33)	(0.121, 0.082, 0.062, 0.109, 0.036, 0.081)	0.491	1.756
Case B	(3, 8, 11, 23, <u>25</u> , <u>35</u>)	(0.100, 0.098, 0.088, 0.085, 0.043, 0.060)	0.474	1.748
Case C	(3, 8, 11, <u>17</u> , <u>21</u> , <u>32</u>)	(0.097, 0.057, 0.078, 0.119, 0.018, 0.095)	0.464	1.741
Case D	(3, 8, <u>10</u> , <u>16</u> , <u>26</u> , <u>34</u>)	(0.086, 0.075, 0.055, 0.086, 0.122, 0.062)	0.486	1.754
Case E	(3, <u>5</u> , <u>12</u> , <u>19</u> , <u>24</u> , <u>31</u>)	(0.114, 0.056, 0.067, 0.081, 0.026, 0.153)	0.497	1.771
Case F	(<u>4</u> , <u>7</u> , <u>13</u> , <u>18</u> , <u>22</u> , <u>30</u>)	(0.091, 0.076, 0.054, 0.085, 0.104, 0.083)	0.493	1.762

Table 3-4 compares PV integration size for each candidate locations, PV hosting capacity of the grid and SVC planning cost under different combinations of potential PV energy penetration sites. As seen in this table, both PV hosting capacity values and the corresponding SVC planning cost will be changed with different locations of PV energy integration. Hence, it can be concluded that the sites of PV generations connection affect the PV hosting capacity and SVC planning cost. From the perspective of practical implementation, candidate locations for PV generators installation should be included in the SVC planning scheme so that the most economic benefits can be obtained. Nevertheless, the distribution network planners try to minimize the total cost of SVC devices investment and operation meanwhile maintaining the reliability and security of distribution networks. Therefore, distribution network planners determine the reasonable sites for PV energy integration in terms of the policy-making process.

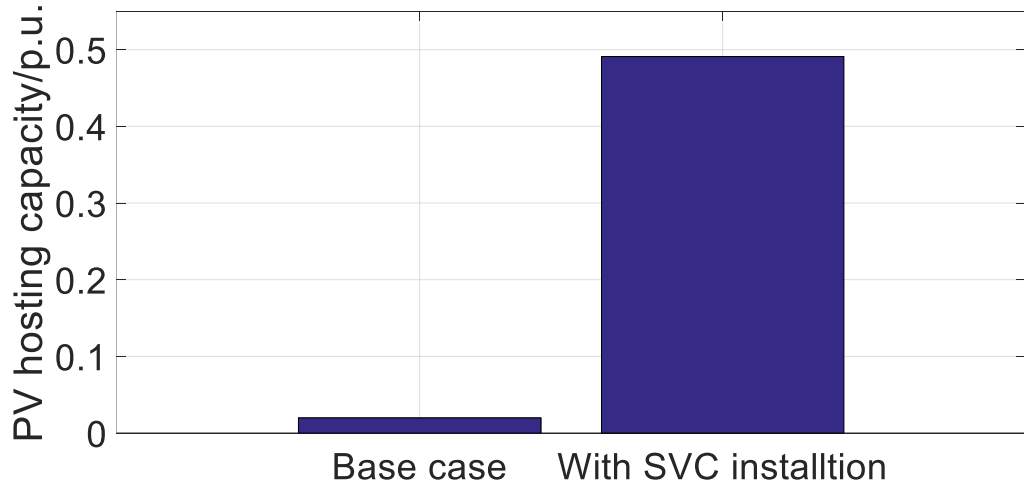


Fig. 3-7 PV hosting capacity with and without SVC installation

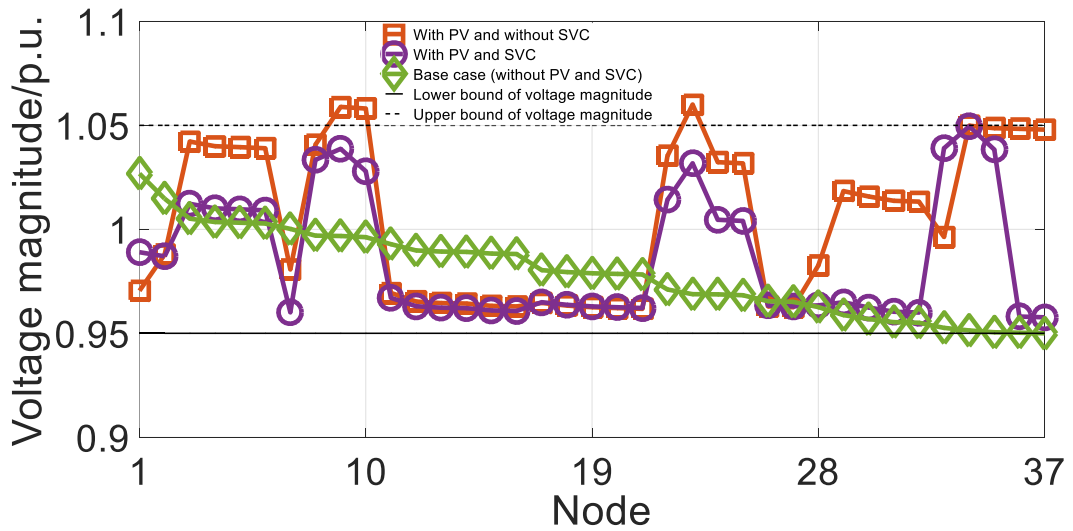


Fig. 3-8 Comparison on daily voltage profiles

Fig. 3-7 compares the PV hosting capacity in two cases, the first one is the base case without SVC devices installation and the second one is the case with optimal SVC planning as shown in Table 3-3. As seen in this figure, the PV hosting capacity is significantly improved after SVC devices placement. Besides, Fig. 3-8 depicts three daily voltage profiles of node 13 at 1:00 pm in three cases, which are described as follows,

1) Case 1: base case without PV generation penetration and SVC devices installation.

2) Case 2: the case with PV generation penetration as the result in Table 3-2 but without SVC devices installation.

3) Case 3: the case with PV generation penetration as the result in Table 3-2 and SVC devices installation as the result in Table 3-3.

According to Fig. 3-8, voltage violations can be observed in Case 2 where the voltage magnitudes at some nodes (i.e. nodes 9, 10, and 21) exceed the upper bound (1.05 p.u.). However, all overvoltage issues are solved after optimal SVC devices placement, as shown in Case 3.

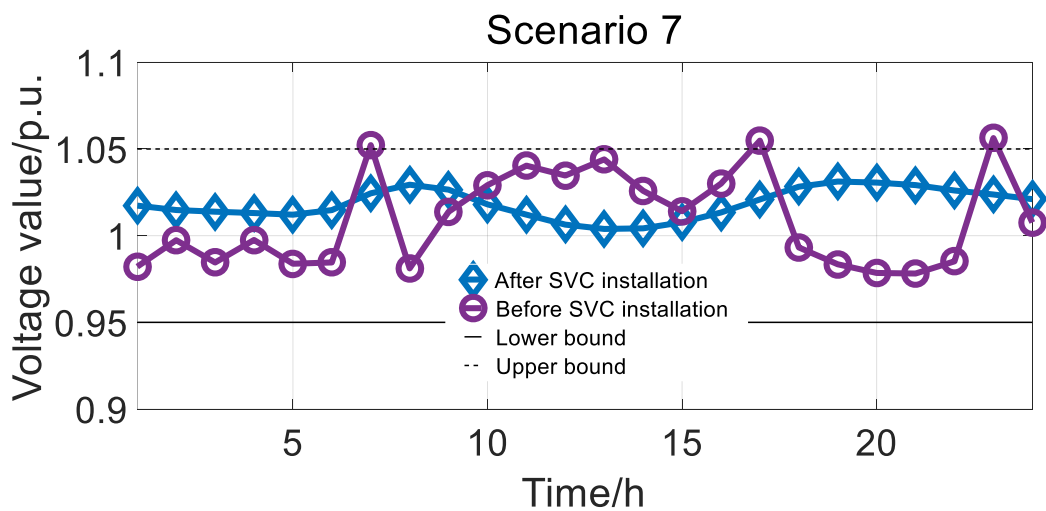


Fig. 3-9 Daily voltage profiles of node 30 in scenario 7 with and without SVC installation

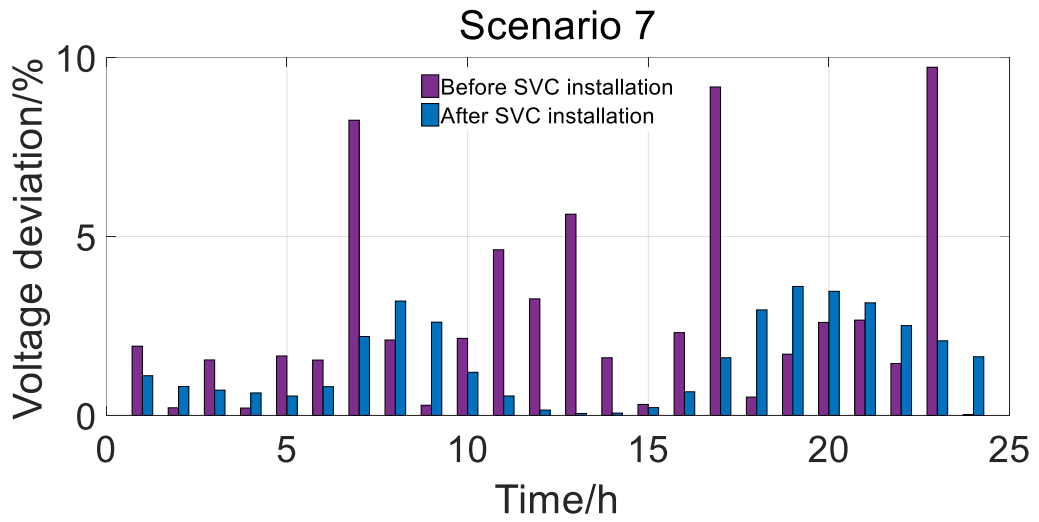


Fig. 3-10 Daily voltage deviations of node 30 in scenario 7 with and without SVC installation

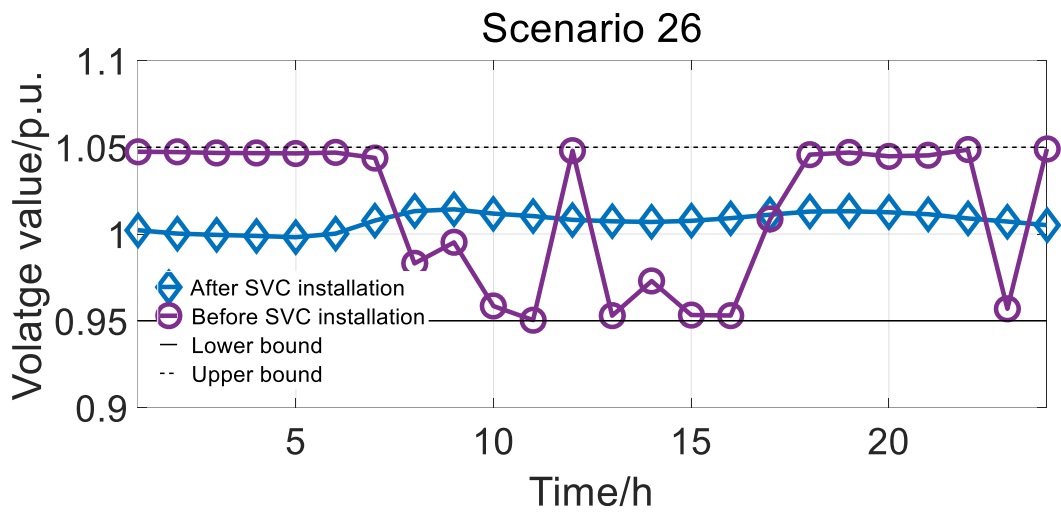


Fig. 3-11 Daily voltage profiles on node 4 in scenario 26 with and without SVC installation

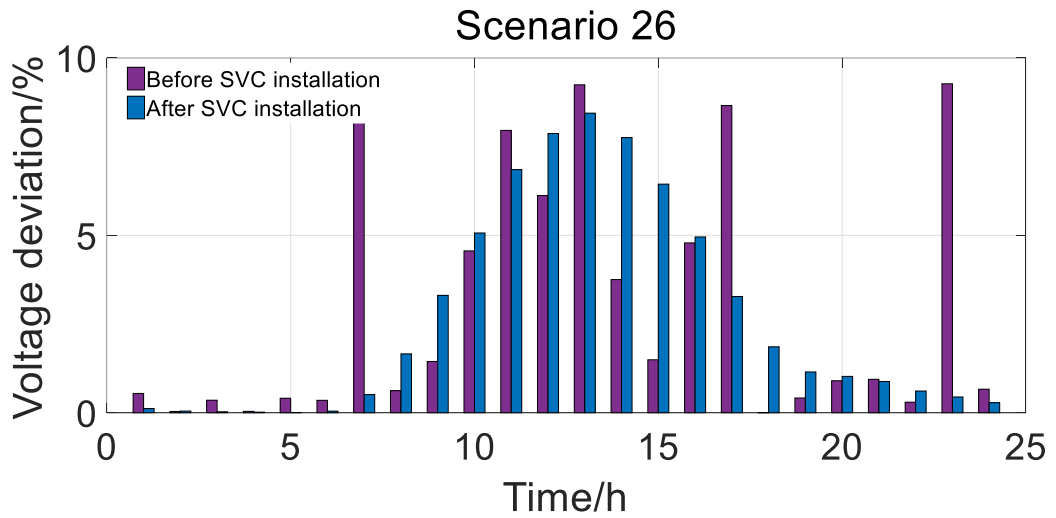


Fig. 3-12 Daily voltage deviations on node 4 in scenario 26 with and without SVC installation

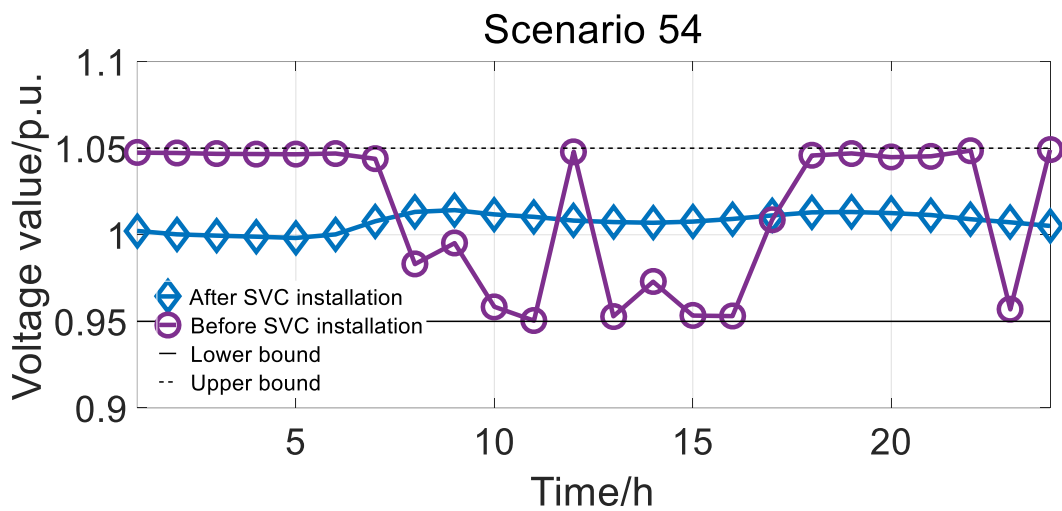


Fig. 3-13 Daily voltage profiles on node 15 in scenario 54 with and without SVC installation

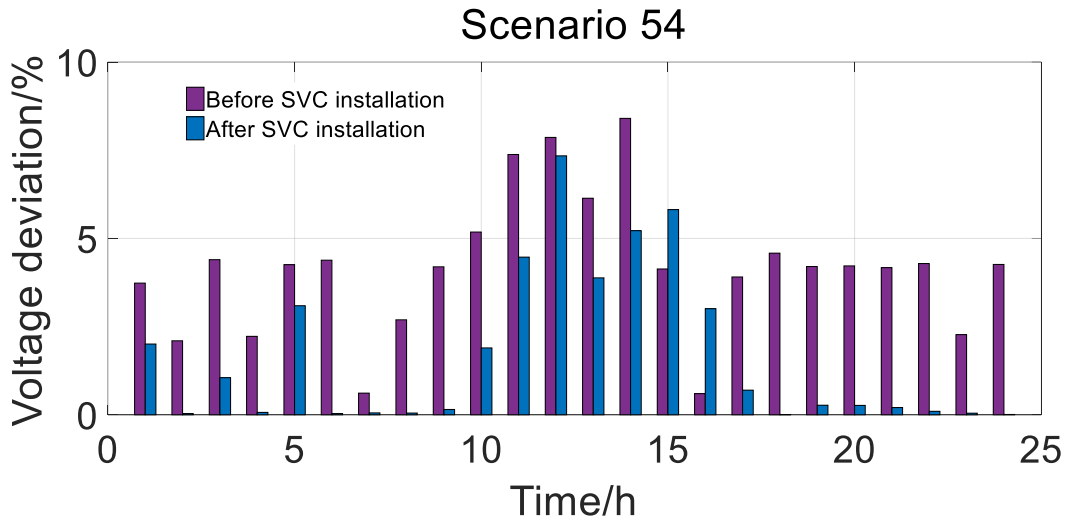


Fig. 3-14 Daily voltage deviations on node 15 in scenario 54 with and without SVC installation

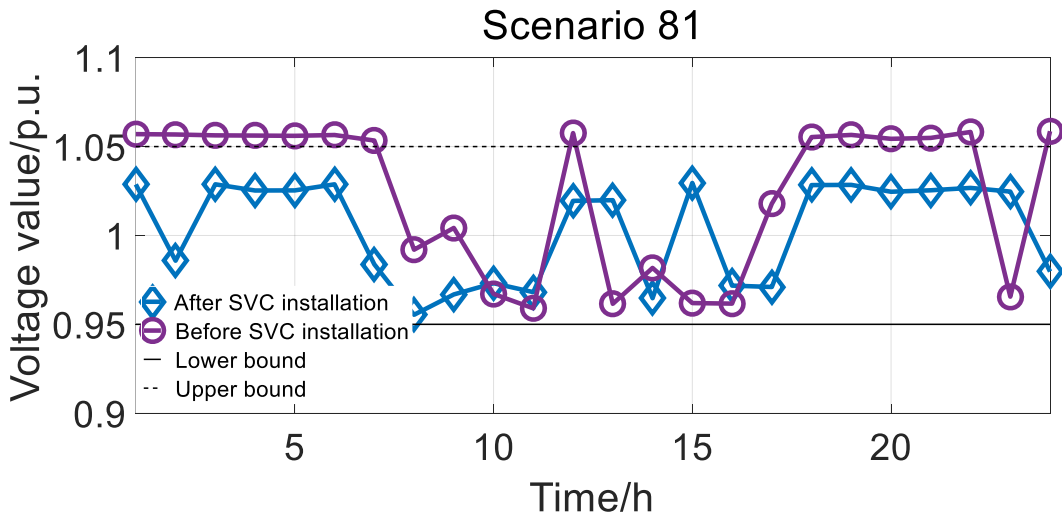


Fig. 3-15 Daily voltage profiles on node 23 in scenario 81 with and without SVC installation

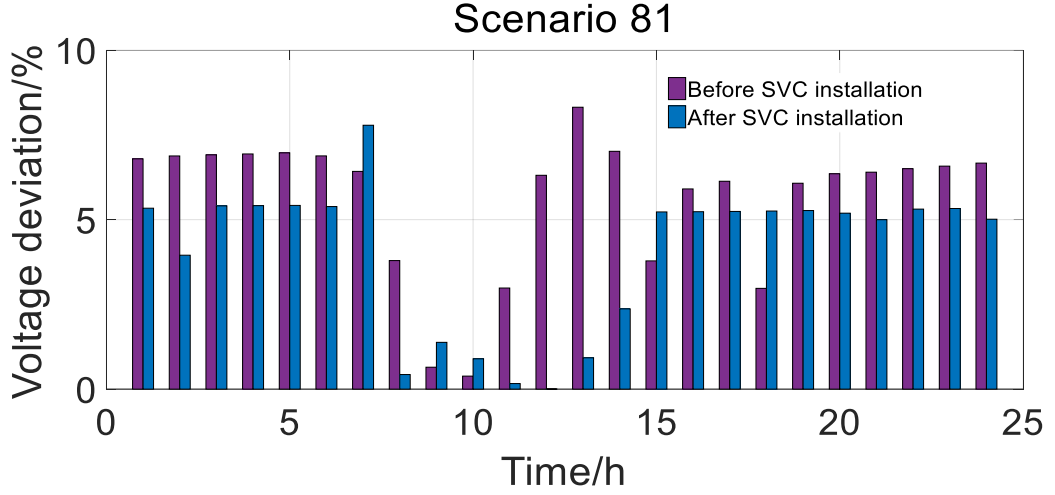


Fig. 3-16 Daily voltage deviations on node 23 in scenario 81 with and without SVC installation

Figs. 3-9 to 3-16 compare the voltage magnitude and voltage deviation of nodes 4, 15, 23 and 30 in scenarios 7, 26, 54, and 81. Note that the voltage deviation can be obtained by the following equation,

$$\text{Voltage deviation} = \sum_{i \in N} \frac{(V_i - V_{Ni})^2}{V_{Ni}^2} \quad (3.40)$$

where V_i represents the voltage magnitude at the node i , V_{Ni} denotes the nominal voltage at the node i . It should be noted that $V_{Ni} = 1$, where unit quantity is adopted.

In some unfavorable operation conditions like scenario 7 and scenarios 81, overvoltage occurs when the SVC devices are not installed in the distribution network. By contrast, all voltage magnitudes are in the normal range, namely 0.95 p.u. to 1.05 p.u., after SVC devices installation. In addition, the voltage deviations at most nodes become small with SVC placement. By conducting these comparisons, it can be concluded that the optimal SVC planning cannot only relieve overvoltage violations but also decrease voltage deviations, which ensures the reliability and security of normal distribution network operation.

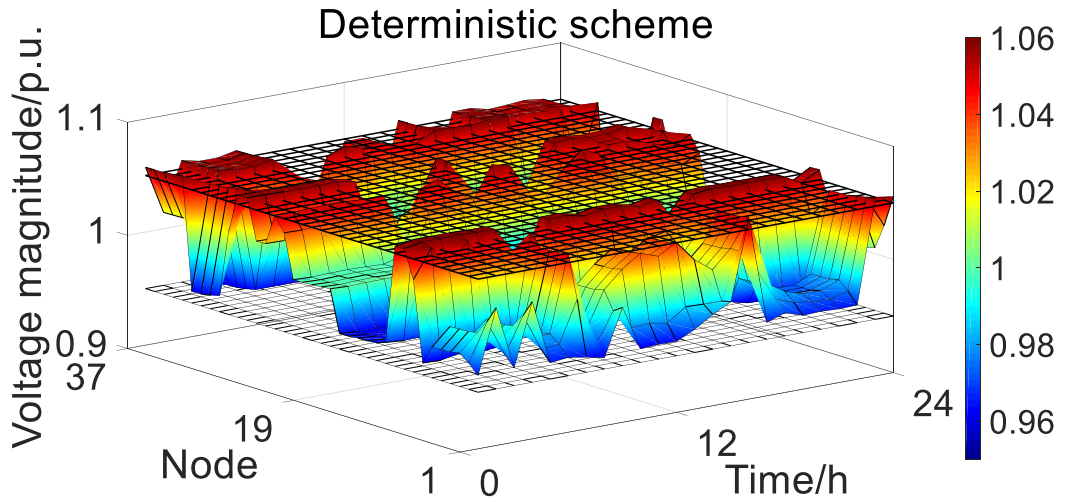


Fig. 3-17 Daily voltage profiles obtained from the deterministic scheme under the critical scenario

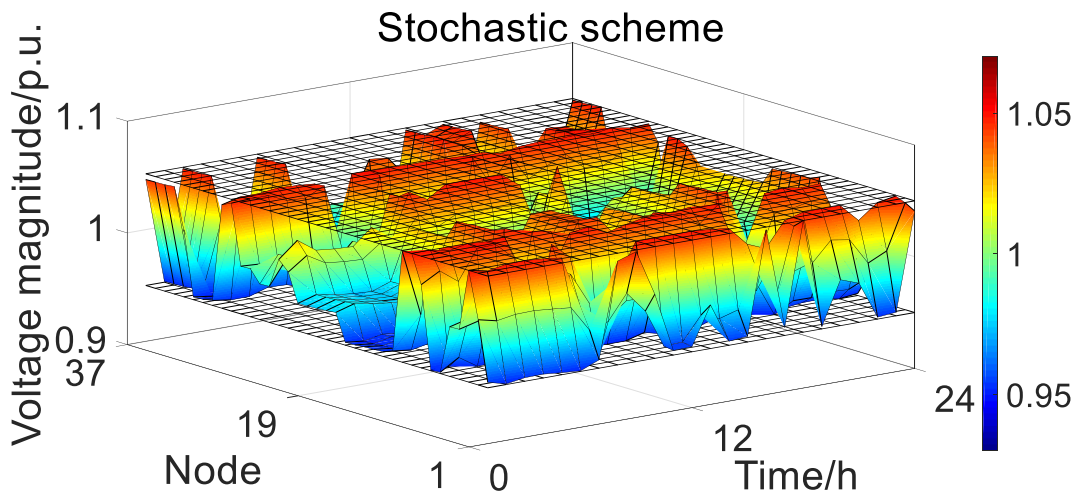


Fig. 3-18 Daily voltage profiles obtained from the stochastic scheme under the critical scenario

To demonstrate the performance of the proposed stochastic scheme for SVC planning, the deterministic scheme is employed as the benchmark. The mathematical formulation of the deterministic SVC planning problem is similar to the original formulation (3.10)-(3.29) of stochastic SVC planning problem while the only expected operation condition is considered. After

solving the deterministic SVC planning problem, the optimal SVC planning decisions and PV hosting capacity can be obtained. The optimal sites for SVC installation are node 6, 7, 8, 9, 10, 11, 23, 24, 26, 29, 33, 34 and the corresponding SVC capacity are 0.02, 0.035, 0.05, 0.05, 0.019, 0.05, 0.05, 0.043, 0.05, 0.05, 0.05, 0.043 p.u., respectively. The PV hosting capacity for the candidate nodes 3, 8, 11, 23, 29, and 33 are 0.1, 0.07, 0.04, 0.1, 0.03 and 0.06 p.u, respectively. The critical combination of uncertainty scenario is used to compare the performance of the stochastic scheme and deterministic scheme. In this critical PV-load scenario, the PV power output is high and the load level is low. Fig. 3-17 and Fig. 3-18 depict the voltage magnitude at all nodes in the critical scenarios of the deterministic scheme and stochastic scheme, respectively. It can be seen from these two figures that the overvoltage problem caused by high PV energy integration can be issued by the stochastic scheme. This is because the stochastic scheme takes various uncertainties into consideration and thus it is more robust against the critical condition.

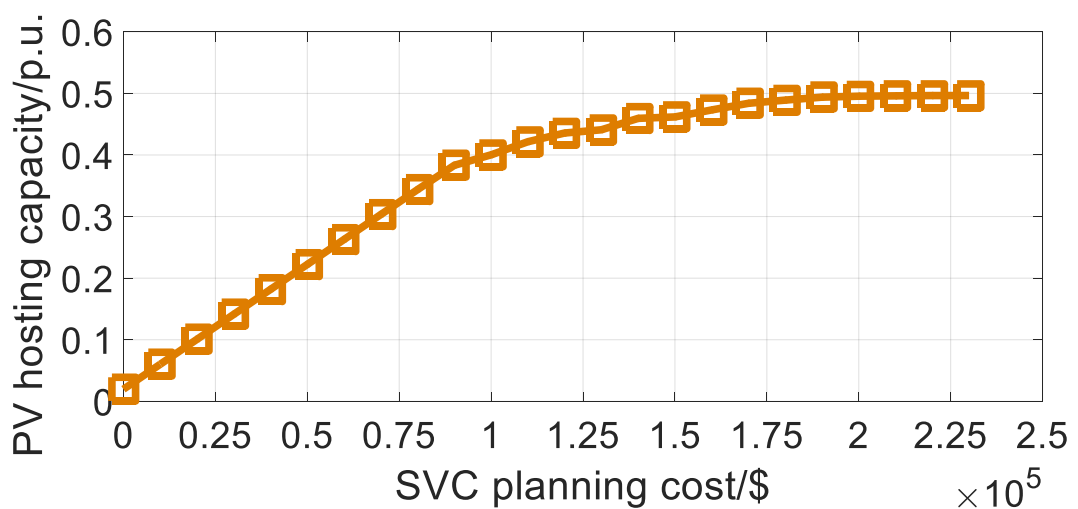


Fig. 3-19 Tradeoff curve between PV hosting capacity and SVC planning cost

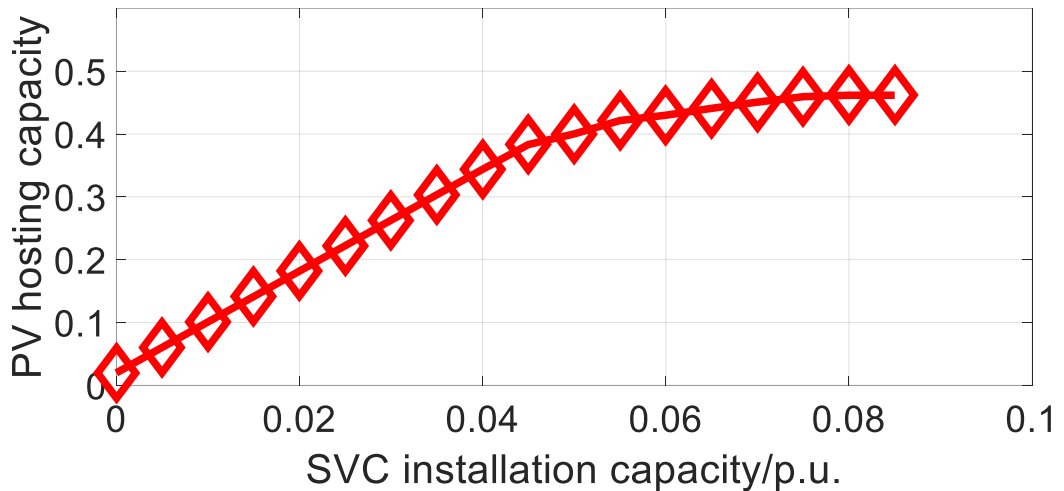


Fig. 3-20 Impact of SVC installation capacity on PV hosting capacity (with same installation number)

Fig. 3-19 shows the tradeoff curve between PV hosting capacity and SVC planning cost. As seen in this figure, the PV hosting capacity rises gradually with the increase of SVC planning cost until it reaches \$75,000. Next, the increasing rate of the PV hosting capacity decreases to zero so that the PV hosting capacity is insensitive to any increased SVC planning cost. The reason is that the large PV energy integration leads to overload on distribution lines so there is a threshold beyond which the PV hosting capacity cannot improve with increasing SVC planning cost. Under such circumstance, if the PV hosting capacity is too low to be accepted by the decision makers, the distribution system expansion is suggested.

Sensitivity analysis is conducted to investigate the impacts of SVC installation capacity/number on PV hosting capacity enhancement. Fig. 3-20 illustrates the impact of SVC installation capacity on PV hosting capacity improvement with fixed installation number. It can be observed from this figure that the PV hosting capacity improves almost linearly until the SVC installation capacity reaches 0.045 p.u.. Fig. 3-21 depicts the impact of SVC

installation number on PV hosting capacity improvement with fixed installation capacity. As seen in this figure, before the SVC installation number reaches nine, the PV hosting capacity increase rapidly. Beyond the threshold, more SVC devices or larger SVC sizes will have a minor effect on the PV hosting capacity enhancement since overload cannot be issued by distribution lines.

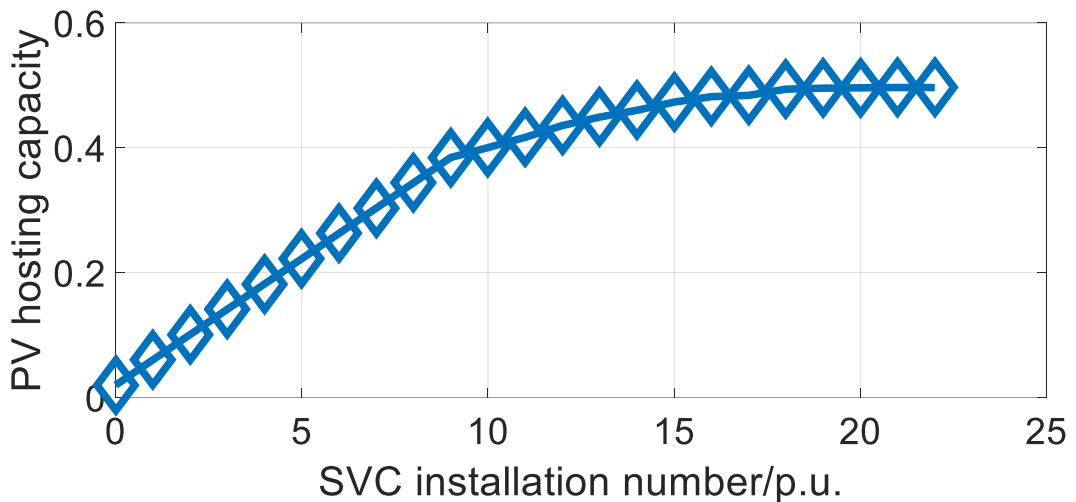


Fig. 3-21 Impact of SVC installation number on PV hosting capacity (with same installation capacity: 0.05p.u.)

3.4.2 IEEE 123-node Distribution Network

To verify the performance of the proposed SVC location-allocation model and solution approach on the large-scale distribution network, a modified IEEE 123-node is adopted, as shown in Fig. 3-22. In this case, the base value, operation scenarios and weight factors are the same as those described in the 37-node case. The 123-node test system is modified by selecting twelve candidate sites for the PV energy generators installation, such as nodes 5, 23, 31, 34, 45, 58, 62, 77, 84, 93, 109 and 118. Table 3-5 and Table 3-6 list the optimal results of the PV hosting capacity and SVC location-allocation

decisions, respectively. Fig. 3-23 demonstrates the daily voltage magnitudes at all nodes in the critical scenario. As seen in this figure, the voltage magnitudes are ensured within the allowable ranges with optimal SVC placement.

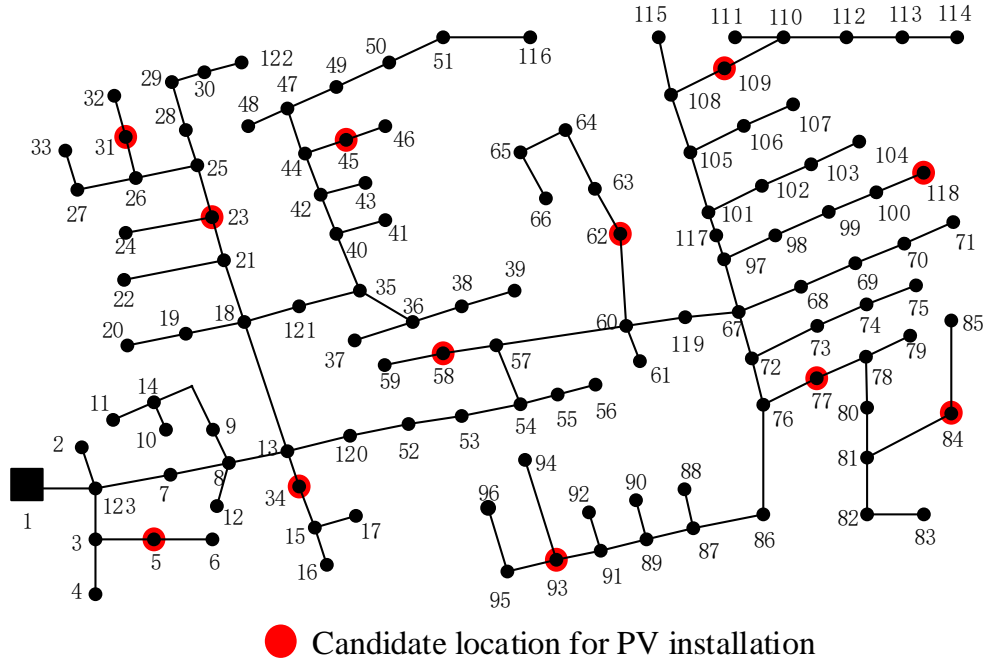


Fig. 3-22 The modified IEEE 123-node test system

Table 3-5 PV hosting capacity value of candidate locations in the 123-node system

Candidate location (Node)	PV size (p.u.)	Candidate location (Node)	PV size (p.u.)
5	0.209	62	0.093
23	0.224	77	0.102
31	0.214	84	0.315
34	0.181	93	0.243
45	0.212	109	0.102
58	0.339	118	0.225

Table 3-6 SVC planning decisions in the 123-node system

Location (Node)	SVC size (p.u.)	Location (Node)	SVC size (p.u.)	Location (Node)	SVC size (p.u.)
5	0.050	37	0.009	84	0.050
6	0.034	45	0.050	85	0.036
22	0.015	47	0.040	93	0.050
23	0.050	57	0.043	94	0.048
25	0.003	58	0.050	109	0.050
30	0.043	59	0.050	117	0.008
31	0.050	62	0.050	118	0.050
33	0.044	77	0.050	119	0.028
34	0.050	83	0.050	-	-

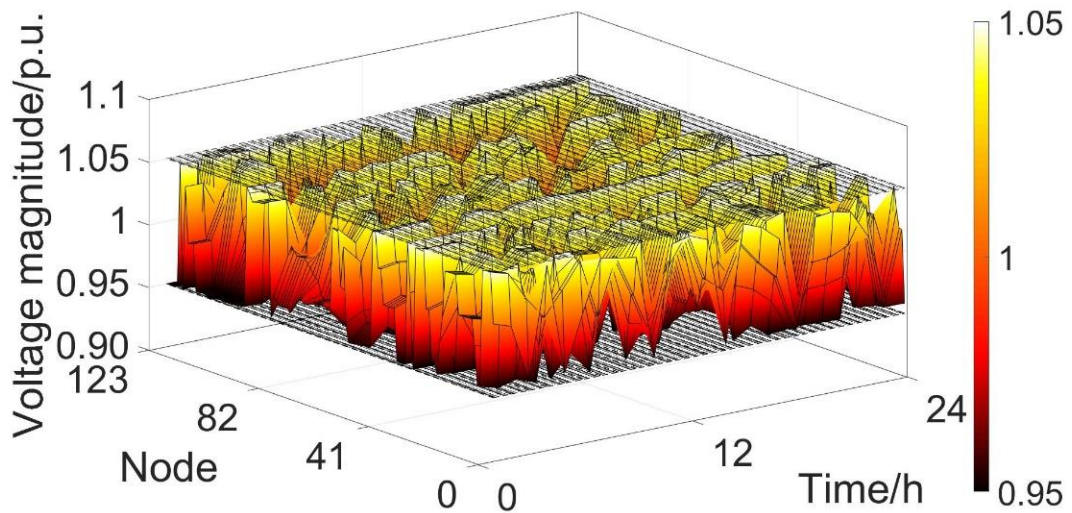


Fig. 3-23 Daily voltage profiles of the modified 123-node distribution system under the critical scenario

3.5 Summary

In this chapter, a two-stage stochastic optimal SVC location-allocation model is proposed. The primary goal of this planning model is to maximize the PV hosting capacity of the distribution networks by finding the optimal sites and sizes of SVC devices. In this two-stage problem, the PV hosting capacity and the corresponding SVC location-allocation decisions are determined in the first-stage before the uncertainty realization, while the operational constraints are evaluated with given first-stage results under representative PV-load scenarios in the second stage. The numerous time-coupled constraints result in an intractable problem, so a solution approach is developed where the Benders decomposition algorithm is used to decompose the original problem into master problem and subproblems. Thus, commercial solvers can be used to directly solve this two-stage problem. The modified IEEE 37-node and 123-node distribution networks are employed to demonstrate the effectiveness of the proposed model and the solution method.

The main conclusions are summarized as follows,

1) The main contribution of this work is that it investigates the extent of the potential benefits from optimal SVC planning as an option to improve the PV hosting capacity of distribution networks. Considering the widespread application of SVC in power systems, this work has practical significance.

2) Simulation-based methods are widely adopted to assess PV hosting capacity but they are inapplicable in studying its improvement. Conversely, the PV hosting capacity is originally modeled as the decision variable and incorporate it into the objective function. Hence, a tradeoff between PV hosting capacity and SVC planning cost can be achieved.

3) The proposed two-stage stochastic optimal SVC location-allocation problem is practically intractable because coupled objective and constraints across the time periods and numerous uncertainty scenarios. In this regard, based on Benders decomposition, an efficient solution approach is proposed to solve this two-stage problem so as to reduce computational complexity.

4) At first, the PV hosting capacity improves gradually with the increasing static var compensator planning cost. However, because of the limit of distribution line capacity, there is a threshold (about $\$1.75 \times 10^5$) beyond which the PV hosting capacity becomes insensitive to the additional SVC planning cost.

Chapter 4 Optimal Voltage Regulators Placement

Considering Photovoltaic Accommodation Capability

Enhancement

4.1 Introduction

In the previous chapter, an optimal static var compensator (SVC) planning model is proposed for photovoltaic (PV) hosting capacity enhancement in the distribution networks. By optimizing the sitting and sizing of SVC devices, the maximum PV hosting capacity of the given locations can be obtained. Similarly, this chapter aims at improving the hourly PV accommodation capability (PVAC) via optimal advanced devices placement. The concept of PVAC is proposed to describe the amount of PV generation that can be reliably accommodated at a certain node of a distribution network within a certain time period. Installing voltage regulators (VRs) in the distribution networks is an appropriate alternative to enhance the operational capacity of the existing distribution networks. Compared with optimal SVC devices planning, this method is economically and technically preferable to distribution system planners due to its advantages on flexible placement, economic efficiency and short installation time [87]. Besides, two criteria are introduced to maintain the safety and reliability of the distribution network operation, i.e., voltage variation and distribution line capacity. Therefore, this chapter gives a continue study of the previous chapter.

Optimal VR placement is an effective approach to enhance the PVAC of the distribution network since VR has the ability to regulate voltage magnitude. The VR is known as the step voltage regulator and includes an autotransformer

[88]. During the voltage regulation process, the voltage magnitude variation can be obtained by changing the number of turns (tap changers) of the series winding of the autotransformer. VR has many advantages, especially fast and efficient operation metrics [87]. To some extent, VR can address the voltage fluctuation problem caused by renewable energy and thus has an influence on PVAC enhancement by alleviating overvoltage violations.

Many heuristic algorithms based approaches have been proposed to find the optimal locations of VRs. In Ref. [89], genetic algorithm (GA) is employed to solve the coordinated VR and capacity bank (CB) planning problem where the multi-objective function is considered. Ref. [90] proposes a local controller model to determine the number and location of VR and GA is also employed to solve this problem. Ref. [91] develops a fuzzy adaptive Particle Swarm Optimization (PSO) algorithm to find the optimal nodes for VR installation in the distribution networks. However, due to the lack of mathematically proven basis for obtaining global optimal solutions, the final results of these heuristic methods may be locally optimal. Also, there are other methods to deal with VR placement problem. In Ref. [92], a multicriteria model, including technical, regulatory, economic and social criteria, is presented to evaluate the prioritizing sites of VR placement in the distribution networks. Ref. [93] presents a plant growth simulation algorithm to select the optimal locations of VR with the consideration of voltage control and loss decrease. Ref. [94] solves the optimal VR placement problem by using a novel multi-objective optimization method, which is based on modified teaching-learning-based optimization (MTLBO) algorithm. Ref. [95] investigates the optimal placement of VR in low voltage(LV) distribution networks by using an existing

method based upon centralized voltage regulation compared to the distributed voltage control schemes. However, these works have no regard for the uncertainties of renewable output and load, which may result in an unreasonable VR placement solution. Besides, these classic works also overlook the potential of VR placement for improving the PVAC. Therefore, this chapter endeavors to improve the PVAC via optimal VR placement in distribution networks.

In this chapter, a novel two-stage stochastic programming based VR placement model considering the PVAC enhancement is presented. The first stage determines the hourly PVAC values and the corresponding VR allocation decisions while the second stage is related to the proposed stochastic feasibility checking model which is imposed to ensure that the distribution network operation always remains secure under different uncertainty scenarios. Firstly, the VR allocation model is formulated as a deterministic mixed integer nonlinear programming (MINLP) problem. Then a technique approach is employed to transform the MINLP model to the mixed integer linear programming (MILP) model. To model the uncertainties of PV generation and load consumption, the scenario method is employed to obtain representative PV-load scenarios, creating a two-stage stochastic MILP problem. The decomposition-based solution method is proposed to solve this two-stage problem. To illustrate the effectiveness of the proposed allocation model and decomposition method, the IEEE 33-node distribution network is utilized as the test system. The major contributions are summarized in threefold as below,

- 1) The main contribution of this work is that it investigates the extent of the potential benefits from optimal VR placement as an option to improve the

hourly PVAC of distribution networks. Considering the widespread application of VR in power systems, this work has practical significance.

2) Two criteria are introduced to maintain the safety and reliability of the distribution network operation, i.e., voltage variation and distribution line capacity. Then a stochastic programming based feasibility check model is proposed to guarantee the security of distribution networks for any considered operation scenarios.

3) Since numerous time-coupled constraints result in a huge computation burden, decomposition algorithm is developed to decompose the two-stage problem into a master program problem (the first-stage problem) and many subprogram problems (the second-stage problems), which can be directly solved by commercial solvers.

The nomenclature of symbols used in this chapter is given as follows,

Sets and Indices

j/J	Index/set of distribution nodes.
t/T	Index/set of time periods.
w/W	Index/set of scenarios.
$i/\varphi(j)$	Index/set of child nodes of node j .
α	Index of piecewise linearization approximation method.
Ω^{AP}/Ω^{RP}	Sets for the quadratic term of active/reactive power.

Variables

P_{jtw}/Q_{jtw}	Active/Reactive power flow at j, t, w .
$P_{jtw}^{QT}/Q_{jtw}^{QT}$	Quadratic terms of active/reactive power flow at j, t, w .
Q_{jtw}^{PV}	Reactive PV output at j, t, w .
V_{jtw}	Node voltage magnitude at j, t, w .
\tilde{V}_{jtw}	Voltage magnitude at the point of VR installation, near to the node j , at t, w .
$rr\%$	Regulator range of VR.

u_j^{VR}	Binary decision variable flagging VR installation or not at j .
u_j^{PV}	Binary decision variable flagging PV energy connection or not at j .
E_j^{PV}	Size of PV integration at j .
Z_j^{PV}	The auxiliary variable representing the bilinear term $u_j^{PV} E_j^{PV}$.
Parameters	
c^{PV}	Subsidy for accommodating capability of PV generation (\$).
c_{inv}^{VR}	The objective coefficient associated with the investment cost of VR devices (\$).
$c_{o\&m}^{VR}$	The objective coefficient associated with the operation and maintenance cost of VR devices (\$/day).
$c^{Penalty}$	The objective coefficient associated with the penalty cost for voltage deviation and overload (\$).
p_w	Probability of the combined scenario w .
C^{VR}	Maximum allowed total VR installation budget.
ξ_{tw}^{PV}	PV output factor (ratio of the accommodating capability of PV generation) at t, w .
κ	Daily capital recovery factor for VR.
r_{ij}/x_{ij}	Resistance/Reactance of the distribution branch ij .
θ_{pv}	Power factor angle for PV power systems.
p_{jtw}/q_{jtw}	Active/Reactive load at j, t, w .
\underline{V}/\bar{V}	Lower/Upper bound of voltage magnitude.
LC_{ij}	The capacity of distribution network branch ij .
SC	The capacity of distribution network substation.
P_{jtw}^{PV}	Active PV output at j, t, w .
\bar{Q}^{PV}	Upper bound of reactive PV output.

4.2 Problem Formulation

4.2.1 Mathematical Formulation based on Deterministic Mixed Integer Nonlinear Programming

In this chapter, the proposed VR placement model considers two goals simultaneously, identifying the optimal VR installation locations and improving hourly PVAC of the distribution network. This optimization model minimizes the sum of VR investment, maintenance and operation cost, and meanwhile maximizes the economic benefits of the PVAC. Based on piecewise linearized DistFlow equations [96], the deterministic formulation can be presented by a MINLP, simplified as DMINLP,

DMINLP:

$$\underset{\Theta^{DMINLP}}{\text{Min}} \sum_{j \in J} (\kappa c_{inv}^{VR} + c_{o\&m}^{VR}) u_j^{VR} - \sum_{t \in T} \sum_{j \in J} c^{PV} \xi_t^{PV} u_j^{PV} E_j^{PV} \quad (4.1)$$

$$\Theta^{DMINLP} = [u_j^{PV}, E_j^{PV}, u_j^{VR}, P_{jt}, Q_{jt}, P_{jt}^{QT}, Q_{jt}^{QT}, Q_{jt}^{PV}, V_{jt}, \tilde{V}_{jt}]$$

Subject to

$$P_{jt} = \sum_{i \in \varphi(j)} P_{it} + \sum_{i \in \varphi(j)} r_{ij} \frac{P_{it}^{QT} + Q_{it}^{QT}}{V_0^2} + P_{jt}^{PV} - p_{jt}, \forall j \in J, \forall t \in T \quad (4.2)$$

$$\text{where } P_{jt}^{PV} = \xi_t^{PV} u_j^{PV} E_j^{PV}$$

$$Q_{jt} = \sum_{i \in \varphi(j)} Q_{it} + \sum_{i \in \varphi(j)} x_{ij} \frac{P_{it}^{QT} + Q_{it}^{QT}}{V_0^2} + Q_{jt}^{PV} - q_{jt}, \forall j \in J, \forall t \in T \quad (4.3)$$

$$P_{jt}^{QT} \geq M_{\alpha jt}^{AP} P_{jt} + N_{\alpha jt}^{AP}, \forall \alpha \in \Omega^{AP}, \forall j \in J, \forall t \in T \quad (4.4)$$

$$Q_{jt}^{QT} \geq M_{\alpha jt}^{RP} Q_{jt} + N_{\alpha jt}^{RP}, \forall \alpha \in \Omega^{RP}, \forall j \in J, \forall t \in T \quad (4.5)$$

$$0 \leq P_{jt}^{QT} \leq \bar{P}^2, \forall j \in J, \forall t \in T \quad (4.6)$$

$$0 \leq Q_{jt}^{QT} \leq \bar{Q}^2, \forall j \in J, \forall t \in T \quad (4.7)$$

$$V_{jt} = V_{it} + \frac{r_{ij} P_{it} + x_{ij} Q_{it}}{V_0}, \forall j \in J \setminus 1, i \in \varphi(j), \forall t \in T \quad (4.8)$$

$$V_{jt} = V^{Sub}, j=1, \forall t \in T \quad (4.9)$$

$$\underline{V} \leq V_{jt} \leq \bar{V}, \forall j \in J, \forall t \in T \quad (4.10)$$

$$\tilde{V}_{jt} = V_{jt} + \frac{r_{ij}P_{it} + x_{ij}Q_{it}}{V_0}, \forall j \in J, i \in \varphi(j), \forall t \in T \quad (4.11)$$

$$(1 - rr\%) \tilde{V}_{jt} \leq V_{jt} \leq (1 + rr\%) \tilde{V}_{jt}, \forall j \in J, \forall t \in T \quad (4.12)$$

$$|V_{jt} - \tilde{V}_{jt}| \leq (\bar{V} - \underline{V}) u_j^{VR}, \forall j \in J, \forall t \in T \quad (4.13)$$

$$\sum_{j \in J} c_{inv}^{VR} u_j^{VR} \leq C^{VR} \quad (4.14)$$

$$u_j^{PV} \in [0, 1], u_j^{PV} \in R, j \in J \quad (4.15)$$

$$E_j^{PV} \geq 0, j \in J \quad (4.16)$$

$$-\bar{Q}_{jt}^{PV} \leq Q_{jt}^{PV} \leq \bar{Q}_{jt}^{PV}, j \in J, \forall t \in T \quad (4.17)$$

$$\text{where } \bar{Q}_{jt}^{PV} = P_{jt}^{PV} \tan \theta^{PV}$$

where the objective function (4.1) consists of two terms: the first term is the sum of investment, maintenance and operation cost of VR and the second term is daily economic benefit obtained from the PVAC. PV energy output factor ξ_t^{PV} represents the ratio of the PVAC $u_j^{PV} E_j^{PV}$, which is introduced to capture the hourly generation of PV generators, so the PV energy out P_{jt}^{PV} can be obtained, $P_{jt}^{PV} = \xi_t^{PV} u_j^{PV} E_j^{PV}$. To match the unit of daily VR maintenance and operation cost $c_{o\&m}^{VR}$, daily capital recovery factor $\kappa = \frac{r^{VR}(1+r^{VR})^y}{365((1+r^{VR})^y - 1)}$ is employed to transfer the VR investment cost c_{inv}^{VR} from planning horizon to daily horizon, where r^{VR} is the interest rate and y is the planning horizon. Note that the coefficient c^{PV} , representing the subsidy for the PVAC, is introduced to sum these two objectives in the single-dimensional case, e.g. \$.

The actual value of c^{PV} is governed by practical considerations according to the preference of distribution network planners and have to be established on a case by case basis. For example, if the distribution network needs to obtain a relatively high PVAC, then the value of c^{PV} should be adjusted to be large.

To deal with nonlinearity caused by quadratic terms, like P_{it}^2 and Q_{it}^2 , the piecewise linearized DistFlow model [96] is utilized. This model linearizes the quadratic terms P_{it}^2 and Q_{it}^2 , so the apparent power flow can be calculated more accurately. Constraints (4.2)-(4.10) are related to piecewise linearized DistFlow model, which describes the complex power flows at the node j in a distribution network. (4.2) and (4.3) describe the active and reactive power flow balance, respectively. The quadratic terms P_{jt}^{QT} and Q_{jt}^{QT} are employed to estimate P_{jt}^2 and Q_{jt}^2 with two auxiliary inequality constraints (4.4) and (4.5) so P_{jt}^{QT} and Q_{jt}^{QT} can be estimated by applying the piecewise linearization approximation (PLA) approach. (4.6) and (4.7) define the limits of active and reactive quadratic power flows P_{jt}^{QT} and Q_{jt}^{QT} , respectively. (4.8) denotes the voltage along the distribution line ij , (4.9) gives the voltage of the substation and (4.10) includes the voltage magnitude limits.

Constraints (4.11)-(4.14) are related to the ideal VR model, as shown in Fig. 4-1. For the simplification, it is assumed that each VR has a regulator range of $rr\%$ and the VR tap position is considered as a continuous variable [97]. (4.11) describes the voltage transit along the distribution branch between the node i and the VR installation point. (4.12) and (4.13) describe the relationship of the voltage magnitude between the VR installation point and the node j . Note that if $u_j^{VR} = 0$, (without VR installation), then $V_{jt} = \tilde{V}_{jt}$,

otherwise, V_{jt} varies in the range of $[(1 - rr\%), (1 + rr\%)]\tilde{V}_{jt}$. Besides, (4.14) considers the practical total VR capital cost limit.

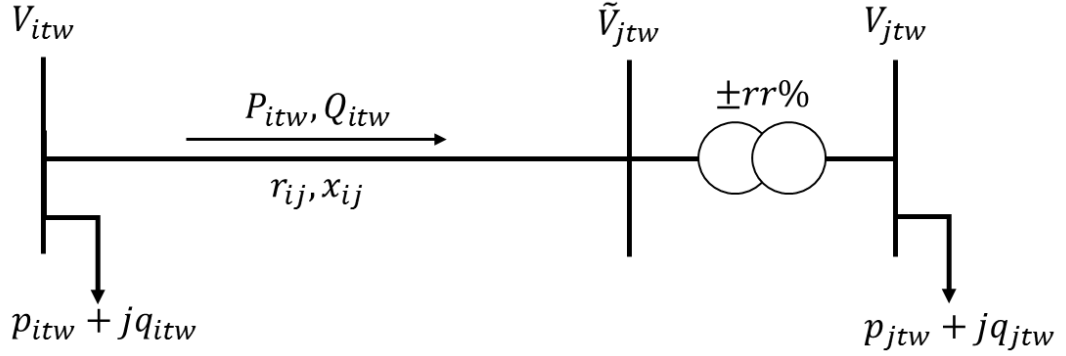


Fig. 4-1 One distribution branch diagram with a voltage regulator

Constraints (4.15)-(4.17) are related to the PVAC limits. In (4.15), the binary variable u_j^{PV} represents whether the PV generation is connected to the node j . The continuous variable E_j^{PV} in (4.16) denotes the size of PV generation connected to the node j and this constraint guarantees that E_j^{PV} is non-negative. In this thesis, it is assumed that PV systems can provide reactive power support to the distribution network, the range of reactive power output is given in (4.17).

4.2.2 Linearization Techniques for DMINLP Model

Note that the proposed DMINLP problem (4.1)-(4.17) cannot be directly solved by some cutting-edge solvers, such as CPLEX and GUROBI, since this problem is nonconvex due to the presence of the bilinear term $E_j^{PV}u_j^{PV}$. To reduce the computational complex, a continuous variable Z_j^{PV} is introduced to replace the bilinear term $E_j^{PV}u_j^{PV}$, in other words, $Z_j^{PV} = E_j^{PV}u_j^{PV}$. Then the following inequations should be considered,

$$0 \leq Z_j^{PV} \leq u_j^{PV} B^M, \forall j \in J \quad (4.18)$$

$$Z_j^{PV} \leq E_j^{PV}, \forall j \in J \quad (4.19)$$

$$Z_j^{PV} + B^M - E_j^{SVC} - u_j^{PV} B^M \geq 0, \forall j \in J \quad (4.20)$$

where B^M is a quite large positive constant.

By doing so, the deterministic mixed integer linear programming (DMILP) model can be written as follows,

DMILP:

$$\text{Min}_{\Theta^{DMILP}} \sum_{j \in J} (\kappa c_{inv}^{VR} + c_{o\&m}^{VR}) u_j^{VR} - \sum_{t \in T} \sum_{j \in J} c^{PV} \xi_t^{PV} Z_j^{PV} \quad (4.21)$$

$$\Theta^{DMILP} = [u_j^{PV}, E_j^{PV}, Z_j^{PV}, u_j^{VR}, P_{jt}, Q_{jt}, P_{jt}^{QT}, Q_{jt}^{QT}, Q_{jt}^{PV}, V_{jt}, \tilde{V}_{jt}]$$

Subject to

$$(4.2)-(4.17) \quad (4.22)$$

$$(4.18)-(4.20) \quad (4.23)$$

$$\text{where } P_{jt}^{PV} = \xi_t^{PV} Z_j^{PV}, \forall j \in J, \forall t \in T$$

where the objective (4.21) in the DMILP formulation is the same as (4.1) in DMINLP formulation except the bilinear term $u_j^{PV} E_j^{PV}$ is replaced by the auxiliary continuous variable Z_j^{PV} . The constraint set (4.22) refers to the constraints (4.2)-(4.17) of the DMINLP formulation and the constraint set (4.23) refers to the constraints (4.18)-(4.20) which are included to make the equation $Z_j^{PV} = u_j^{PV} E_j^{PV}$ workable.

4.2.3 Stochastic Programming based Feasibility Checking Model

The proposed DMILP model (4.21)-(4.23) determines the optimal placement solution from the economic aspects without considering the reliability and security of the distribution network operation. Due to time-

varying load demand and uncertain PV energy output, these two uncertainties should be incorporated in the DMILP model. In this thesis, the scenario approach is employed since it allows us to take representative combinations of load and PV generation into account with reasonable computation complexity. By using the scenario approach, uncertainties of load demand and PV output can be denoted in the form of daily uncertainty scenarios which can be sampled from historical data in [71] and then a well-established backward-reduction algorithm [98] is utilized for representative scenarios selection since this reduction algorithm can generate the probability of each scenario. Note that these associated probabilities have a direct effect on the optimal solutions since they are able to distinguish the significance of scenarios.

Finally, a set of probabilistic scenarios describing most potential load and PV production can be acquired, which transforms the DMILP model described above to a two-stage stochastic model, as shown in Fig. 4-2 and Fig. 4-3. Specifically, in the first stage, the hourly PVAC and VR placement decisions are determined. Then in the second stage, considering the uncertainties of PV output and load demand, the feasibility of the first-stage results is checked to ensure no operation constraints violations, especially node voltage constraints violations and distribution line capacity constraints violations.

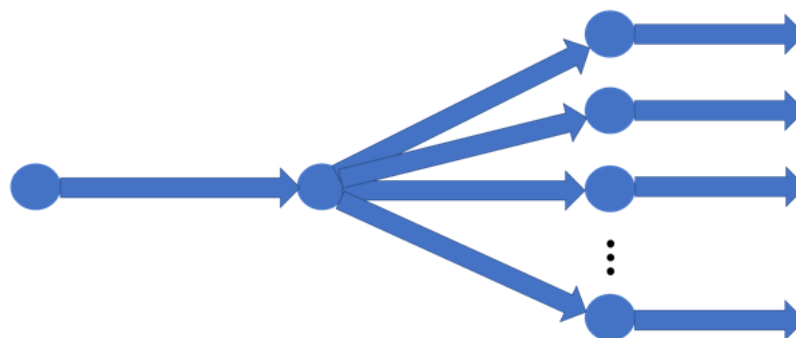


Fig. 4-2 Decision-making process of the proposed VR placement problem

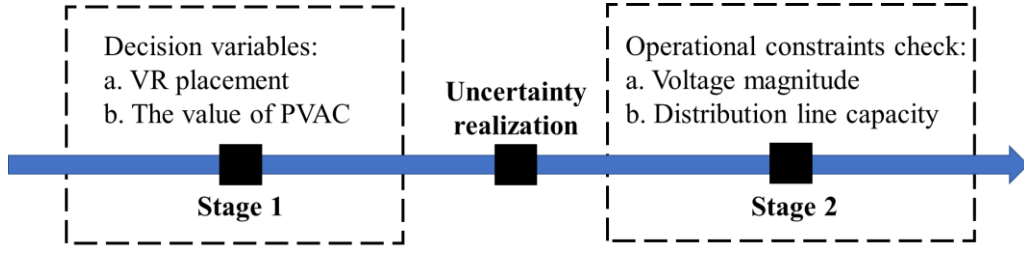


Fig. 4-3 Two-stage stochastic framework of the proposed voltage regulator placement problem

In this regard, the feasibility checking constraints should be added into the DMILP formulation to ensure that the distribution network is able to remain secure under any considered operation scenarios. To guarantee the reliability and safety of the distribution network operation, the technical constraint should not be violated. Hence, non-negative slack variables are introduced to relax the voltage constraints and distribution line capacity constraints and then the stochastic programming based feasibility checking (SPFC) model is formulated as follows,

SPFC:

$$\text{Min} \text{ Min}_{\Theta_1 \in \Pi^1} \sum_{w \in W} \sum_{t \in T} \sum_{j \in J} c^{Penalty} (s_{jtw}^{V,LB} + s_{jtw}^{V,UB} + s_{jtw}^{PQ}) \quad (4.24)$$

where $s_{jtw}^{V,LB}$ and $s_{jtw}^{V,UB}$ represent the slack variables for upper voltage and lower voltage constraints, respectively. s_{jtw}^{PQ} denotes the slack variable for distribution line capacity constraints. Since the positive penalty coefficient $c^{Penalty}$ is large enough, the value (4.24) should be zero since all slack variables $s_{jtw}^{V,LB}$, $s_{jtw}^{V,UB}$ and s_{jtw}^{PQ} will converge to zero.

The uncertainty set Π^1 and the first-stage variables describing the uncertainty Θ_1 are given as follows,

$$\Pi^1 = \{\Theta_1 | \Theta_1 = [u_j^{PV}, E_j^{PV}, Z_j^{PV}, u_j^{VR}]\}$$

$$(4.14)-(4.16) \quad (4.25)$$

$$(4.18)-(4.20) \quad (4.26)$$

where (4.25) describes the first-stage constraints as described in the (4.14)-(4.16) of the DMINLP model and (4.26) represents the auxiliary constraints (4.18)-(4.20) which are imposed to linear the DMINLP model.

The uncertainty set Π^2 and the second-stage variables describing the uncertainty Θ_2 are given as follows,

$$\Pi^2 = \{\Theta_2 | \Theta_2 = [P_{jtw}, Q_{jtw}, P_{jtw}^{QT}, Q_{jtw}^{QT}, Q_{jtw}^{PV}, V_{jtw}, \tilde{V}_{jtw}, S_{jtw}^{V, LB}, S_{jtw}^{V, UB}, S_{jtw}^{PQ}]\}$$

$$P_{jtw} = \sum_{i \in \varphi(j)} P_{itw} + \sum_{i \in \varphi(j)} r_{ij} \frac{P_{itw}^{QT} + Q_{itw}^{QT}}{V_0^2} + P_{jtw}^{PV} - p_{jtw}, \forall j \in J, \forall t \in T, \forall w \in W \quad (4.27)$$

$$\text{where } P_{jtw}^{PV} = \xi_{tw}^{PV} Z_j^{PV}$$

$$Q_{jtw} = \sum_{i \in \varphi(j)} Q_{itw} + \sum_{i \in \varphi(j)} x_{ij} \frac{P_{itw}^{QT} + Q_{itw}^{QT}}{V_0^2} + Q_{jtw}^{PV} - q_{jtw}, \forall j \in J, \forall t \in T, \forall w \in W \quad (4.28)$$

$$P_{jtw}^{QT} \geq M_{\alpha jtw}^{AP} P_{jtw} + N_{\alpha jtw}^{AP}, \forall \alpha \in \Omega^{AP}, \forall j \in J, \forall t \in T, \forall w \in W \quad (4.29)$$

$$Q_{jtw}^{QT} \geq M_{\alpha jtw}^{RP} Q_{jtw} + N_{\alpha jtw}^{RP}, \forall \alpha \in \Omega^{RP}, \forall j \in J, \forall t \in T, \forall w \in W \quad (4.30)$$

$$0 \leq P_{jtw}^{QT} \leq \bar{P}^2, \forall j \in J, \forall t \in T, \forall w \in W \quad (4.31)$$

$$0 \leq Q_{jtw}^{QT} \leq \bar{Q}^2, \forall j \in J, \forall t \in T, \forall w \in W \quad (4.32)$$

$$V_{jtw} = V_{itw} + \frac{r_{ij} P_{itw} + x_{ij} Q_{itw}}{V_0}, \forall j \in J, i \in \varphi(j), \forall t \in T, \forall w \in W \quad (4.33)$$

$$V_{jtw} = V^{Sub}, j=1, \forall t \in T, \forall w \in W \quad (4.34)$$

$$\tilde{V}_{jtw} = V_{itw} + \frac{r_{ij} P_{itw} + x_{ij} Q_{itw}}{V_0}, \forall j \in J, i \in \varphi(j), \forall t \in T, \forall w \in W \quad (4.35)$$

$$(1-rr\%)\tilde{V}_{jtw} \leq V_{jtw} \leq (1+rr\%)\tilde{V}_{jtw}, \forall j \in J, \forall t \in T, \forall w \in W \quad (4.36)$$

$$|V_{jtw} - \tilde{V}_{jtw}| \leq (\bar{V} - \underline{V})u_j^{VR}, \forall j \in J, \forall t \in T, \forall w \in W \quad (4.37)$$

$$-\bar{Q}_{jtw}^{PV} \leq Q_{jtw}^{PV} \leq \bar{Q}_{jtw}^{PV}, j \in J, \forall t \in T, \forall w \in W \quad (4.38)$$

$$\text{where } \bar{Q}_{jtw}^{PV} = P_{jtw}^{PV} \tan\theta^{PV}$$

$$V_{jtw} + s_{jtw}^{V,LB} \geq \underline{V}, \forall j \in J, \forall t \in T, \forall w \in W \quad (4.39)$$

$$V_{jtw} - s_{jtw}^{V,UB} \leq \bar{V}, \forall j \in J, \forall t \in T, \forall w \in W \quad (4.40)$$

$$P_{jtw}^{QT} + Q_{jtw}^{QT} - s_{jtw}^{PQ} \leq LC_{ij}^2, \forall j \in J \setminus 1, \forall t \in T, \forall w \in W \quad (4.41)$$

$$P_{jtw}^{QT} + Q_{jtw}^{QT} - s_{jtw}^{PQ} \leq SC^2, j=1, \forall t \in T, \forall w \in W \quad (4.42)$$

$$s_{jtw}^{V,LB}, s_{jtw}^{V,UB}, s_{jtw}^{PQ} \in R^+, \forall j \in J, \forall t \in T, \forall w \in W \quad (4.43)$$

where (4.27)-(4.43) are the second-stage constraints. (4.27)-(4.34) describe the power flow in the scenario w . (4.35)-(4.37) represent the voltage regulator operation in the scenario w . (4.38) limits the reactive PV energy output in the scenario w . (4.39)-(4.43) describe the relaxed voltage constraints with the non-negative slack variables $s_{jtw}^{V,LB}$, $s_{jtw}^{V,UB}$ and the relaxed distribution line capacity constraints with non-negative slack variable s_{jtw}^{PQ} .

4.2.4 Final Formulation of Stochastic VR Placement Model

The two-stage stochastic MILP (SMILP) model is finally formulated by integrating the SPFC model (4.27) into the DNILP model, given as follows,

SMILP:

$$\begin{aligned} \text{Min}_{\Theta_1, \Theta_2} & \sum_{j \in J} (\mathcal{K}c_{inv}^{VR} + c_{ope}^{VR})u_j^{VR} - \sum_{w \in W} P_w \sum_{t \in T} \sum_{j \in J} c^{PV} \xi_{tw}^{PV} Z_j^{PV} \\ & + \sum_{w \in W} \sum_{t \in T} \sum_{j \in J} c^{Penalty} (s_{jtw}^{V,LB} + s_{jtw}^{V,UB} + s_{jtw}^{PQ}) \end{aligned} \quad (4.44)$$

$$\Theta_1 = [u_j^{PV}, E_j^{PV}, Z_j^{PV}, u_j^{VR}]$$

$$\Theta_2 = [P_{jtw}, Q_{jtw}, P_{jtw}^{QT}, Q_{jtw}^{QT}, Q_{jtw}^{PV}, V_{jtw}, \tilde{V}_{jtw}, s_{jtw}^{V,LB}, s_{jtw}^{V,UB}, s_{jtw}^{PQ}]$$

Subject to

$$(4.14)-(4.16), (4.18)-(4.20) \quad (4.45)$$

$$(4.27)-(4.43) \quad (4.46)$$

where (4.45) and (4.46) formulate the first-stage constraints and second-stage constraints, respectively. Note that the sum of all probabilities of uncertainty scenarios should be equal to one, $\sum_w p_w = 1$.

4.3 Decomposition Algorithm for Solving SMILP

Due to numerous uncertainty scenarios and time-coupling constraints, the computation burden of the proposed two-stage SMILP problem (4.44)-(4.46) is quite heavy. Fortunately, the two-stage structure of SMILP formulation permits decomposing this model into a master program corresponding to the first-stage problem and subprograms corresponding to the second-stage problems of all time periods in all scenarios, which can significantly reduce the computation complexity. Therefore, Benders decomposition algorithm [76] can be properly applied to solve this intractable two-stage problem.

4.3.1 Subprograms Formulation

Each subprogram is associated with each time period in each considered uncertainty. After solving all subprogram problems, operation variables can be obtained. The subprogram (SP) formulation in each iteration v is given as follows, SP:

$$Z_{tw}^{Sub(v)} := \text{Min}_{\Theta^{SP}} \sum_{j \in J} c^{Penalty} (s_{jtw}^{V, LB} + s_{jtw}^{V, UB} + s_{jtw}^{PQ}) \quad (4.47)$$

$$\Theta^{SP} = \{Z_{tw}^{sub(v)}, P_{jtw}^{(v)}, Q_{jtw}^{(v)}, P_{jtw}^{QT(v)}, Q_{jtw}^{QT(v)}, Q_{jtw}^{PV(v)}, V_{jtw}^{(v)}, \tilde{V}_{jtw}^{(v)}, s_{jtw}^{V, LB(v)}, s_{jtw}^{V, UB(v)}, s_{jtw}^{PQ(v)}\}$$

Subject to

$$(4.27)-(4.43) \quad (4.48)$$

$$Z_j^{PV(v)} = Z_j^{PV*} : \lambda_{jtw}^{PV(v)}, \forall j \in J, \forall t \in T, \forall w \in W \quad (4.49)$$

$$u_j^{VR(v)} = u_j^{VR*} : \lambda_{jtw}^{VR(v)}, \forall j \in J, \forall t \in T, \forall w \in W \quad (4.50)$$

The objective function (4.47) is to minimize the objective value of the feasibility checking model (SFC) to ensure the constraints security of the distribution networks. (4.48) summarizes the second-stage constraints. (4.49) and (5.50) fix the first-stage variables $Z_j^{PV(v)}$ and $u_j^{VR(v)}$ to the given value obtained from the solution of the master problem in each iteration v , respectively.

The upper bound $Z^{Upper(v)}$ for the optimal value of the objective function in the SMILP problem in each iteration v can be calculated by the following equation,

$$\begin{aligned} Z^{Upper(v)} = & \sum_{w \in W} \rho_w \sum_{t \in T} Z_{tw}^{Sub(v)} + \sum_{j \in J} (\kappa c_{inv}^{VR} + c_m^{VR}) u_j^{VR(v)} \\ & - \sum_{w \in W} p_w \sum_{t \in T} \sum_{j \in J} c_{tw}^{PV} \xi_{tw}^{PV} Z_j^{PV} \end{aligned} \quad (4.51)$$

Dual variables $\lambda_{jtw}^{PV(v)}$ and $\lambda_{jtw}^{VR(v)}$ of the first-stage variables can be used to provide sensitivities $\lambda_j^{PV(v)}$ and $\lambda_j^{VR(v)}$, which are further fed into the master problem to build the Benders cut, linking the subproblem and the master problem. These sensitivities can be acquired from the following equations,

$$\lambda_j^{PV(v)} = \sum_w \rho^W \sum_t \lambda_{jtw}^{PV(v)}, \forall j \in J, \forall t \in T, \forall w \in W \quad (4.52)$$

$$\lambda_j^{VR(v)} = \sum_w \rho^W \sum_t \lambda_{jtw}^{VR(v)}, \forall j \in J, \forall t \in T, \forall w \in W \quad (4.53)$$

4.3.2 Master Program Formulation

The hourly PVAC values and VR placement decisions are determined in the master problem, which is subject to the first-stage constraints. The master program (MP) formulation in each iteration v is given as follows,

MP:

$$Z^{Lower(v)} := \underset{\Xi^{MP}}{\text{Min}} \gamma^{(v)} + \sum_{j \in J} (\kappa c_{inv}^{VR} + c_m^{VR}) u_j^{VR(v)} - \sum_{w \in W} p_w \sum_{t \in T} \sum_{j \in J} c^{PV} \xi_{tw}^{PV} Z_j^{PV} \quad (4.54)$$

$$\Theta^{MP} = \{Z^{Lower(v)}, \gamma^{(v)}, u_j^{PV(v)}, E_j^{PV(v)}, Z_j^{PV(v)}, u_j^{VR(v)}\}$$

Subject to

$$(4.14)-(4.16), (4.18)-(4.20) \quad (4.55)$$

$$\begin{aligned} \gamma^{(v)} \geq & \sum_{w \in W} \rho_w \sum_{t \in T} Z_{tw}^{Sub(k)} + \sum_{j \in J} \lambda_j^{VR(v)} (u_j^{VR(v)} - u_j^{VR(\tau)}) \\ & + \sum_{j \in J} \lambda_j^{PV(v)} (Z_j^{PV(v)} - Z_j^{PV(\tau)}) \quad \tau = 1, 2, \dots, v-1 \end{aligned} \quad (4.56)$$

$$\gamma^{(v)} \geq \gamma^{down} \quad (4.57)$$

$$Z^{Lower(v)} \leq Z^{Opt} \quad (4.58)$$

The objective value of the master problem (4.54) is the lower bound of the SMILP problem in each iteration v since the master program relaxes the second-stage constraints. (4.55) summarizes the first-stage constraints. (4.56) represents the Benders cut $\gamma^{(v)}$, which is generated to link the master problem and the subproblem in each iteration. (4.57) gives a lower bound γ^{down} of $\gamma^{(v)}$ to accelerate the convergence. (4.58) is to ensure that the lower bound

$Z^{Lower(v)}$ is not greater than the minimum optimal solution value Z^{Opt} acquired from the subproblem.

4.3.3 Solution Algorithm Process

The convergence is guaranteed until the upper bound meets the lower bound according to [79]. The proposed Benders decomposition algorithm procedure is as follows,

Algorithm 1 Benders Decomposition Algorithm

Step 1. Initialization:

- a) Set the iteration counter $v = 0$, $Z^{Lower(v)} = -\infty$, $Z^{Upper(v)} = -\infty$, $Z^{Opt} = \infty$.
- b) Set a small tolerance ε to control convergence.

Step 2. Iteration:

- a) Solve MP and update $Z_j^{PV(v)}$ and $u_j^{VR(v)}$ and $Z^{Lower(v)}$.
- b) For each $t \in T$, $w \in W$, solve SP and update $Z^{Upper(v)}$.
- c) If $Z^{Upper(v)} < Z^{Opt}$, then update $Z^{Opt} = Z^{Upper(v)}$.

Step 3. Convergence check: If $|Z^{Upper(v)} - Z^{Lower(v)}| \leq \varepsilon$, terminate the iteration with an optimal solution. Otherwise, build the next Benders cut, update $v \leftarrow v + 1$ and continue from Step 2.

4.4 Numerical Results

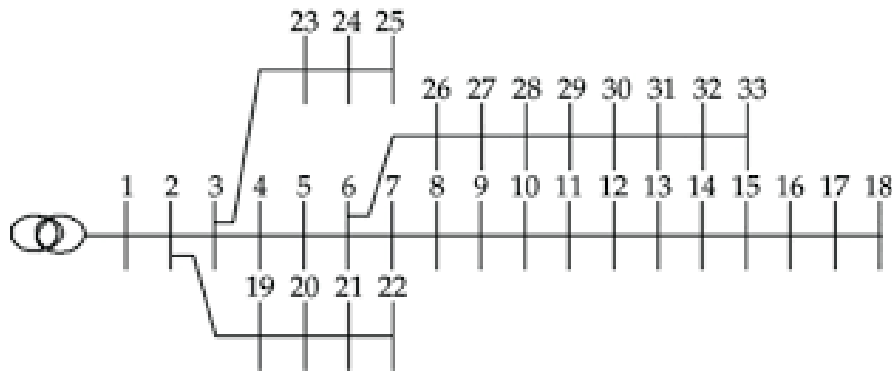


Fig. 4-4 IEEE 33-node test distribution system

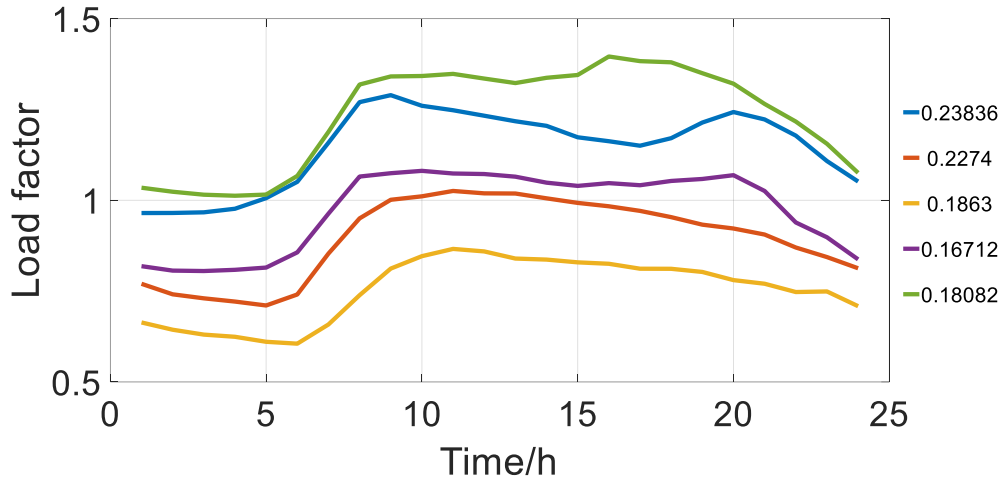


Fig. 4-5 Load factor

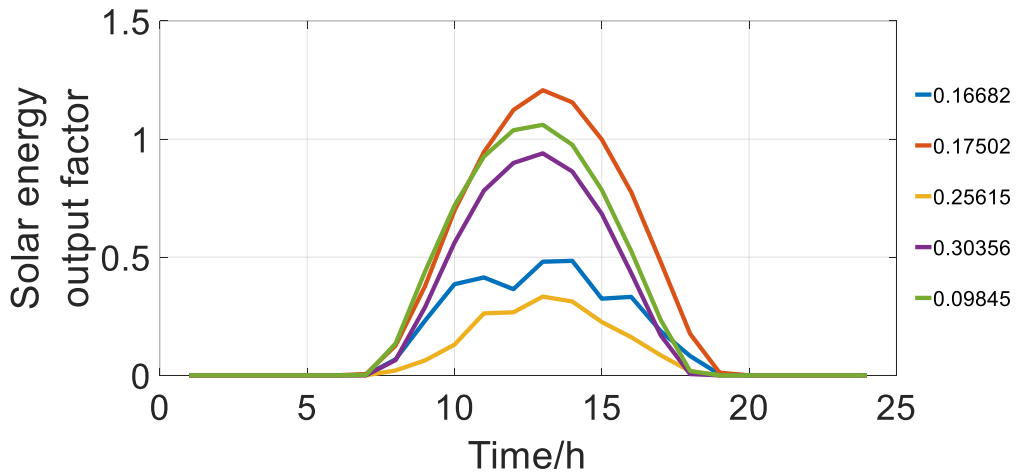


Fig. 4-6 Solar energy output factor

The performance of the proposed method is validated on the IEEE 33-node distribution system, as shown in Fig. 4-4. Details about this test system can be found in [99]. In this case study, the base energy value is 1 MVA and the base voltage value is 12.66 kV. The per-unit value is used. A five-year planning horizon is taken into consideration. One thousand scenarios are sampled from the history data and 125 representative ones ($5*5*5$) with probabilities are selected as representatives in the proposed model, as shown in Fig. 4-5 and Fig. 4-6.

4.4.1 Performance of Computational Efficiency

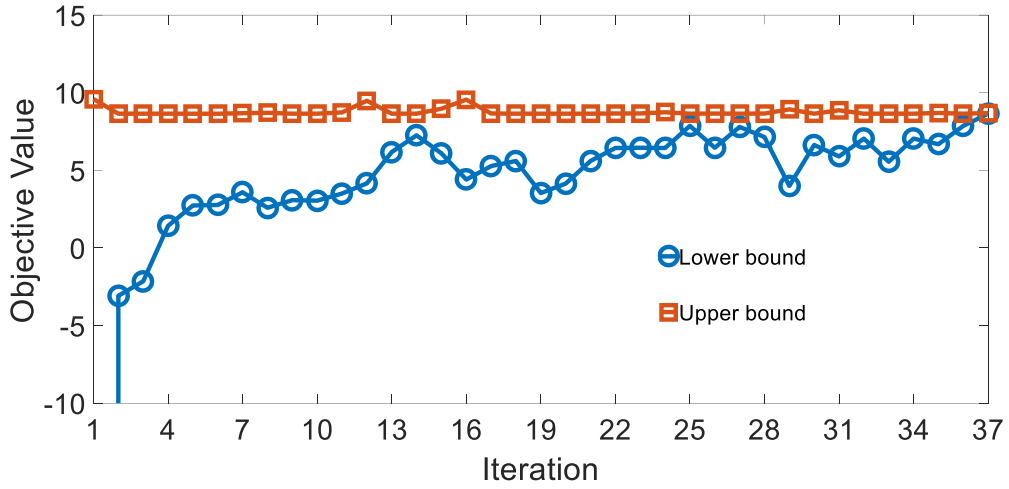


Fig. 4-7 Evolution of Benders decomposition algorithm

Table 4-1 Comparison of computation time by two methods

Scenario number	Computation time (min)	
	CVX_GUROBI	BD
1 (1*1*1)	0.22	0.19
8 (2*2*2)	27.36	4.57
27 (3*3*3)	132.27	18.56
64 (4*4*4)	N.A.	53.33
125 (5*5*5)	N.A.	105.28

Fig. 4-7 depicts the evolution of the proposed Benders decomposition algorithm. In the 37th iteration, this algorithm converges, where the gap between the upper bound $Z^{Upper(v)}$ and the lower bound $Z^{Lower(v)}$ is smaller than the predefined toleration ε . To demonstrate the performance of the computational efficiency of the developed solution approach, a comparison between different solution methods is conducted. The first method is based on

the widely-used solver GUROBI [78] with the platform of CVX [81], marked as CVX_GUROBI. The second method is the proposed solution method, which is based on Benders decomposition algorithm via the same commercial solver and platform, marked as BD. As shown in Table 4-1, both two solution methods can be used to solve the proposed problem with low considered scenario numbers (e.g. 1, 8, 27) while the proposed method shows a clear advantage over the first method, and this advantage widened as the scenario number increases. With high scenarios numbers (e.g. 64, 125), the original problem cannot be directly solved by the first solution method due to huge computation burden. By contrast, the solution algorithm is able to solve the same problem with acceptable computation time.

4.4.2 Performance of Optimal VR Placement

Table 4-2 The result of the daily PVAC in the 33-node test system

Locations for PV generation connection (node)	ACPVG for PV generation location (p.u.)
5	0.0187
10	0.0028
16	0.0042
21	0.0044
23	0.0123
27	0.0010
32	0.0010

Table 4-3 The result of VR placement in the 33-node test system

VR allocation locations (node)	5, 6, 22, 25, 26, 28, 30, 31
--------------------------------	------------------------------

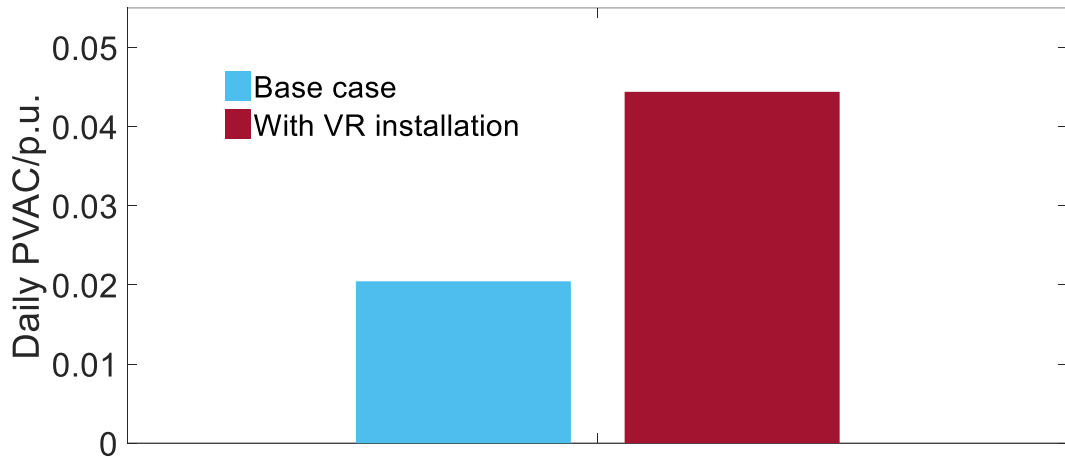


Fig. 4-8 Comparison on daily PVAC

In this subsection, the performance of optimal VR placement is demonstrated. It can be seen from Table 4-2 that the daily PVAC is 0.0444 p.u. and Table 4-3 shows the corresponding VR placement decisions. In order to demonstrate the performance of VR placement on the PVAC enhancement, Case 1 (the base case without VR installation), and Case 2 (the case with VR installation as the result in Table 3) are compared, as shown in Fig. 4-8. It can be observed from this figure that the daily PVAC is of Case 2 significantly larger than that of the Case 1, in other words, the daily PVAC is significantly improved after VR installation.

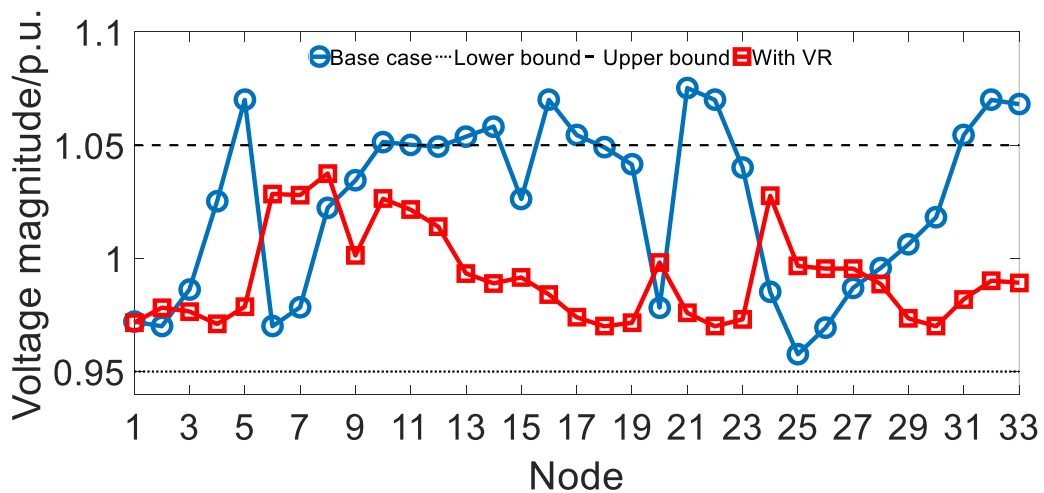


Fig. 4-9 Comparison on voltage magnitude

Fig. 4-9 depicts two voltage profiles at 12:00 pm under the expected scenario: (1) voltage profile of the case with PV integration as the result in Table 2 but without VR installation, and (2) voltage profile of the case with both PV integration and VR installation, as the results in Table 2 and Table 3. It can be observed from this figure that the voltage magnitudes on some nodes (i.e. nodes 5, 14, 16, 17, 21, 22, 31, 32, and 33) exceed the upper bound (1.05 p.u.) in the first case due to lack of the voltage adjustment of VR. However, the overvoltage violations caused by high PV penetration is able to be avoided after optimal VR placement, as shown in the second case.

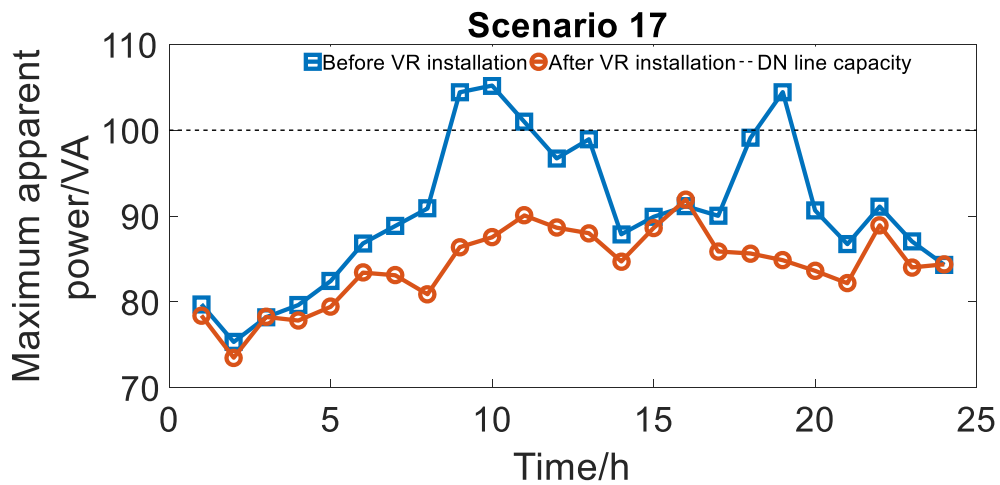


Fig. 4-10 Comparison of maximum apparent power in scenario 17

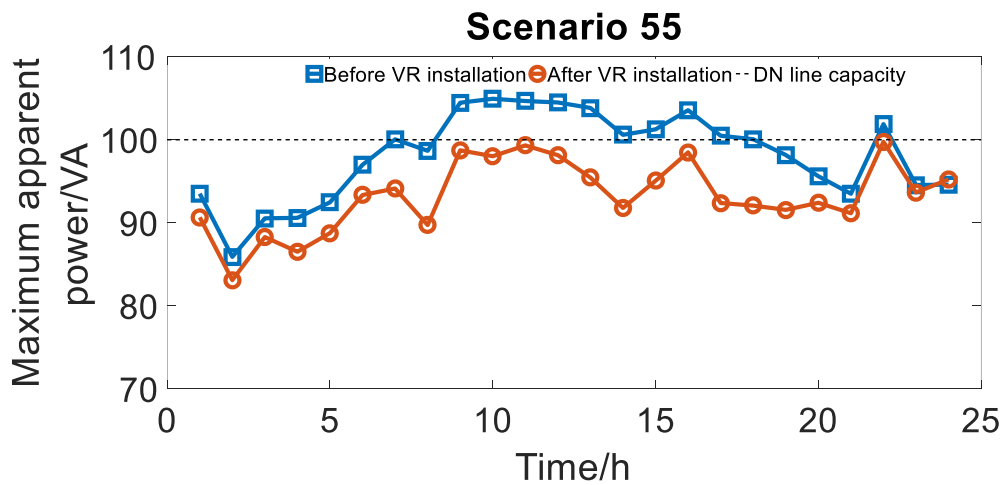


Fig. 4-11 Comparison of maximum apparent power in scenario 55

Fig. 4-10 and Fig. 4-11 show the comparison results about the apparent power of the 33-node test system in two representative scenarios, i.e. scenario 17 and scenario 55. Note the apparent power S_{jtw} can be calculated by using the following equation,

$$S_{jtw} = \sqrt{P_{jtw}^{QT} + Q_{jtw}^{QT}}, \forall j \in J \setminus 1, \forall t \in T, \forall w \in W \quad (4.63)$$

As shown in these two figures, before VR installation, distribution line overload can be observed. By comparison, after VR installation, apparent power flow is maintained within its desired range. According to these two comparisons, it can be concluded that optimal VR allocation cannot only avoid overvoltage occurrence but also ensure the safe and reliable operation of distribution lines.

4.4.3 Comparison with Deterministic Model

In this subsection, the deterministic VR placement model is employed as a benchmark. The formulation of the deterministic optimal VR placement problem is similar to the stochastic model but the deterministic model only uses one operation scenario as its input, in which the PV output and load demand are replaced by their expected values. By solving the deterministic VR placement problem, the optimal VR installation sites can be obtained: nodes 15, 16, 19, 21, 23, and 27. Together with deterministic VR placement decisions, the daily PVAC values are obtained: 0.0106, 0.0001, 0.0007, 0.0064, 0.0021, 0.0036 and 0.0079 p.u. for nodes 5, 10, 16, 21, 23, 27 and 32, respectively.

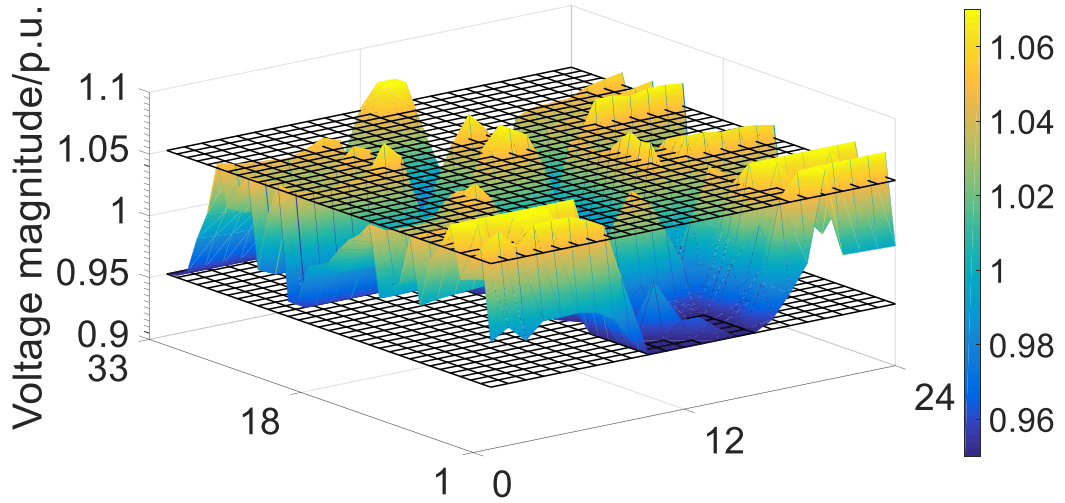


Fig. 4-12 Voltage profile of the deterministic model under the critical scenario

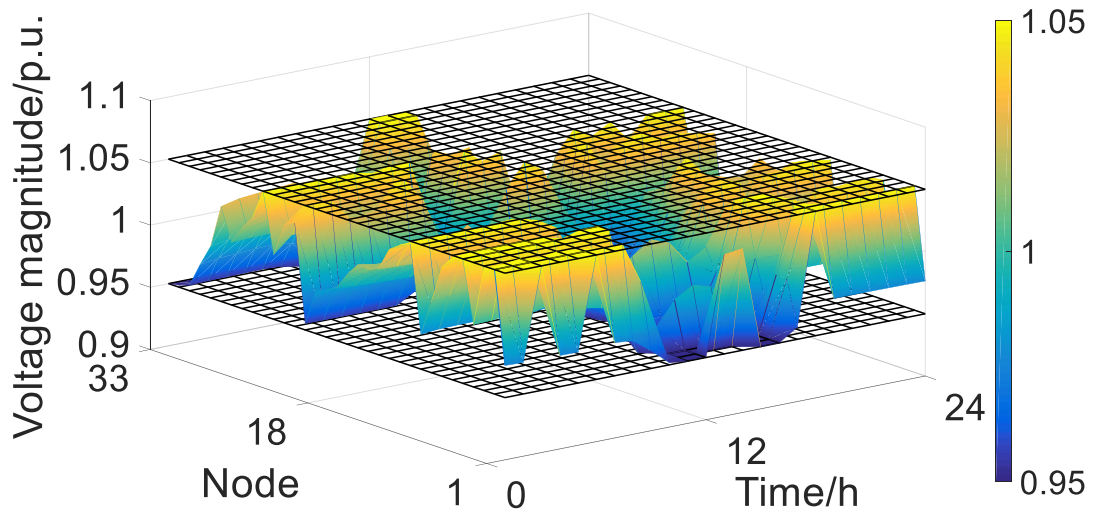


Fig. 4-13 Voltage profile of the stochastic model under the critical scenario

To compare the performance of the deterministic model and the stochastic model, a critical scenario corresponds to the maximum PV output factor μ_{tw}^{PV} with minimum load demand level is utilized. Fig. 4-12 and Fig. 4-13 depict the voltage profiles of the deterministic model and stochastic model under this critical scenario, respectively. From these two figures, overvoltage violation can be seen in Fig. 4-12 while this violation cannot be observed in Fig. 4-13.

Therefore, it can be concluded that the stochastic model shows a better performance on voltage profiles under the critical scenario. This is because the stochastic model takes numerous representative scenarios into account and thus its solution is more comprehensive and robust when dealing with the uncertainties of electrical networks.

4.4.4 Tradeoff Curve between Daily PVAC and VR Planning Cost

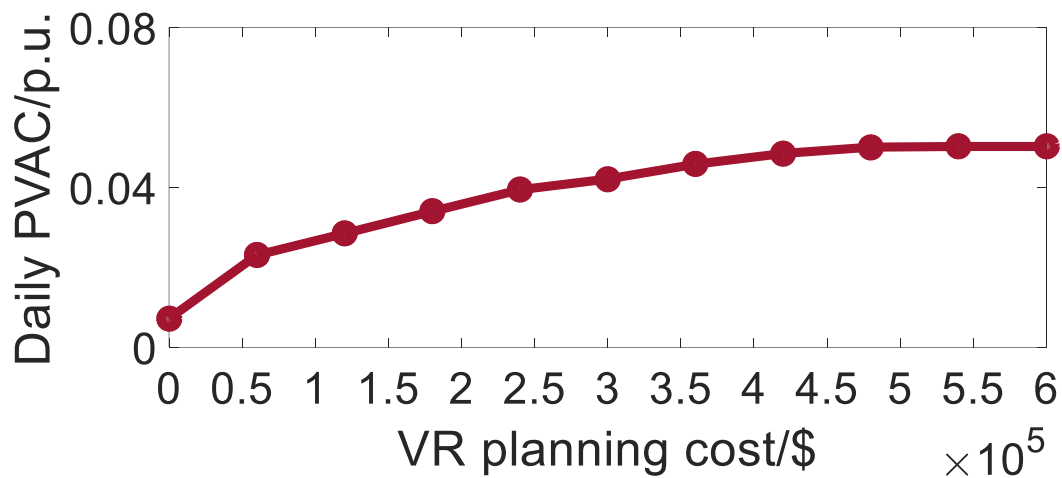


Fig. 4-14 Optimal tradeoff curve between the daily PVAC and VR planning cost

The tradeoff curve between daily PVAC and VR planning cost (including the cost of investment, operation and maintenance) is depicted in Fig. 4-14. It can be seen from this figure that the PVAC enhances gradually with the increase of the VR planning cost until it reaches around \$450,000. Then the increasing rate becomes zero, which means the PVAC is insensitive to the additional VR planning cost after it exceeds \$450,000. The reason is that there is a threshold determined by the loadability of the distribution network, so overload may occur with the large PV energy integration. When the PVAC

improvement is too low to be accepted by distribution network planners, the network expansion is recommended.

4.4.5 Impact of VR Installation Number on PVAC Enhancement

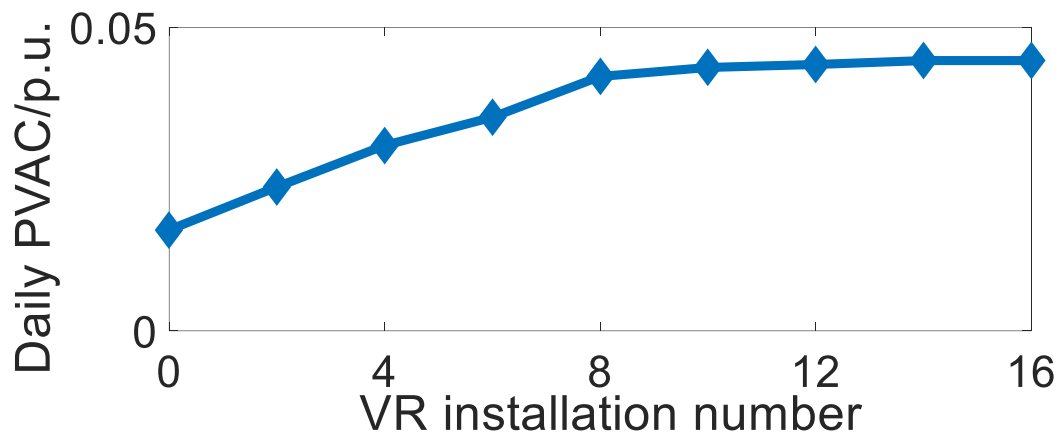


Fig. 4-15 Impact of VR installation number on PVAC

A sensitivity analysis is conducted to investigate the impact of the VR installation number on PVAC enhancement in this subsection. Fig. 4-15 depicts the impact of VR installation number on the daily PVAC under the expected scenario. As seen in this figure, with the increase of the VR installation number, the PVAC improves linearly until the VR installation number reaches eight. Then the PVAC increases slowly until the installation number reaches twelve, after which the PVAC becomes insensitive to the increase of VR installation number. This is because larger PV penetration level may lead to the distribution line overload.

4.5 Summary

In this chapter, a novel two-stage stochastic programming based VR placement model considering the daily PVAC enhancement in distribution

networks is considered. Firstly, the VR allocation model is formulated as a deterministic mixed integer nonlinear programming (MINLP) problem. Then a technique approach is utilized to transform the MINLP model to the mixed integer linear programming (MILP) model. To model the uncertainties of PV generation and load consumption, the scenario method is employed to obtain representative PV-load scenarios, creating a two-stage stochastic MILP problem. Since numerous time-coupled constraints result in a huge computation burden, decomposition algorithm is used to decompose the two-stage MILP problem into a master program problem (the first-stage problem) and many subprogram problems (the second-stage problems), which can be directly solved by commercial solvers. To illustrate the effectiveness of the proposed allocation model and decomposition method, the IEEE 33-node distribution network is utilized as the test system.

The main conclusions are summarized as follows,

(1) The proposed VR planning model can appropriately take the PVAC improvement into consideration. According to the numerical results, it can be concluded that the PVAC is significantly enhanced after optimal VR placement.

(2) From the observation and analysis of the case study, it can also be concluded that optimal VR placement can effectively eliminate the overvoltage violations so as to ensure the reliability and security of normal distribution network operation.

(3) The proposed solution method on the basic of Benders decomposition algorithm is quite suitable for solving the proposed two-stage stochastic problem considering a large number of uncertainty scenarios. The developed solution approach can be suggested when dealing with similar problems.

(4) With the increase of VR planning cost, the PVAC improves accordingly at first. However, there is a threshold beyond which the PVAC improvement becomes insensitive to the VR planning cost increase. And this threshold is determined by the distribution network loadability.

Chapter 5 Conclusions and Future Works

5.1 Conclusions

The over-proliferation of renewable energy generators impact on normal operating conditions of power systems due to their stochastic characteristic of power output. This thesis mainly focuses on dealing with these negative impacts and improving the ability of power systems to accommodate more renewable power integration via advanced devices planning approaches. Stochastic programming based planning strategy is developed to address economic and technical problems within the domain of power system planning and operation. Specifically, the power system planning problem is investigated in the following aspects, given as follows,

- 1) In this thesis, the classical copula theory is used to sample uncertainties of wind generation and load demand in transmission networks, where the temporal interdependence between wind energy output and load is taken into account. Especially, the inverse transform method is used to model these two uncertainties. Previous works usually use Monte Carlo simulation method to generate scenarios. In comparison, this method has been widely applied to the generation of forecasted operational scenarios for renewable production, which can better resemble reality.
- 2) The stochastic programming based framework is proposed for TCSC planning model considering uncertainties in the transmission networks. This planning model is formulated to a two-stage model where the first stage determines the TCSC location-allocation decisions and the second stage is to minimize the expected system operation cost under different

wind-load scenarios. The proposed TCSC planning model is originally formulated a mixed integer nonlinear programming (MINLP), then a linearization technique and an approximation method are utilized to transform this MINLP into a mixed integer linear programming (MILP). Numerical results demonstrate that the performance of the proposed stochastic scheme is better than that of the traditional deterministic scheme.

- 3) The PV hosting capacity is innovatively modeled as a decision variable in the optimization text. Empirically, PV hosting capacity is difficult to be evaluated and it is generally assessed by using simulation-based approaches. In this thesis, the PV hosting capacity is incorporated into the objective function of optimal SVC planning problem by using sum weighted method. Therefore, the tradeoff between the PV hosting capacity and the SVC planning cost can be obtained, which is enforceable for practical application.
- 4) VR has the potential to improve the hourly PVAC of distribution networks since it can handle the overvoltage issue caused by PV energy integration through its continuous voltage regulation, which is not well studied in the existing works. To fill this research gap, a novel two-stage framework is proposed to investigate the extent of the potential benefits from optimal VR placement as an option to improve the PVAC. The hourly PVAC is modeled as a continuous variable which is formulated in the objective function. Two criteria are introduced to maintain the safety and reliability of the distribution network operation, i.e., voltage variation and distribution line capacity. Moreover, a stochastic programming based feasibility checking model is established to ensure that the distribution

network always remains secure operation under different uncertainty scenarios. Considering the widespread application of VR in power systems, this thesis has practical significance.

- 5) Time-coupling constraints across the time periods and numerous uncertainty scenarios result in an intractable two-stage stochastic planning problem. To reduce the computation burden, an efficient solution approach based on Benders decomposition is developed to solve this two-stage problem. Specifically, the two-stage problem can be decomposed into a master problem and multiple subproblems corresponding to all time periods in all scenarios. Furthermore, stochastic Benders cuts are built to link the master problem with the subproblems. To the best knowledge, this is the first study to employ the Benders decomposition algorithm to solve the two-stage planning problem for PV hosting capacity improvement by far.

5.2 Future Works

In this thesis, several advanced methods have been proposed for both transmission systems and distribution systems with the high integration level of renewable generations. In order to reduce the complexity arising from the complicated realistic issues, some assumptions have been made. In the future, the following aspects need to be considered for making the proposed approaches to be more practical.

- 1) Line flow based equation model is used to describe power flows of transmission networks without consideration of voltage angle and Distflow model is adopted to describe power flows of distribution networks.

However, in fact, the model of real transmission and distribution systems presents considerable complexity, resulting in complicated issues in power system planning problems. In this regard, the research efforts should be paid to the improvement of the existing models and development of models with high accuracy, like multi-phase OPF model, which enables us to deal with planning problems in power systems in a more realistic manner.

2) In this thesis, the stochastic programming is used as the optimization methodology, which has its inherent disadvantages. The main difficulty of the stochastic programming is that the probability distribution functions associated with uncertain parameters should be provided. Therefore, a huge burden may arise from this requirement since related information is unavailable to acquire in many realistic situations. In most cases, when dealing with input uncertainty, stochastic programming assumes that some uncertain parameters can represent all possible operating conditions of the power systems and ensures that the obtained solution is able to be robust against all considered scenarios. Therefore, all underlying stochastic parameters should be selected to build uncertainty scenarios and thus the obtained solution is itself random, which seems inapplicable for practical implementation. In this thesis, decisionmakers are allowed to manage the degree of robustness of the solution by using a backward-reduction algorithm to obtain representative uncertainty scenarios. With the consideration of realistic implementation, the way to control the robustness of the solution should be carefully estimated. Moreover, the stochastic programming based algorithms generally have two stages and make all decisions before the uncertainty realizations. Thus, multi-period

optimization is suggested to address uncertainties and manage the robustness of the solution since it makes a series of decisions in different time occurs.

References

- [1] Ellabban O, Abu-Rub H, Blaabjerg FJR, Reviews SE. Renewable energy resources: Current status, future prospects and their enabling technology. 2014;39:748-64.
- [2] Breeze P. Power generation technologies: Newnes; 2019.
- [3] Muttaqi KM, Islam MR, Sutanto DJIToAS. Future Power Distribution Grids: Integration of Renewable Energy, Energy Storage, Electric Vehicles, Superconductor, and Magnetic Bus. 2019;29:1-5.
- [4] Renewable Capacity Highlights. International Renewable Energy Agency; 2019.
- [5] Willis HL. Distributed power generation: planning and evaluation: Crc Press; 2018.
- [6] Revesz R, Unel BJELI. The future of Distributed Generation: Moving past net metering. 2018;48:I0719-I25.
- [7] Rehmani MH, Reisslein M, Rachedi A, Erol-Kantarci M, Radenkovic MJIToII. Integrating renewable energy resources into the smart grid: recent developments in information and communication technologies. 2018;14:2814-25.
- [8] Barbose GL, Darghouth NR, LaCommare KH, Millstein D, Rand J. Tracking the Sun: Installed Price Trends for Distributed Photovoltaic Systems in the United States-2018 Edition. 2018.
- [9] Abdmouleh Z, Alammari RA, Gastli AJR, Reviews SE. Review of policies encouraging renewable energy integration & best practices. 2015;45:249-62.
- [10] Boyle GJRE, by Edited by Godfrey Boyle, pp. 456. Oxford University Press, May . ISBN-10: 0199261784. ISBN-13: 9780199261789. Renewable energy. 2004:456.
- [11] Buonocore JJ, Luckow P, Norris G, Spengler JD, Biewald B, Fisher J, et al. Health and climate benefits of different energy-efficiency and renewable energy choices. 2016;6:100.
- [12] Novan KJAEJEP. Valuing the wind: renewable energy policies and air pollution avoided. 2015;7:291-326.
- [13] Adefarati T, Bansal RJIRPG. Integration of renewable distributed generators into the distribution system: a review. 2016;10:873-84.
- [14] Ziaee O, Mousavi OA, Choobineh F. Co-optimization of transmission expansion planning and TCSC placement considering the correlation between wind and demand scenarios. IEEE Transactions on Power Systems. 2017;PP:1-.

- [15] Helton JC, Johnson JD, Sallaberry CJ, Storlie CB. Survey of sampling-based methods for uncertainty and sensitivity analysis. *Reliability Engineering & System Safety*. 2006;91:1175-209.
- [16] Batalla-Bejerano J, Trujillo-Baute EJEP. Impacts of intermittent renewable generation on electricity system costs. 2016;94:411-20.
- [17] Song Y-H, Johns A. Flexible ac transmission systems (FACTS): IET; 1999.
- [18] Mohanty AK, Barik AKJIJoMER. Power system stability improvement using FACTS devices. 2011;1:666-72.
- [19] Acharya N, Sode-Yome A, Mithulananthan N. Facts about flexible AC transmission systems (FACTS) controllers: practical installations and benefits. *Australasian universities power engineering conference (AUPEC), Australia2005*. p. 533-8.
- [20] Donsion MP, Guemes J, Rodriguez J. Power Quality. Benefits of Utilizing FACTS Devices in Electrical Power Systems. 2007 7th International Symposium on Electromagnetic Compatibility and Electromagnetic Ecology: IEEE; 2007. p. 26-9.
- [21] Habur K, O'Leary DJS-WBdFDR, Erlangen. FACTS-flexible alternating current transmission systems: for cost effective and reliable transmission of electrical energy. 2004:46.
- [22] Galiana F, Almeida K, Toussaint M, Griffin J, Atanackovic D, Ooi B, et al. Assessment and control of the impact of FACTS devices on power system performance. *IEEE Transactions on power systems*. 1996;11:1931-6.
- [23] Perez MA, Messina AR, Fuerte-Esquivel CR. Application of FACTS devices to improve steady state voltage stability. 2000 Power Engineering Society Summer Meeting (Cat No00CH37134)2000. p. 1115-20 vol. 2.
- [24] Rahimzadeh S, Tavakoli M, Viki BAH. Simultaneous application of multi-type FACTS devices to the restructured environment: achieving both optimal number and location. *IET Generation, Transmission & Distribution*. 2010;4:349-62.
- [25] Brunet-Watson M, Leighfield J, America PN. Review of Series Compensation for Transmission Lines. 2014.
- [26] L'Abbate A, Migliavacca G, Hager U, Rehtanz C, Ruberg S, Ferreira H, et al. The role of facts and HVDC in the future paneuropean transmission system development. *AC and DC Power Transmission, 2010 ACDC 9th IET International Conference on: IET; 2010*. p. 1-8.

- [27] Hamidi A, Nazarpour D, Golshannavaz S. Multiobjective Scheduling of Microgrids to Harvest Higher Photovoltaic Energy. *IEEE Transactions on Industrial Informatics*. 2018;14:47-57.
- [28] Jia Y, Xu Z, Lai LL, Wong KP. Risk-based power system security analysis considering cascading outages. *IEEE Transactions on Industrial Informatics*. 2016;12:872-82.
- [29] Tsai Y-C, Chan Y-K, Ko F-K, Yang J-T. Integrated operation of renewable energy sources and water resources. *Energy Conversion and Management*. 2018;160:439-54.
- [30] Smith J, Rylander MJEPRI, Palo Alto, CA, Tech. Rep. Stochastic analysis to determine feeder hosting capacity for distributed solar PV. 2012;1026640:0885-8950.
- [31] Smith J, Rylander M. Stochastic analysis to determine feeder hosting capacity for distributed solar PV. Electric Power Research Inst, Palo Alto, CA, Tech Rep. 2012;1026640.
- [32] Ayres H, Freitas W, De Almeida M, Da Silva L. Method for determining the maximum allowable penetration level of distributed generation without steady-state voltage violations. *IET generation, transmission & distribution*. 2010;4:495-508.
- [33] Baran ME, Hooshyar H, Shen Z, Huang A. Accommodating high PV penetration on distribution feeders. *IEEE Transactions on smart grid*. 2012;3:1039-46.
- [34] Gang Q, Haozhong C, Liangzhong Y, Bazargan M, Zeliang M, Zhonglie Z, et al. Power transmission expansion planning considering large bulk power injection. 8th International Conference on Advances in Power System Control, Operation and Management (APSCOM 2009)2009. p. 1-5.
- [35] Hingorani NG. Flexible AC transmission. *IEEE spectrum*. 1993;30:40-5.
- [36] Hingorani NG, Gyugyi L. *Understanding facts*: IEEE press; 2000.
- [37] Leonidaki E, Georgiadis D, Hatziargyriou N. Decision trees for determination of optimal location and rate of series compensation to increase power system loading margin. *IEEE Transactions on Power Systems*. 2006;21:1303-10.
- [38] Ashpazi MA, Mohammadi-Ivatloo B, Zare K, Abapour M. Probabilistic allocation of thyristor-controlled phase shifting transformer for transient stability enhancement of electric power system. *IETE Journal of Research*. 2015;61:382-91.
- [39] Duan C, Fang W, Jiang L, Niu S. FACTS Devices Allocation via Sparse Optimization. *IEEE Transactions on Power Systems*. 2016;31:1308-19.

- [40] Gerbex S, Cherkaoui R, Germond AJ. Optimal location of multi-type FACTS devices in a power system by means of genetic algorithms. *IEEE Transactions on Power Systems*. 2001;16:537-44.
- [41] Saravanan M, Slochanal SMR, Venkatesh P, Abraham JPS. Application of particle swarm optimization technique for optimal location of FACTS devices considering cost of installation and system loadability. *Electric Power Systems Research*. 2007;77:276-83.
- [42] Yang GY, Hovland G, Majumder R, Dong ZY. TCSC Allocation Based on Line Flow Based Equations Via Mixed-Integer Programming. *IEEE Transactions on Power Systems*. 2007;22:2262-9.
- [43] Ziaee O, Choobineh F. Optimal Location-Allocation of TCSCs and Transmission Switch Placement Under High Penetration of Wind Power. *IEEE Transactions on Power Systems*. 2016;PP:1-.
- [44] Hemmati R, Hooshmand R-A, Khodabakhshian A. Comprehensive review of generation and transmission expansion planning. *IET Generation, Transmission & Distribution*. 2013;7:955-64.
- [45] De Oliveira E, Lima JM, De Almeida K. Allocation of FACTS devices in hydrothermal systems. *IEEE Transactions on Power Systems*. 2000;15:276-82.
- [46] Mann NR, Singpurwalla ND, Schafer RE. *Methods for statistical analysis of reliability and life data*. 1974.
- [47] Charytoniuk W, Chen M, Kotas P, Van Olinda P. Demand forecasting in power distribution systems using nonparametric probability density estimation. *IEEE Transactions on Power Systems*. 1999;14:1200-6.
- [48] Pinson P, Girard R. Evaluating the quality of scenarios of short-term wind power generation. *Applied Energy*. 2012;96:12-20.
- [49] Growe-Kuska N, Heitsch H, Romisch W. Scenario reduction and scenario tree construction for power management problems. *Power tech conference proceedings, 2003 IEEE Bologna: IEEE; 2003. p. 7 pp. Vol. 3.*
- [50] Grainger JJ, Stevenson WD, Stevenson WD. *Power system analysis* 2003.
- [51] Powell L. *Power System Load Flow Analysis (Professional Engineering)*: McGraw-Hill Professional; 2004.
- [52] Yan P, Sekar AJIP-G, Transmission, Distribution. Steady-state analysis of power system having multiple FACTS devices using line-flow-based equations. *IEEE Transactions on Power Systems*. 2005;152:31-9.

- [53] Yan P, Sekar AJIToPS. Analysis of radial distribution systems with embedded series FACTS devices using a fast line flow-based algorithm. 2005;20:1775-82.
- [54] Ping Y, Sekar A. Analysis of radial distribution systems with embedded series FACTS devices using a fast line flow-based algorithm. IEEE Transactions on Power Systems. 2005;20:1775-82.
- [55] Blumsack S. Network topologies and transmission investment under electric-industry restructuring: ProQuest; 2006.
- [56] Lofberg J. YALMIP : a toolbox for modeling and optimization in MATLAB. 2004 IEEE International Conference on Robotics and Automation (IEEE Cat No04CH37508)2004. p. 284-9.
- [57] Cplex IJIBMC. V12. 1: User's Manual for CPLEX. 2009;46:157.
- [58] Karmellos M, Mavrotas G. Multi-objective optimization and comparison framework for the design of Distributed Energy Systems. Energy Conversion and Management. 2019;180:473-95.
- [59] Zakariazadeh A, Jadid S, Siano P. Integrated operation of electric vehicles and renewable generation in a smart distribution system. Energy Conversion and Management. 2015;89:99-110.
- [60] Song J, Oh S-D, Yoo Y, Seo S-H, Paek I, Song Y, et al. System design and policy suggestion for reducing electricity curtailment in renewable power systems for remote islands. Applied Energy. 2018;225:195-208.
- [61] Ding F, Mather B. On Distributed PV Hosting Capacity Estimation, Sensitivity Study, and Improvement. IEEE Transactions on Sustainable Energy. 2017;8:1010-20.
- [62] Rabiee A, Mohseni-Bonab SM. Maximizing hosting capacity of renewable energy sources in distribution networks: A multi-objective and scenario-based approach. Energy. 2017;120:417-30.
- [63] Hashemi S, Østergaard J, Degner T, Brandl R, Heckmann W. Efficient control of active transformers for increasing the pv hosting capacity of lv grids. IEEE Transactions on Industrial Informatics. 2017;13:270-7.
- [64] Soroudi A, Rabiee A, Keane A. Distribution networks' energy losses versus hosting capacity of wind power in the presence of demand flexibility. Renewable Energy. 2017;102:316-25.
- [65] Hashemi S, Ostergaard J. Efficient control of energy storage for increasing the PV hosting capacity of LV grids. IEEE Transactions on Smart Grid. 2016.

- [66] Wang S, Chen S, Ge L, Wu L. Distributed generation hosting capacity evaluation for distribution systems considering the robust optimal operation of oltc and svc. *IEEE Transactions on Sustainable Energy*. 2016;7:1111-23.
- [67] Savić A, Đurišić Ž. Optimal sizing and location of SVC devices for improvement of voltage profile in distribution network with dispersed photovoltaic and wind power plants. *Applied Energy*. 2014;134:114-24.
- [68] Mínguez R, Milano F, Zárate-Miñano R, Conejo AJ. Optimal network placement of SVC devices. *IEEE Transactions on Power Systems*. 2007;22:1851-60.
- [69] Kall P, Wallace SW, Kall P. *Stochastic programming*: Springer; 1994.
- [70] Ben-Tal A, El Ghaoui L, Nemirovski A. *Robust optimization*: Princeton University Press; 2009.
- [71] da Silva PP, Dantas G, Pereira GI, Câmara L, De Castro NJJR, Reviews SE. Photovoltaic distributed generation—An international review on diffusion, support policies, and electricity sector regulatory adaptation. 2019;103:30-9.
- [72] Baran M, Wu FF. Optimal sizing of capacitors placed on a radial distribution system. *IEEE Transactions on Power Delivery*. 1989;4:735-43.
- [73] Baran ME, Wu FF. Optimal capacitor placement on radial distribution systems. *IEEE Transactions on Power Delivery*. 1989;4:725-34.
- [74] Stott B, Jardim J, Alsaç OJIToPS. DC power flow revisited. 2009;24:1290-300.
- [75] Marler RT, Arora JS. The weighted sum method for multi-objective optimization: new insights. *Structural and multidisciplinary optimization*. 2010;41:853-62.
- [76] Geoffrion AM. Generalized benders decomposition. *Journal of optimization theory and applications*. 1972;10:237-60.
- [77] Lofberg J. YALMIP: A toolbox for modeling and optimization in MATLAB. *Computer Aided Control Systems Design, 2004 IEEE International Symposium on: IEEE*; 2004. p. 284-9.
- [78] Optimization G. Inc., “Gurobi optimizer reference manual,” 2015. Google Scholar. 2014.
- [79] Sahinidis N, Grossmann IE. Convergence properties of generalized Benders decomposition. *Computers & Chemical Engineering*. 1991;15:481-91.
- [80] Patel MR. *Wind and solar power systems: design, analysis, and operation*: CRC press; 2005.
- [81] Grant M, Boyd S, Ye Y. *CVX: Matlab software for disciplined convex programming*. 2008.

- [82] Jenkins J, Zhou Z, Ponciroli R, Vilim R, Ganda F, de Sisternes F, et al. The benefits of nuclear flexibility in power system operations with renewable energy. 2018;222:872-84.
- [83] Han X, Chen X, McElroy MB, Liao S, Nielsen CP, Wen JJA. Modeling formulation and validation for accelerated simulation and flexibility assessment on large scale power systems under higher renewable penetrations. 2019;237:145-54.
- [84] Adefarati T, Bansal RJA. Reliability, economic and environmental analysis of a microgrid system in the presence of renewable energy resources. 2019;236:1089-114.
- [85] Atems B, Hotaling CJEP. The effect of renewable and nonrenewable electricity generation on economic growth. 2018;112:111-8.
- [86] Kabalci E, Kabalci Y. Introduction to Smart Grid Architecture. Smart Grids and Their Communication Systems: Springer; 2019. p. 3-45.
- [87] Nakashima S. Voltage regulator. Google Patents; 2019.
- [88] Semiconductor OJOS. Linear & switching voltage regulator handbook. 2002.
- [89] Szuvovivski I, Fernandes T, Aoki AJIJoEP, Systems E. Simultaneous allocation of capacitors and voltage regulators at distribution networks using genetic algorithms and optimal power flow. 2012;40:62-9.
- [90] Attar M, Homae O, Falaghi H, Siano PJIJoEP, Systems E. A novel strategy for optimal placement of locally controlled voltage regulators in traditional distribution systems. 2018;96:11-22.
- [91] Niknam T, Narimani MR, Azizipanah-Abarghooee RJIJoC, Automation, Systems. A multi-objective fuzzy adaptive PSO algorithm for location of automatic voltage regulators in radial distribution networks. 2012;10:772-7.
- [92] de Lima MAX, Clemente TRN, de Almeida AT. Prioritization for allocation of voltage regulators in electricity distribution systems by using a multicriteria approach based on additive-veto model. International Journal of Electrical Power & Energy Systems. 2016;77:1-8.
- [93] Rao PR, Raju SSJIJoE, Science, Technology. Voltage regulator placement in radial distribution system using plant growth simulation algorithm. 2010;2.
- [94] Niknam T, Azizipanah-Abarghooee R, Narimani MRJEAoAI. A new multi objective optimization approach based on TLBO for location of automatic voltage regulators in distribution systems. 2012;25:1577-88.

- [95] Efkarpidis N, De Rybel T, Driesen J. Optimal placement and sizing of active in-line voltage regulators in flemish LV distribution grids. *IEEE Transactions on Industry Applications*. 2016;52:4577-84.
- [96] Zhao J, Xu Z, Wang J, Wang C, Li J. Robust Distributed Generation Investment Accommodating Electric Vehicle Charging in a Distribution Network. *IEEE Transactions on Power Systems*. 2018.
- [97] Gonçalves RR, Franco JF, Rider MJ. Short-term expansion planning of radial electrical distribution systems using mixed-integer linear programming. *IET Generation, Transmission & Distribution*. 2014;9:256-66.
- [98] Heitsch H, Römisch W. Scenario reduction algorithms in stochastic programming. *Computational optimization and applications*. 2003;24:187-206.
- [99] Kersting WH. Radial distribution test feeders. *Power Engineering Society Winter Meeting, 2001 IEEE: IEEE; 2001*. p. 908-12.